

Higgs branch of 6D (1, 0) SCFTs and little string theories with Dynkin DE-type SUSY enhancement

Craig Lawrie^{*} and Lorenzo Mansi[†]

Deutsches Elektronen-Synchrotron DESY, Notkestraße 85, 22607 Hamburg, Germany



(Received 11 June 2024; accepted 20 August 2024; published 19 September 2024)

We detail the Higgs branches of 6D (1, 0) superconformal field theories (SCFTs) and little string theories (LSTs) that exhibit supersymmetry-enhancing Higgs branch renormalization group flows to the 6D (2, 0) SCFTs and LSTs of type DE. Generically, such theories are geometrically engineered in F-theory via a configuration of (-2) -curves, arranged in an (affine) DE-type Dynkin diagram, and supporting special unitary gauge algebras; this describes the effective field theory on the tensor branch of the SCFT. For the Higgsable to D-type (2, 0) SCFTs/LSTs, there generically also exists a type IIA brane description, involving a Neveu-Schwarz orientifold plane, which allows for the derivation of a magnetic quiver for the Higgs branch. These are 3D $\mathcal{N} = 4$ unitary-orthosymplectic quivers whose Coulomb branch is isomorphic to the Higgs branch of the 6D theories. From this magnetic quiver, together with an extended quiver subtraction algorithm that we explain, the foliation structure of the Higgs branch as a symplectic singularity is unveiled. For this class of 6D SCFTs, we observe a simple rule, which we refer to as “slice subtraction,” to read off the transverse slice in the foliation from the tensor branch. Based on this slice subtraction observation, we conjecture the transverse slices in the Higgsable to E-type (2, 0) Hasse diagram, where the SCFTs lack any known magnetic quiver for their Higgs branches.

DOI: [10.1103/PhysRevD.110.066014](https://doi.org/10.1103/PhysRevD.110.066014)

I. INTRODUCTION

In recent years, the study of six-dimensional superconformal fields theories (SCFTs) with minimal supersymmetry has been burgeoning. While the existence of these novel quantum fields theories has been established for many years [1–4], their concrete construction and the extraction of their physical features has been rendered challenging by the absence of supersymmetry-preserving relevant or marginal deformations [5–9], and thus of direct bottom-up Lagrangian descriptions.

Nevertheless, 6D SCFTs have been fruitfully explored via top-down constructions from string theory.¹ The maximally supersymmetric SCFTs in 6D were first constructed [15] by considering the compactification of type IIB string theory on the orbifold

$$\mathbb{C}^2/\Gamma \quad \text{with} \quad \Gamma \subset SU(2). \quad (1.1)$$

^{*}Contact author: craig.lawrie1729@gmail.com

[†]Contact author: lorenzo.mansi@desy.de

¹See [10–14] for recent reviews of such explorations.

Published by the American Physical Society under the terms of the Creative Commons Attribution 4.0 International license. Further distribution of this work must maintain attribution to the author(s) and the published article's title, journal citation, and DOI. Funded by SCOAP³.

The finite subgroups, Γ , of $SU(2)$ organize themselves into an *ADE* classification, consisting of two infinite series and three sporadics,

$$A_{n \geq 1}, \quad D_{n \geq 4}, \quad E_6, \quad E_7, \quad E_8, \quad (1.2)$$

and thus, each 6D (2, 0) SCFT is associated with a choice of simple and simply-laced Lie group via the McKay correspondence [16].

To construct 6D SCFTs with minimal supersymmetry, one can replace type IIB, used in the construction of 6D (2, 0) SCFTs, with F-theory [17–19]. In [11,12], it was argued that F-theory compactified on certain noncompact elliptically fibered Calabi-Yau threefolds engineers 6D (1, 0) SCFTs, and furthermore a mechanism was provided for the construction of a vast landscape of such Calabi-Yau spaces. In particular, we need a noncompact Calabi-Yau threefold Y that is elliptically-fibered over a noncompact base B , containing no compact complex curves, and such that the elliptic fiber over every point of B is irreducible. Since we are interested in nonproduct SCFTs, B may contain at most one singular point, b_0 , and at most one nonminimal fiber, which must be supported over b_0 .² A method to determine such elliptically fibered Calabi-Yau threefolds was provided

²An explanation of these technical conditions can be found in the review [13].

in [11,12]. In particular, take a noncompact elliptically fibered Calabi-Yau threefold

$$\pi: \tilde{Y} \rightarrow \tilde{B}, \quad (1.3)$$

such that \tilde{B} has no singular points, and the fiber over each point of B is irreducible and minimal. Suppose that \tilde{B} contains a network of connected compact curves, C_i . If there exists a contraction map

$$\rho: \tilde{B} \rightarrow B, \quad (1.4)$$

that shrinks all compact curves to zero volume such that either the image of the C_i under the map is singular, or, uplifting ρ to a map $\rho: \tilde{Y} \rightarrow Y$, the singular fiber above the image of the C_i is nonminimal, then the resulting Y engineers a 6D (1, 0) SCFT. All possible \tilde{Y} can be constructed from a small set of building blocks; see [20] for a recent review. F-theory compactified on \tilde{Y} directly gives rise to a 6D (1, 0) quantum field theory, not an SCFT, which is referred to as the SQFT living at the generic point of the tensor branch of the SCFT associated with Y . Therefore, we often refer to \tilde{Y} as the “tensor branch geometry” or the “tensor branch curve configuration.” Since \tilde{Y} is nonsingular, it is generally easier to extract physical properties from \tilde{Y} rather than Y directly; therefore this tensor branch description is particularly powerful for determining SCFT properties which are protected under the curve contraction map.

There is an extensive family of 6D (1, 0) SCFTs associated with each 6D (2, 0) SCFT in the following manner. Let Y be a noncompact elliptically fibered Calabi-Yau threefold that engineers some 6D (1, 0) SCFT in F-theory, and further suppose that there exists a sequence of complex structure deformations of Y such that

$$Y \xrightarrow{\text{cx.str.def.}} T^2 \times \mathbb{C}^2 / \Gamma, \quad (1.5)$$

where Γ is a finite subgroup of $SU(2)$. Then the SCFT engineered by Y belongs to the family of the (2, 0) SCFT labeled by Γ .³ Since complex structure deformations correspond physically to Higgs branch renormalization group (RG) flows, we can refer to any such 6D (1, 0) SCFT as “Higgsable to the 6D (2, 0) SCFT of type Γ ” [21,22]. The most famous examples are the rank N $(\mathfrak{g}, \mathfrak{g})$ conformal matter theories [23], which are Higgsable to the 6D (2, 0) SCFT of type $\Gamma = A_{N-1}$. Our focus in this paper is precisely this set of 6D (1, 0) SCFTs where Γ is of DE-type; such theories have received limited attention (see, e.g., [24,25]) compared to their A-type cousins.

³It is straightforward to see that if there exists a Γ such that Eq. (1.5) is satisfied, then it is unique.

A vital aspect of the study of any supersymmetric quantum field theory is the exploration of the moduli space of supersymmetric vacua. A 6D (1, 0) SCFT can have a Higgs branch which captures the half-BPS (Bogomol’nyi–Prasad–Sommerfield) operators of the theory. There are many interesting physical questions related to the Higgs branch, for example:

- (1) What are the interacting fixed points on the Higgs branch? How are they related?
- (2) What are the half-BPS operators belonging to the Higgs branch chiral ring?
- (3) Is the Higgs branch chiral ring freely generated?
- (4) What are the generators (and relations if it is not freely generated)?

As an eight-supercharge theory, the Higgs branch of a 6D (1, 0) SCFT is both a hyperkähler space and a symplectic singularity [26,27]. A symplectic singularity possesses a natural foliation by symplectic leaves, and this induces a partial ordering on the leaves given by inclusion; from this partial ordering, we can associate a Hasse diagram, the so-called Higgs branch Hasse diagram. The physical interpretation of this Hasse diagram is that it encompasses all of the patterns of partial Higgsing of a given theory; a 6D SCFT is associated with each symplectic leaf in the foliation, and the transverse slice between two leaves captures the parameters that need to be tuned to perform a Higgs branch renormalization group flow between the two associated SCFTs [28,29].

In terms of the elliptically fibered Calabi-Yau threefold, Y , engineering the SCFT, the Higgs branch is related to the space of complex structure deformations of Y [30]. In particular, if there exists a complex structure deformation

$$Y \xrightarrow{\text{cx.str.def.}} Y', \quad (1.6)$$

then there exists a Higgs branch renormalization flow between the SCFTs associated with Y and Y' . However, the question of whether such complex structure deformations exist can be difficult to answer from the study of the nonsingular Calabi-Yau geometries engineering the tensor branch effective field theories; \tilde{Y} and \tilde{Y}' . As the geometry does not provide a particularly transparent window on the structure of the Higgs branch, especially on the vacuum expectation values that are given to trigger a particular flow, we use alternative methods to study the Higgs branch Hasse diagram in this paper, and we then compare to the expected geometric structure.

One particularly powerful method to study the structure of the Higgs branch of a 6D (1, 0) SCFT is the method of magnetic quivers [31–33]. Let \mathcal{T} be an arbitrary 6D (1, 0) SCFT; if we can find a 3D $\mathcal{N} = 4$ Lagrangian theory \mathcal{T}_M such that the Higgs branch of \mathcal{T} is the same as the Coulomb branch of \mathcal{T}_M ,

$$\text{HB}[\mathcal{T}] = \text{CB}[\mathcal{T}_M], \quad (1.7)$$

then we say that \mathcal{T}_M is a magnetic quiver for the Higgs branch of \mathcal{T} .⁴ Of course, for this to be a useful perspective, it is necessary to have an algorithm for the construction of a \mathcal{T}_M . Luckily, if \mathcal{T} can be engineered via a brane system in type IIA (or type I) string theory, then one can pass to the magnetic phase of the brane system to obtain a quiver \mathcal{T}_M satisfying Eq. (1.7). This process has been carried out for certain 6D (1, 0) SCFTs in [34–36].

Knowing that the Higgs branch of the 6D SCFT is isomorphic to the Coulomb branch of a Lagrangian 3D $\mathcal{N} = 4$ quiver is particularly powerful, as we can then use the sophisticated tools developed to study the Coulomb branches of such quivers. For example, we can use the monopole formulas [37] to calculate the Coulomb branch Hilbert series, and thus understand the structure of the 6D Higgs branch chiral ring, or we can use a quiver subtraction algorithm [38] or the decay and fission algorithm [29, 39] to determine the structure of the interacting fixed points on the 6D Higgs branch. As one of the principle results of this paper, we use the type IIA brane system description of the Higgsable to (2, 0) D-type SCFTs, which involves a Neveu-Schwarz orientifold [40], to determine unitary-orthosymplectic magnetic quivers for their Higgs branches. Then, we use the quiver subtraction algorithm to study the interacting fixed points and compare them to the 6D (1, 0) SCFTs expected to lie along subloci of the Higgs branch.

The structure of this paper is as follows. First, in Sec. II, we review the geometric construction of 6D (1, 0) SCFTs via F-theory and introduce the classes of theories that are of interest in this paper. In Sec. III, we determine the magnetic quivers for the Higgs branches of the $D_N^{\text{su}(2k)}(O)$ SCFTs from the type IIA brane engineering description involving ON^- -planes. We perform a consistency check by comparing the unitary magnetic quivers obtained when $\Gamma = A_3$ with the unitary-orthosymplectic magnetic quivers obtained when $\Gamma = D_3$ in Sec. IV. With the magnetic quiver firmly in hand, we turn, in Sec. V, to the determination of the Higgs branch Hasse diagram, and we observe that the quiver subtraction algorithm leads to the same result as expected from the F-theory geometry. In Sec. VI, we make a brief digression to discuss the complex structure deformations behind Higgsings that break an SCFT into a product of SCFTs. In Sec. VII, we explore the 6D (1, 0) SCFTs with supersymmetry-enhancing RG flows to 6D (2, 0) SCFTs of E-type; due to the lack of a magnetic

quiver, we study the Higgs branch purely from the 6D perspective. Next, in Sec. VIII, we study the 6D (1, 0) little strings theories (LSTs) that have DE-type supersymmetry-enhancing Higgs branch RG flows, and determine the magnetic quivers capturing the structure of their Higgs branches. Finally, in Sec. IX, we summarize our results and discuss some suggested future directions.

II. 6D (1, 0) SCFTs WITH SUSY-ENHANCING RENORMALIZATION GROUP FLOWS

As we have mentioned in Sec. I, 6D (1, 0) SCFTs can be engineered by considering F-theory compactified on certain noncompact elliptically fibered Calabi-Yau threefolds. The atomic construction [11, 12] provides a constructive algorithm to produce such threefolds. This geometric procedure has been reviewed in detail in [13], as well as in recent work of the current authors [20], and so we only briefly summarize the necessary aspects of the construction here, and refer to these references for a fuller exposition.

We begin with a noncompact elliptically-fibered Calabi-Yau threefold \tilde{Y} . The base of the fibration, \tilde{B} , contains a collection of intersecting smooth rational curves, C_i , and the intersection matrix of these compact curves is presumed to be negative-definite,

$$C_i \cdot C_j < 0. \quad (2.1)$$

Furthermore, the fibration over every point of \tilde{B} is assumed to be minimal, in the technical sense explained in [11, 12]. Then, there exists a (unique) contraction map $\pi: \tilde{Y} \rightarrow Y$, which simultaneously takes the volume of all the C_i to zero, such that F-theory compactified on Y leads to a 6D (1, 0) SCFT.⁵ The construction of LSTs from F-theory [41] proceeds in a similar way, except that the intersection matrix of compact curves is negative semidefinite with a single zero eigenvalue. Then, there exists a (possibly nonunique) contraction map which simultaneously shrinks all-but-one of the compact curves; F-theory compactified on the Calabi-Yau space obtained after contraction gives rise to an LST. We return to LSTs in Sec. VIII.

Therefore, a 6D (1, 0) SCFT engineered in such a way can be encoded in the relevant data of \tilde{Y} , which is simply the configuration of curves C_i , and the singular fibers supported over the generic points of each C_i . Each C_i has a negative self-intersection number, $(-n)$ for some positive n , due to the condition in Eq. (2.1). The minimal singular fiber supported over the curve C_i can be captured by a simple

⁴More generally, the Higgs branch can be isomorphic to a union of Coulomb branches of magnetic quivers,

$$\text{HB}[\mathcal{T}] = \bigcup_i \text{CB}[\mathcal{T}_M^{(i)}]. \quad (1.8)$$

This will not be relevant for this paper, where the Higgs branch is always given by a single magnetic quiver.

⁵Depending on the \tilde{Y} , the 6D SCFT engineered in this way may be noninteracting.

Lie algebra, \mathfrak{g}_i .⁶ The intersections of the C_i necessarily occur pairwise, and with intersection number 1, for the contraction to lead to a Y that gives rise to a 6D (1, 0) SCFT. Therefore, we can simply use the now standard notation where we denote a curve C_i of self-intersection number $(-n_i)$ and supporting singular fiber associated with the Lie algebra \mathfrak{g}_i as

$$\begin{array}{c} \mathfrak{g}_i \\ n_i \end{array} \quad (2.2)$$

Then, we can depict several such expressions adjacent to each other to indicate a nontrivial intersection of the associated curves. Such a notation captures all the salient data of the elliptically fibered Calabi-Yau threefold \tilde{Y} . For example,

$$\begin{array}{c} \mathfrak{su}_3 \\ 1 \ 3 \ 1, \end{array} \quad (2.3)$$

denotes three genus-zero curves, with self-intersection numbers (-1) , (-3) , and (-1) , that intersect in a linear chain, where only the (-3) -curve carries a nontrivial singular fiber,⁷ which is associated with the Lie algebra $\mathfrak{su}(3)$. Such data, which we refer to as a “curve configuration,” then specifies an interacting 6D (1, 0) SCFT.⁸

When considering F-theory compactified on \tilde{Y} , as opposed to Y , we obtain a 6D (1, 0) QFT; this is a gauge theory where the gauge algebras are specified by the singular fibers over the C_i . In addition to the gauge sector, there are also hypermultiplets associated with matter fields. In the cases of interest to us, the number of hypermultiplets and the representations of \mathfrak{g}_i under which they transform are prescribed, via gauge-anomaly cancellation, by the choice of self-intersection number of the corresponding curve C_i . The resulting QFT is the effective description at the generic point of the tensor branch of the 6D (1, 0) SCFT associated with the Calabi-Yau geometry Y .

A. Higgsable to D-type (2, 0)

The first family of theories that we explore in this paper are those that possess supersymmetry-enhancing Higgs branch renormalization group flows to the (2, 0) SCFT of type D_N . In the atomic construction, the 6D (2, 0) SCFT of

type D_N is associated with the following curve configuration:

$$\begin{array}{c} 2 \\ 2 \ 2 \cdots 2 \\ N-3 \end{array} \quad (2.4)$$

That is, a D_N Dynkin diagram formed out of intersecting (-2) -curves, where the elliptic fiber over each (-2) -curve is just a smooth torus.⁹

One family of theories that are Higgsable to the 6D (2, 0) SCFTs of type D_N are associated with the curve configurations where the (-2) -curves in Eq. (2.4) are decorated with singular fibers associated with special unitary gauge algebras,

$$\begin{array}{c} \mathfrak{su}_{k_2} \\ 2 \\ \mathfrak{su}_{k_1} \ \mathfrak{su}_{k_3} \ \mathfrak{su}_{k_4} \ \mathfrak{su}_{k_N} \\ 2 \ 2 \ \underbrace{2 \cdots 2}_{N-3} \end{array} \quad (2.5)$$

Gauge-anomaly cancellation mandates that when an $\mathfrak{su}(k)$ gauge algebra is supported over a (-2) -curve there must be precisely $2k$ -hypermultiplets transforming in the fundamental representation of $\mathfrak{su}(k)$.¹⁰ Thus, we need to have that

$$\sum_{j=1}^N A^{ij} k_j = m_i \geq 0, \quad (2.6)$$

where A^{ij} is the (positive-definite) Cartan matrix for the D_N Lie algebra and all the k_i and m_i are non-negative. In general, this is a necessary condition, but it is not sufficient; for example, any curve configuration of the form

$$\begin{array}{c} \mathfrak{su}_2 \\ 2 \\ \mathfrak{su}_2 \ \mathfrak{su}_3 \ \mathfrak{su}_4 \cdots \end{array} \quad (2.7)$$

does not, in fact, correspond to a 6D (1, 0) SCFT [43], even though it may satisfy Eq. (2.6). The m_i appearing in Eq. (2.6) are referred to as “dangling hypermultiplets,” and they are associated with $\mathfrak{su}(m_i)$ flavor algebras rotating these hypermultiplets. We can depict all this information together in one curve configuration as

$$\begin{array}{c} [m_2] \\ \mathfrak{su}_{k_2} \\ 2 \\ \mathfrak{su}_{k_1} \ \mathfrak{su}_{k_3} \ \mathfrak{su}_{k_4} \ \mathfrak{su}_{k_N} \\ 2 \ 2 \ \underbrace{2 \cdots 2}_{N-3} \\ [m_1] \ [m_3] \ [m_4] \ [m_N] \end{array} \quad (2.8)$$

⁶There are Kodaira-Neron singular fibers that correspond to the same simple Lie algebra, e.g., I_3 and IV fibers both correspond to $\mathfrak{su}(3)$, however, such distinctions are not generally relevant in this paper.

⁷For ease of notation, we refer to the smooth torus as the trivial singular fiber.

⁸In some circumstances, such as those discussed in [42], additional data may be required to uniquely describe the 6D (1, 0) SCFT, however, for the theories discussed in this paper, this is not necessary.

⁹One can continue to $N = 1$ and $N = 2$, which correspond to either a single (-2) -curve, or to two disjoint (-2) -curves, respectively. Throughout this paper, we assume that $N \geq 3$ to avoid these edge cases.

¹⁰Care must be taken when any $k = 0, 1$.

although the m_i are, of course, already implicitly fixed when writing the configuration as in Eq. (2.5).¹¹

For theories described by tensor branch configurations as in Eq. (2.5), there is a straightforward approach to understanding the Higgs branch renormalization group flows between theories. Consider a pair of consistent SCFTs of the form in Eq. (2.5), with the same value of N , where the gauge algebras are captured by the tuples

$$(k_1, k_2, \dots, k_N) \quad \text{and} \quad (k'_1, k'_2, \dots, k'_N), \quad (2.10)$$

respectively. Then, there exists a Higgs branch renormalization group flow from the unprimed to the primed theory if and only if

$$k'_i \leq k_i, \quad (2.11)$$

for all i . This is equivalent to the existence of a complex structure deformation of the Calabi-Yau engineering the unprimed SCFT, Y , to that engineering the primed SCFT, Y' .

The formulation in Eq. (2.5) is highly redundant; most combinations of positive integers (k_1, \dots, k_N) are ruled out as they violate the condition in Eq. (2.6). Instead, all valid tensor branch configurations of the form in Eq. (2.5) arise as elements of a family parametrized by a choice of algebra $\mathfrak{g} = \mathfrak{su}(2k)$ and a nilpotent orbit, O , of \mathfrak{g} . For fixed N with $N \geq 2k + 1$,¹² every combination of (\mathfrak{g}, O) corresponds to an interacting SCFT, and every interacting SCFT arises via a unique pair (\mathfrak{g}, O) . These families are obtained by starting with a parent theory with a \mathfrak{g} flavor symmetry, and the children in the family are those that can be obtained from the parent theory by giving a nilpotent vacuum expectation value to the moment map of the \mathfrak{g} flavor symmetry. The parent of each family is an SCFT which we denote as

$$D_N^{\mathfrak{su}(2k)}. \quad (2.12)$$

The description of these SCFTs at the generic point of their tensor branch is given by the configuration

¹¹As almost all of the theories studied in detail in this paper consist of $\mathfrak{su}(k)$ algebras supported over (-2) -curves, we introduce a simplifying notation where we write the dual Coxeter numbers of the gauge algebras arranged in the same way as the (-2) -curves. For example,

$$\begin{array}{c} \mathfrak{su}_3 \\ 2 \\ \mathfrak{su}_3 \quad \mathfrak{su}_6 \quad \mathfrak{su}_5 \quad \mathfrak{su}_4 \\ 2 \quad 2 \quad 2 \quad 2 \\ [1] \quad [3] \end{array} \xrightarrow[\text{denoted as}]{\text{will be}} \begin{array}{c} 3 \\ 3 \quad 6 \quad 54[3] \\ [1] \end{array} \quad (2.9)$$

While this could, *a priori*, be confusing, in every case that we consider in this paper, it is unambiguous whether we are referring to a curve configuration in the usual notation, or in this simplified notation.

¹²When we refer to N as “sufficiently large” throughout this paper, we mean that this condition is satisfied.

$$\begin{array}{c} \mathfrak{su}_k \\ 2 \\ \mathfrak{su}_k \quad \mathfrak{su}_{2k} \quad \mathfrak{su}_{2k} \quad \mathfrak{su}_{2k} \\ 2 \quad 2 \quad \underbrace{2 \quad \dots \quad 2}_{N-3} \end{array} [\mathfrak{su}_{2k}], \quad (2.13)$$

where we have highlighted the existence of an $\mathfrak{su}(2k)$ flavor symmetry.

As we have said, each such $D_N^{\mathfrak{su}(2k)}$ SCFT forms the parent for a whole family of theories related by Higgs branch renormalization group flow via giving nilpotent vacuum expectation values to the moment map of the $\mathfrak{su}(2k)$ flavor symmetry. We label the resulting SCFTs as

$$D_N^{\mathfrak{su}(2k)}(O), \quad (2.14)$$

where O is a nilpotent orbit of $\mathfrak{su}(2k)$. Nilpotent orbits of $\mathfrak{su}(2k)$ are in one-to-one correspondence with integer partitions of $2k$, and the mapping between integer partitions and tensor branch configurations is given in the appendices of [44]. From the tensor branch description, the anomaly polynomial can be determined following the usual algorithm [45–48], and thus the dimensions of the Higgs branches of each of the SCFTs $D_N^{\mathfrak{su}(2k)}(O)$ can be obtained [21,22,44]. We find

$$\dim(\mathcal{H}) = N + 2k^2 - \dim(O), \quad (2.15)$$

where $\dim(O)$ is the dimension of the nilpotent orbit O .¹³ The trivial orbit has dimension zero—consistent with it corresponding to the trivial Higgsing.

More than just the dimension of the Higgs branch, we would like to understand the structure of the Higgs branch. This can mean several things. For example, we would like to understand the effective theory (especially when that is an interacting SCFT) which exists along the different subloci of the Higgs branch; we would like to know when there exists an RG flow from a theory on one subloci to another, the transverse slice corresponding to that transition, as well as the operator(s) to which one gives a vacuum expectation value, and how the spectrum of the theory changes under the flow.

First, it is clear from Eq. (2.10) and the tensor branch description of the $D_N^{\mathfrak{su}(2k)}(O)$ theories that there exists a Higgs branch renormalization group flow between the following SCFTs

$$D_N^{\mathfrak{su}(2k)}(O) \longrightarrow D_N^{\mathfrak{su}(2k)}(O'), \quad (2.16)$$

if $O' < O$ under the partial ordering on nilpotent orbits of $\mathfrak{su}(2k)$ defined via the dominance ordering of their associated integer partitions. That is, there exists a subloci of the

¹³Note: this holds for all $k \geq 0$. When $k = 0$, for notational convenience, we formally consider the existence of a single nilpotent orbit of dimension zero.

Higgs branch of the theory $D_N^{\mathfrak{su}_{2k}}(O)$ along which the theory $D_N^{\mathfrak{su}_{2k}}(O')$ lives, and the Higgs branch of the latter theory is contained within that of the former. The specific operators belonging to the Higgs branch chiral ring whose vacuum expectation value triggers the renormalization group flow for the class of Higgsings in Eq. (2.16) are the same as those studied for (A, A) conformal matter in [49]. In addition, it is straightforward to see that one can Higgs from a family with $\mathfrak{su}(2k)$ to a family with $\mathfrak{su}(2k-2)$,

$$D_N^{\mathfrak{su}_{2k}} \longrightarrow D_N^{\mathfrak{su}_{2k-2}}. \quad (2.17)$$

More generally, it is straightforward to see, using Eq. (2.10),¹⁴ precisely when there exists a Higgs branch renormalization group flow between theories

$$D_N^{\mathfrak{su}_{2k}}(O) \longrightarrow D_N^{\mathfrak{su}_{2k-2}}(O'). \quad (2.18)$$

This provides a partial ordering on the set of theories of the form $D_N^{\mathfrak{su}_{2k}}(O)$, and the Hasse diagram of such theories with this partial ordering provides a subdiagram of the Hasse diagram of the Higgs branch of $D_N^{\mathfrak{su}_{2k}}$. We emphasize that this is *a priori* only a subdiagram, as there may be subloci of the Higgs branch where there are interacting fixed points not of the form $D_N^{\mathfrak{su}_{2k}}(O)$, or else product theories, theories with a free sector. We depict this Hasse diagram for theories $D_N^{\mathfrak{su}_{2\ell}}(O)$, for $2\ell \leq 8$, in Fig. 1.

While the SCFTs associated with tensor branch configurations as in Eq. (2.5) are the main subject of analysis in this paper, there are other 6D (1, 0) SCFTs which are Higgsable to the D-type (2, 0) SCFTs. We briefly review these theories here for completeness. There are 6D (1, 0) SCFTs that we label as

$$D_N^{\mathfrak{e}_6}(O), \quad (2.19)$$

where O is a nilpotent orbit of \mathfrak{e}_6 . These theories are so-named as they behave similarly to the theories described around Eq. (2.14). When O is the nilpotent orbit of dimension zero, the tensor branch configuration takes the form,

¹⁴Without using the tensor branch configuration, we can ask abstractly when there exists a flow between theories defined by the data $(N, 2k, O)$ and $(N, 2\ell, O')$, where O and O' are nilpotent orbits of $\mathfrak{su}(2k)$ and $\mathfrak{su}(2\ell)$, respectively. The answer is a D-type analog of what is called “simultaneous two-box deletion” in [49]. This is triggered via giving a vacuum expectation value to the D-type analog of an “end-to-end” operator, which has been studied in the A-type theories in [49–53]. However, in this paper, we proceed case-by-case, and thus we do not need to explore the general behavior of such transitions.

$$\begin{array}{c} \mathfrak{su}_3 \\ 3 \\ 1 \\ \mathfrak{su}_3 \quad \mathfrak{e}_6 \quad \mathfrak{su}_3 \quad \mathfrak{e}_6 \quad \mathfrak{su}_3 \\ 3 \quad 1 \quad 6 \quad 1 \quad 3 \quad 1 \quad 6 \quad 1 \quad 3 \quad 1 \end{array} \xrightarrow{N-3} \mathfrak{e}_6 \quad \mathfrak{su}_3 \quad \mathfrak{e}_6 \quad \mathfrak{su}_3 \quad \mathfrak{e}_6 \quad \mathfrak{su}_3 \quad 1[\mathfrak{e}_6], \quad (2.20)$$

where we have also depicted the \mathfrak{e}_6 flavor symmetry on the right. When O is nontrivial, the configuration is modified following the rules described in the appendices of [44]. In addition, there are a small number of exceptional theories, which we denote only by their tensor branch configurations. We have the parent theories

$$\begin{array}{c} 2 \\ \mathfrak{su}_2 \quad \mathfrak{su}_3 \quad \mathfrak{su}_3 \\ 2 \quad 2 \quad 2 \quad \cdots \quad 2 \end{array} [\mathfrak{su}_3] \quad \text{and} \quad \begin{array}{c} \mathfrak{su}_2 \\ 2 \\ \mathfrak{su}_2 \quad \mathfrak{so}_7 \quad \mathfrak{so}_8 \quad \mathfrak{so}_8 \\ 2 \quad 3 \quad 1 \quad 4 \quad 1 \quad \cdots \quad 4 \quad 1 \end{array} [\mathfrak{so}_8], \quad (2.21)$$

together with their descendants obtained via nilpotent Higgsing of the $\mathfrak{su}(3)$ and $\mathfrak{so}(8)$ flavor symmetries, respectively.

These four classes of theories exhaust the 6D (1, 0) SCFTs that are Higgsable to D-type (2, 0), where N can be taken to be arbitrarily large. When considering SCFTs Higgsable to the D-type (2, 0) SCFTs with small N , there are more options available.

For an SCFT $D_N^{\mathfrak{su}_{2k}}$ with $N \geq 2k+1$, then for each nilpotent orbit O of $\mathfrak{su}(2k)$ there exists a unique child theory associated with O , and the set of interacting non-product fixed points on the Higgs branch of $D_N^{\mathfrak{su}_{2k}}$ is saturated by the set of theories $D_N^{\mathfrak{su}_{2\ell}}(O)$, for all $\ell \leq k$ and O a nilpotent orbit of $\mathfrak{su}(2\ell)$. We refer to this as the “long quiver” case. In contrast, for short quivers, there may be no child SCFTs associated with particular nilpotent orbits, and there may be interacting nonproduct fixed points on the Higgs branch which are not of the form $D_N^{\mathfrak{su}_{2\ell}}(O)$. Let O be a nilpotent orbit of $\mathfrak{su}(2k)$ associated with a partition

$$P = [p_1, \dots], \quad (2.22)$$

of $2k$, written in weakly decreasing order. It is straightforward to see that the SCFT $D_N^{\mathfrak{su}_{2k}}(O)$ is well-defined when

$$p_1 \leq N-1. \quad (2.23)$$

One can also check that the anomaly polynomial of the $D_N^{\mathfrak{su}_{2k}}(O)$ SCFT is exactly what one would expect from the nilpotent Higgsing of the moment map operator for the $\mathfrak{su}(2k)$ flavor symmetry, as in [44]. Therefore, the first speciality of short quivers is that nilpotent orbits where the partition contains an element $> N-1$ do not exist.

If $N < 2k+1$, then the interacting fixed points on the Higgs branch of $D_N^{\mathfrak{su}_{2k}}$ can be captured by $D_N^{\mathfrak{su}_{2\ell}}(O)$ where

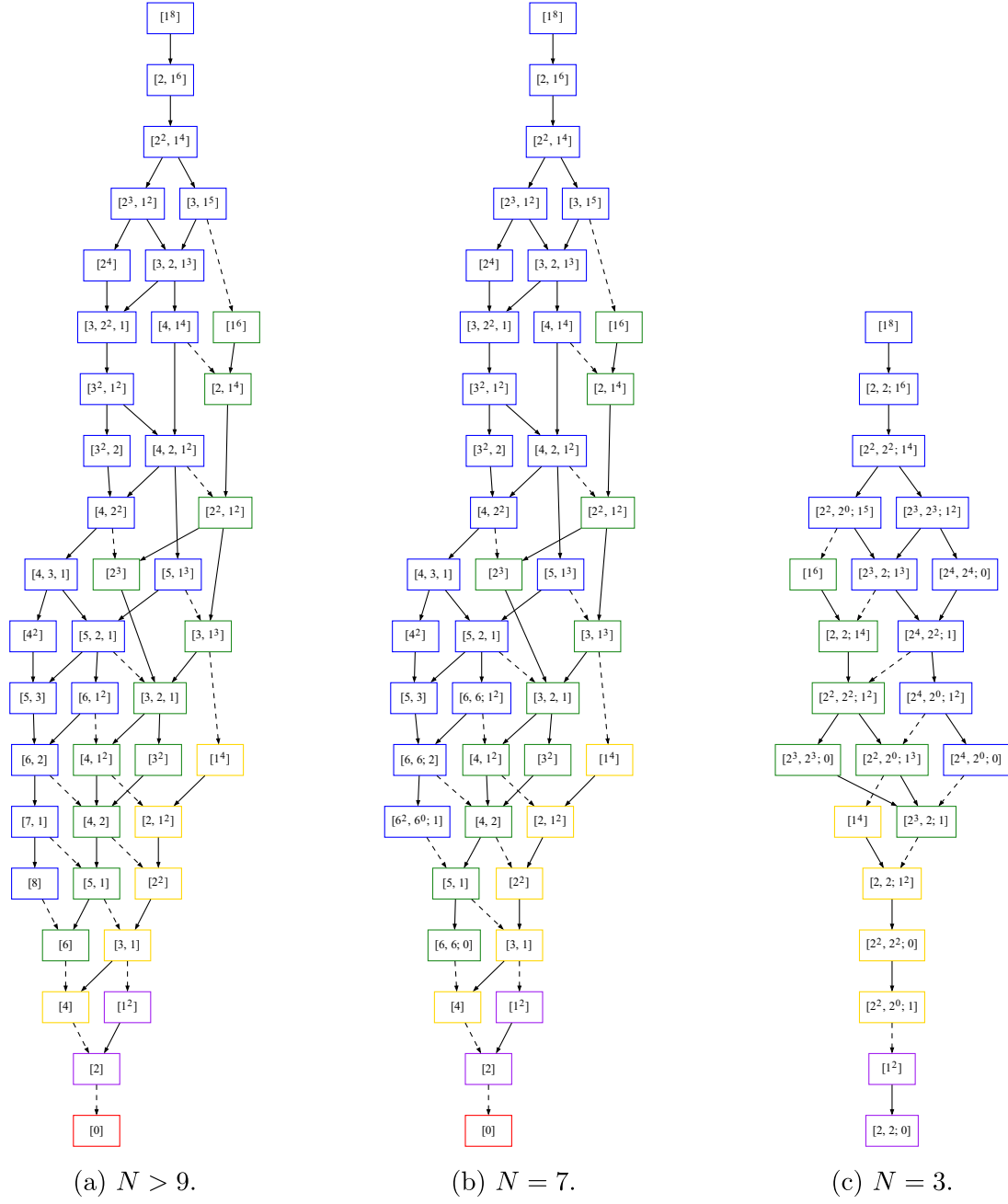


FIG. 1. We depict the Hasse diagram of the theories $D_N^{\text{stu} \leq 8}(O)$ under the partial ordering given in Eq. (2.10). In (a), we assume that $N > 9$. We label each vertex by O , which we write as an integer partition of 2ℓ . Vertices bordered in blue, green, yellow, purple, and red denote $\ell = 4, 3, 2, 1$, and 0 , respectively; dashed edges indicate a change in ℓ . We use $[0]$ for convenience to denote the 6D $(2, 0)$ SCFT of type D_N . In (b) and (c), we depict the Hasse diagrams when $N = 7$ and $N = 3$, respectively, where the labels are instead given by generalized partitions.

$\ell \leq k$ and O is a generalized partition. A generalized partition of 2ℓ is either an integer partition of 2ℓ such no element is larger than $N - 2$,

or else it can be written as

$$[(N-1)^{m_{N-1}^L}, (N-1)^{m_{N-1}^R}; (N-2)^{m_{N-2}}, \dots, 1^{m_1}]. \quad (2.25)$$

$$[(N-2)^{m_{N-2}}, \dots, 1^{m_1}] \quad \text{such that} \quad \sum_{i=1}^{N-2} im_i = 2\ell, \quad (2.24)$$

Here, the exponents are non-negative integers such that there exist non-negative integers $k_i, k_{N-1}^{L,R}$ satisfying,

$$\begin{aligned}
k_{N-1}^L &= \ell, \\
2k_{N-1}^L - k_{N-2} - m_{N-1}^L &= 0, \\
2k_{N-1}^R - k_{N-2} - m_{N-1}^R &= 0, \\
2k_{N-2} - k_{N-1}^L - k_{N-1}^R - k_{N-3} - m_{N-2} &= 0, \\
2k_{N-3} - k_{N-2} - k_{N-4} - m_{N-3} &= 0, \\
&\dots, \\
2k_1 - k_2 - m_1 &= 0,
\end{aligned} \tag{2.26}$$

where we have assumed, without loss of generality, that $m_{N-1}^L \geq m_{N-1}^R$ and $m_{N-1}^L \neq 0$. For the generalized partition written in Eq. (2.24), the description of the associated tensor branch is straightforward, and is written in [44]; in particular, it is treated as a regular partition of 2ℓ . For a generalized partition of the form in Eq. (2.25), the curve configuration follows from the solutions to Eq. (2.26); it is

$$\begin{array}{ccccccc} & & \mathfrak{su}_{N-1}^R & & & & \\ & & 2 & & & & \\ \mathfrak{su}_{N-1}^L & & & \mathfrak{su}_{N-2} & & \mathfrak{su}_{k_1} & \\ 2 & & 2 & \dots & 2 & & \end{array} \quad (2.27)$$

There are simple rules for determining the partial ordering on these generalized partitions, similar in style to those given in [49], however, we do not go into details here as, case-by-case, it is straightforward to determine the partial ordering using Eq. (2.10). To give the reader a clear picture of the generalized partitions, we have included in Fig. 1 the Hasse diagram of interacting fixed points on the Higgs branch of $D_N^{\mathfrak{su}_8}$ for $N = 3, 7$. They are of the form $D_N^{\mathfrak{su}_{2\ell}}(O)$ where $\ell \leq 4$ and O is a generalized partition.¹⁵

The structure of the generalized partition in Eq. (2.25) is particularly natural when considering type IIA brane engineering with ON^- -planes, as we shall see in Sec. III.

B. Higgsable to E-type (2, 0)

We now turn to those 6D (1, 0) SCFTs that have SUSY-enhancing Higgs branch renormalization group flows to the 6D (2, 0) SCFTs of exceptional type. In fact, there is not a lot of variety in such 6D (1, 0) SCFTs. There are three infinite families which are associated with the configurations

¹⁵The observant reader may notice that there is no $[0]$ at the bottom of Fig. 1(c). This is special for $N = 3$ and is related to the fact that $D_3^{\mathfrak{su}_2}([1^2])$ has enhanced $\mathfrak{su}(3)$ flavor symmetry [43], instead of $\mathfrak{su}(2)$.

$$\begin{array}{c}
\mathfrak{su}_{k_6} \\
2 \\
\mathfrak{su}_{k_1} \mathfrak{su}_{k_2} \mathfrak{su}_{k_3} \mathfrak{su}_{k_4} \mathfrak{su}_{k_5} , \quad \mathfrak{su}_{k_1} \mathfrak{su}_{k_2} \mathfrak{su}_{k_3} \mathfrak{su}_{k_4} \mathfrak{su}_{k_5} \mathfrak{su}_{k_6} , \\
2 \quad 2 \quad 2 \quad 2 \quad 2 \quad , \quad 2 \quad 2 \quad 2 \quad 2 \quad 2 \quad 2 \quad , \\
\mathfrak{su}_{k_8} \\
2 \\
\mathfrak{su}_{k_1} \mathfrak{su}_{k_2} \mathfrak{su}_{k_3} \mathfrak{su}_{k_4} \mathfrak{su}_{k_5} \mathfrak{su}_{k_6} \mathfrak{su}_{k_7} \\
2 \quad 2 \quad 2 \quad 2 \quad 2 \quad 2 \quad 2 \quad ,
\end{array} \quad (2.28)$$

which have SUSY-enhancing flows to the 6D (2, 0) SCFTs of type E_6 , E_7 , and E_8 , respectively. We refer to the SCFTs associated with these tensor branch curve configurations as

$$E_N(k_1, \dots, k_N), \quad (2.29)$$

for each of $N = 6, 7, 8$. As in the Higgsable to D-type case, most of the tuples (k_1, \dots, k_N) need to be discarded since they give rise to gauge-anomalous theories; only those obeying the E-type analog of Eq. (2.6), i.e., where the Cartan matrix is the E_N Cartan matrix, realize physical 6D $(1, 0)$ SCFTs.

For each of these theories, it is straightforward to determine the dimension of the Higgs branch using the standard anomaly polynomial machinery, just as we did for the $D_N^{\hat{\mathfrak{su}}_{2k}}(O)$ SCFTs in Sec. II A. We find that the dimension of the Higgs branch of $E_N(k_1, \dots, k_N)$ is

$$\dim(\mathcal{H}) = N + \frac{1}{2} \sum_{i,j=1}^N A^{ij} k_i k_j, \quad (2.30)$$

where A^{ij} is the positive-definite Cartan matrix of E_N . Note that this expression holds for all $k_i \geq 0$ satisfying the E-type analog of Eq. (2.6).

For the families in Eq. (2.29), the presence of a Higgs branch renormalization group flow between two theories is particularly straightforward. If

$$(k'_1, \dots, k'_N) < (k_1, \dots, k_N), \quad (2.31)$$

applied element-by-element,¹⁶ then there exists a flow between the SCFTs,

$$E_N(k_1, \dots, k_N) \rightarrow E_N(k'_1, \dots, k'_N). \quad (2.32)$$

We have depicted a part of the Hasse diagram, under the partial ordering defined in Eq. (2.31), of consistent SCFTs of this form with $N = 6$ in Fig. 2. We further analyze the types of elementary transition in this Hasse diagram in Sec. VII.

In addition to these standard families of 6D (1, 0) SCFTs that have supersymmetry-enhancing RG flows to the 6D (2, 0) SCFTs of type $E_{6,7,8}$, there are a small number of exceptional curve configurations that also realize such

¹⁶I.e., if $k'_i \leq k_i$ for all $i = 1, \dots, N$, excepting the trivial case where the inequality is saturated for all i .

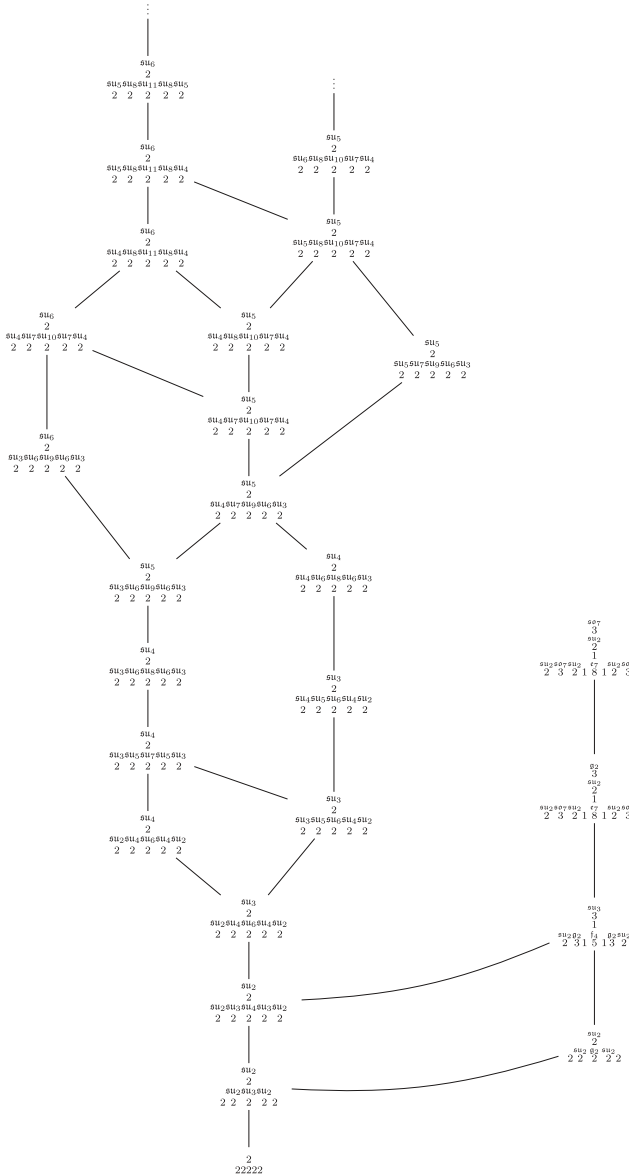


FIG. 2. The Hasse diagram of the 6D (1, 0) SCFTs that have SUSY-enhancing Higgs branch RG flows to the 6D (2, 0) SCFT of type E_6 . For symmetric configurations, we have depicted only one rather than both.

flows. When considering the E_6 theory, there are four such exceptional curve configurations, which are

[illegible]

TABLE I. Spacetime brane extension in type IIA string theory for D-type quivers.

	x^0	x^1	x^2	x^3	x^4	x^5	x^6	x^7	x^8	x^9
D6	X	X	X	X	X	X	X	.	.	.
NS5	X	X	X	X	X	X
D8	X	X	X	X	X	X	.	X	X	X
ON ⁻	X	X	X	X	X	X

We have incorporated the SCFTs associated with these curve configurations into the Hasse diagram that we have drawn in Fig. 2.¹⁷ For the E_7 theory, there is only a single exceptional configuration,

$$\begin{array}{ccccccc} & & \mathfrak{s} u_3 & & & & \\ & & 3 & & & & \\ & & 1 & & & & \\ \mathfrak{s} u_2 & \mathfrak{q}_2 & \mathfrak{f}_4 & \mathfrak{q}_2 & \mathfrak{s} u_2 & & \\ 2 & 2 & 3 & 1 & 5 & 13 & 2 . \end{array} \quad (2.34)$$

There are no exceptional curve configurations which have Higgs branch RG flows to the 6D (2, 0) SCFT of type E_8 since every putative base fibration would be too singular to admit a crepant resolution and therefore fails to construct a consistent Calabi-Yau threefold on which to compactify F-theory [11].

III. MAGNETIC QUIVER FOR THE $D_N^{\text{su}2k}(\mathcal{O})$ SCFTS

Now that we have enumerated the 6D (1, 0) SCFTs that have supersymmetry-enhancing renormalization group flows to the 6D (2, 0) SCFTs of DE-type, we would like to analyze the structure of the Higgs branch of these SCFTs. Conveniently, the $D_N^{\text{su}_{2k}}(\mathcal{O})$ theories can be obtained via a brane construction in type IIA string theory. This allows us to obtain a magnetic quiver for the Higgs branch of $D_N^{\text{su}_{2k}}(\mathcal{O})$, and we can then study the structure of the Higgs branch using techniques from the study of the Coulomb branch of 3D $\mathcal{N} = 4$ Lagrangian theories. This approach will provide nontrivial insights into the Higgs branch renormalization group flows which can then be generalized to the $E_N(k_1, \dots, k_N)$ SCFTs that do not have such a brane construction.

A. The electric type IIA description

A construction in type IIA string theory for D-type quiver theories has been long known [40]. The ingredients are the usual D6-D8-NS5-branes that engineer six-dimensional theories, together with a Neveu-Schwarz orientifold plane; ON^- . These are arranged in the ten-dimensional spacetime as depicted in Table I. This provides us with a mechanism to

¹⁷It is interesting to note that, when Higgsing from these exceptional configurations to the $E_N(k_1, \dots, k_6)$ configurations, not only do the ranks of several algebras get reduced simultaneously but also a sequence of curves are shrunk. This behavior has been appreciated in previous works, such as [54,55].

engineer the 6D SQFTs that are the effective field theory living on the generic point of the tensor branch of the SCFTs of interest.

To understand the gauge theories engineered on the brane world volume, it is useful to pass to the T-dual type IIB description [40]. Of primary importance is the counterpart of the Neveu-Schwarz orientifold plane. This plane, characterized by a negative NS5-charge, is inevitably paired with an NS5-brane to create an uncharged object. Consequently, its type IIB dual is an $O5^-$ -plane paired with a D5-brane, such that the total Ramond-Ramond charge is vanishing. The worldvolume of this combined $O5^-$ -plane plus D5-brane carries an $SO(2)$ gauge theory, and D3-branes ending on this combined object can have one of two possible boundary conditions. Different stacks with different boundary conditions lead to the characteristic bifurcation in the D-type Dynkin diagram. The analogous picture for D6-branes ending on the combined ON^- -plane and paired NS5-brane explains the bifurcation in the 6D tensor branch description.

Focusing on the type IIA engineering, the ON^- orientifold plane can interplay with D8-branes to construct bound states [56]. In fact, binding D8-branes to the ON^- -plane (this case will be drawn as D8-branes between the ON^- and its paired NS5-brane) provides a flavor symmetry factor only in one direction of the bifurcation. Differently, inserting D8-branes between the NS5-brane paired to the ON^- and the adjacent NS5-brane, the heavy branes act as a source of flavor symmetry on both branches of the bifurcation. Both these possibilities are shown in Fig. 3, where for the sake of a more intuitive flavor assignment, we drew the NS5-brane that lives on top of the ON^- -plane as displaced from it and connected to D6 branes wrapping around the orientifold plane, so that the \mathbb{Z}_2 symmetry of the quiver's shape is broken.

Hence, it is straightforward to write down the brane construction for $D_N^{\mathfrak{su}_{2k}}$. It is realized as follows. Consider a linear chain of N NS5-branes, with an ON^- on the left. In the rightmost interval between NS5-branes, we place a stack of $2k$ D8-branes. This configuration is depicted in

Fig. 4(a). The generalization to $D_N^{\mathfrak{su}_{2k}}(O)$, where O is a partition of $2k$ with no element larger than $N - 2$, is also clear; there are instead m_i D8-branes in the interval between the i th and $(i + 1)$ th NS5-branes. Since $m_i = 0$ for $i \geq N - 1$, the D8-branes do not lie in an interval that affect the number of D6-branes in the bifurcation. We show this schematically in Fig. 4(b).

Finally, it remains for us to write down the brane configuration associated with $D_N^{\mathfrak{su}_{2k}}(O)$ where O is a generalized partition given in the form written in Eq. (2.25). Again, there are N NS5-branes arranged in a linear chain, together with the ON^- -plane to the left of the left-most NS5-brane. Between the i th and $(i + 1)$ th NS5-branes, counting from the right, for $i = 1, \dots, N - 2$, there are m_i D8-branes, where m_i is as defined in Eq. (2.25). Furthermore, we define the following two integers:

$$h = \frac{|m_{N-1}^L - m_{N-1}^R|}{2}, \quad s = \min(m_{N-1}^L, m_{N-1}^R). \quad (3.1)$$

From Eq. (2.26), we can see that h is always an integer. In the brane configuration, we have s D8-branes between the $(N - 1)$ th and the N th NS5-branes, and h D8-branes between the N th NS5-brane and the ON^- -plane. The number of D6-branes in each interval is fixed by the anomaly cancellation condition in Eq. (2.26), and this is analogous to setting the number of D6-branes ending on the left and on the right of an NS5-brane via the type IIA cosmological constant whilst taking into account the presence of D8-branes [33,57]. We have depicted this brane system in Fig. 4(c).

While we have given a prescription to associate a brane description to a generalized partition, it remains for us to motivate the connection to Higgsing. Each D6-brane ends on a D8-brane that can be consider as brought in from infinity on the right. The generalized partition then specifies which D6-brane emanating from which NS5-branes end on which D8-branes. The generalized nature of the partition is necessary as the D6-branes coming out of the two left-most NS5-branes are paired due

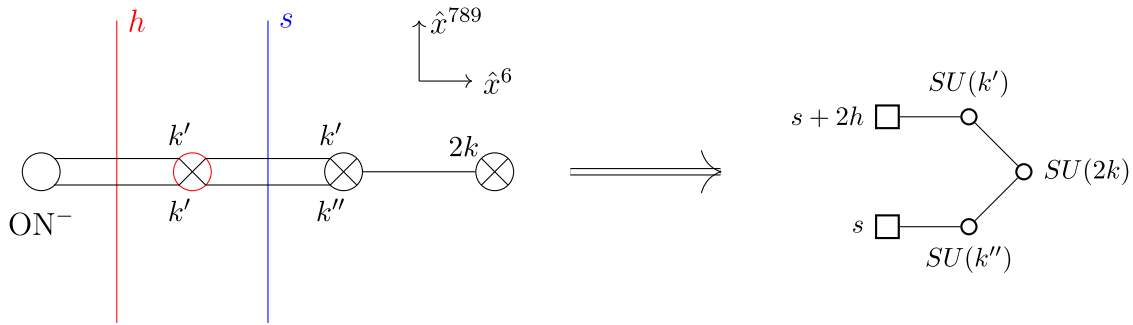


FIG. 3. Quiver obtained by placing D8-branes between the ON^- -plane and its paired NS5-brane (in red) and between the paired NS5-brane and NS5-brane to the right (in blue). We use the standard convention, throughout this paper, of depicting NS5-branes with crossed circles, D6-branes as horizontal lines, and D8-branes as vertical lines.

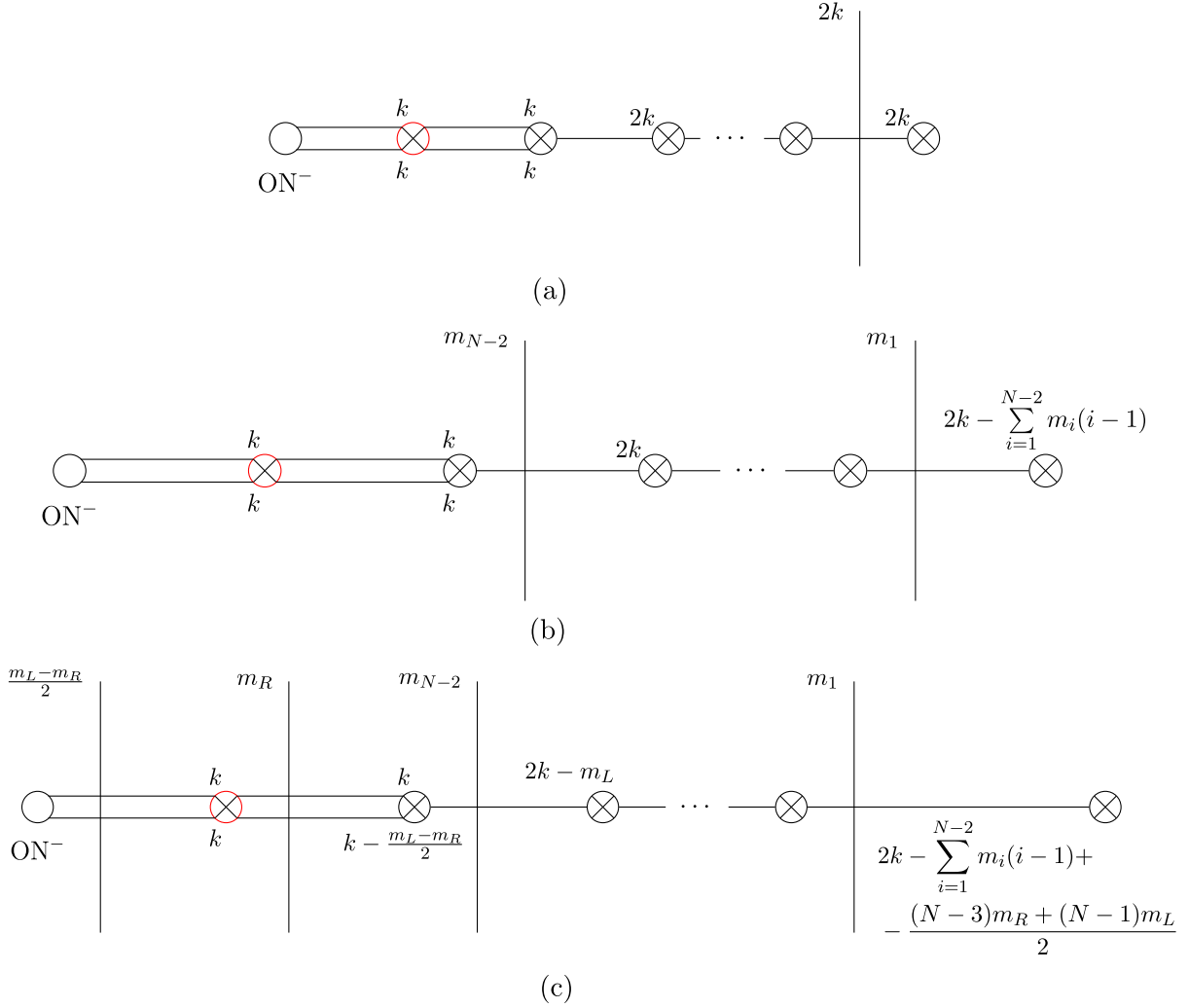


FIG. 4. Type IIA brane configuration engineering the effective field theory on the tensor branch of the $D_N^{\mathfrak{su}_{2k}}(O)$ SCFTs. The number of D6-branes between each pair of NS5-branes, when not written, can be determined from the anomaly cancellation conditions. (a) $D_N^{\mathfrak{su}_{2k}}$. (b) $D_N^{\mathfrak{su}_{2k}}(O)$ where O is a partition of $2k$ with no element larger than $N - 2$. (c) $D_N^{\mathfrak{su}_{2k}}(O)$ where O is a generalized partition of $2k$ of the form in equation (2.25), under the general assumption $m_L \geq m_R$.

to the ON^- . Hanany-Witten transitions can then be transformed to pull all of the D8-branes into the intervals between the necessary pair of NS5-branes, leading to the configurations that we have described in Fig. 4. We have depicted the configurations before and after the Hanany-Witten transitions for an example generalized partition in Fig. 5.

B. Magnetic quivers at finite coupling

The realization via a brane description for the electric phase of the theories $D_N^{\mathfrak{su}_{2k}}(O)$ is significant because it allows us to gain insights into the properties of the Higgs branch of these theories by transitioning to the magnetic phase. This approach has been partially explored in previous works such as [40,56,58–60]. By studying the

brane configurations in the magnetic phase, we can obtain valuable information about the behavior and characteristics of the Higgs branch in the corresponding electric phase. This provides a powerful tool for understanding the dynamics and properties of these six-dimensional theories from a three-dimensional perspective.

The general procedure for transitioning from an electric brane system to a magnetic one in a type IIA D6-D8-NS5 configuration involves two stages. In the first stage, D8-branes are pulled from infinity and used to suspend between them the available D6-branes. In the second stage, the NS5-branes located in the segment between the ON^- -plane and the first (counting from the left) D8-brane are put at different positions on the x^6 axis. The result of the process is illustrated in Fig. 6 for the $D_N^{\mathfrak{su}_{2k}}(O)$ theory,

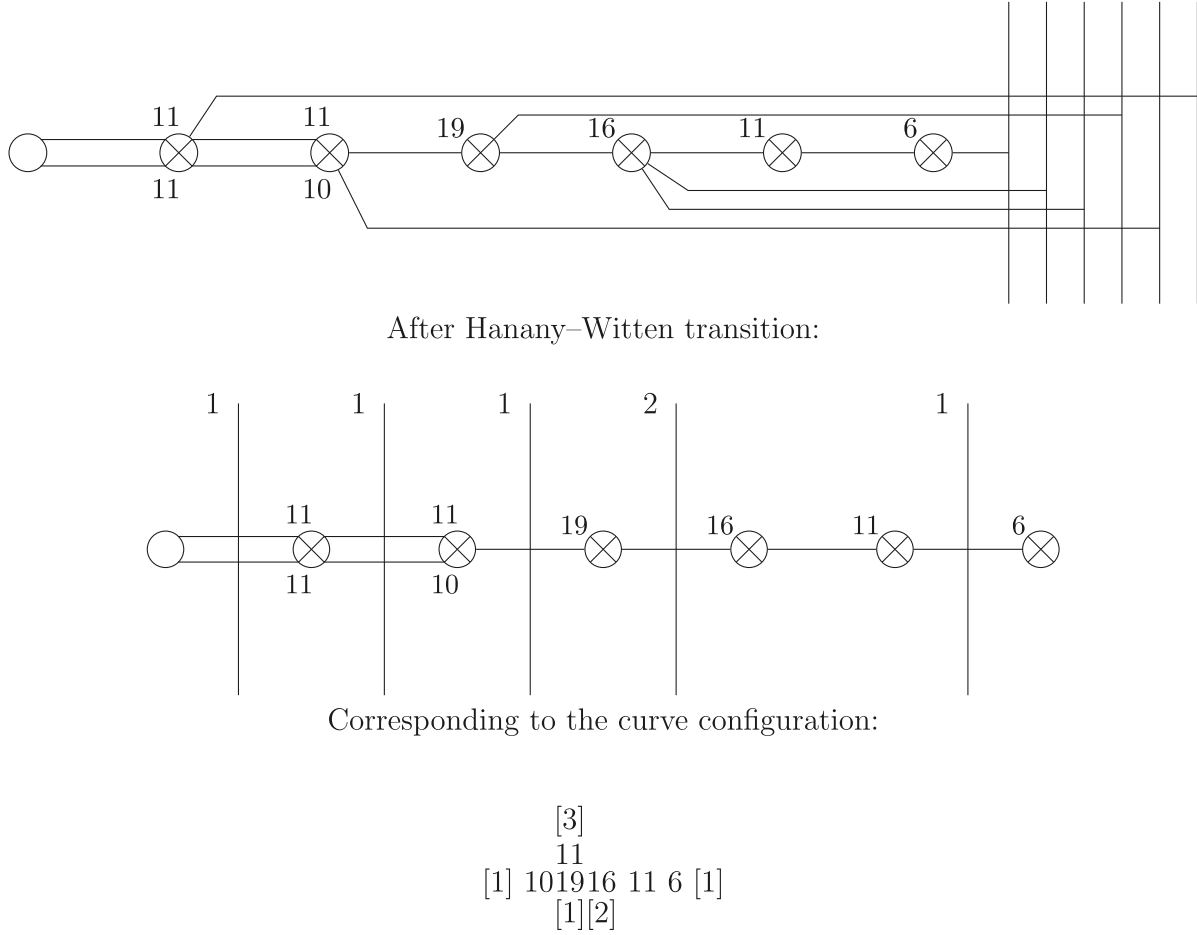


FIG. 5. Type IIA brane configuration associated with the tensor branch of $D_6^{\mathfrak{su}_{22}}(O)$ where the generalized partition of 22 is given by $O = [5^3, 5; 4, 3^2, 1]$. We show the configurations before and after having performed Hanany-Witten transitions to bring the D8-branes from infinity into their respective interval. At the bottom, we depict the corresponding curve configuration.

where O is the nilpotent orbit corresponding to the partition $[1^{2k}]$.

In the brane configuration, be it electric or magnetic, the distance in the x^6 direction between adjacent NS5-branes determines the gauge couplings of the corresponding gauge nodes and, consequently, the volumes of the associated curves in the F-theory description. Similarly, the x^6 -distance between the ON^- -plane and the leftmost NS5-brane determines the gauge coupling of one of the

nodes in the fork. By separating the NS5-branes from the ON^- -plane and the leftmost D6-brane in space, a finite coupling six-dimensional $\mathcal{N} = (1, 0)$ theory is realized. This is then the magnetic description of the $(1, 0)$ SQFT that exists at the generic point of the tensor branch. For the SCFT to emerge no scales can be present, otherwise, conformality would be ruined, and thus all the curves have to be shrunk to zero volume; equivalently, all gauge couplings must be taken to infinity. It is a special feature of the magnetic phase that this infinite-coupling limit can be taken in a controlled manner, and thus information about the SCFT itself is obtained, see Sec. III C.

The rules to read a magnetic quiver from the associated brane system are given in [34,35,60]; a stack of k D6-branes contributes as a $\mathfrak{u}(k)$ gauge node whereas a stack of n NS5-branes is responsible for a $\mathfrak{u}(n)$ node together with an adjoint hypermultiplet, the ON^- -plane is responsible for the projection $\mathfrak{u}(2k) \rightarrow \mathfrak{usp}(2k)$ associated with D6-branes crossing it and $\mathfrak{u}(n) + \text{adjoint} \rightarrow \mathfrak{so}(2n) + \text{antisymmetric}$ associated with a stack of k NS5-branes on top of the orientifold.

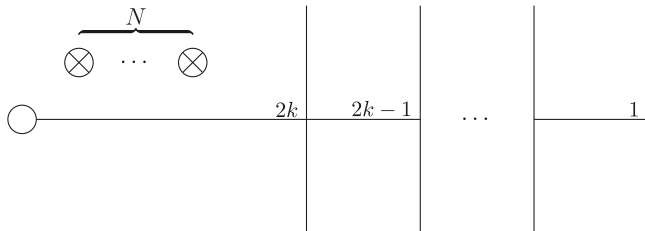


FIG. 6. Magnetic brane system for the tensor branch of the $D_N^{\mathfrak{su}_{2k}}([1^{2k}])$ SCFT.

The characteristic of this finite coupling magnetic quiver is the presence of a bouquet of $\mathfrak{u}(1) = \mathfrak{so}(2)$ nodes coming from the spatially separated NS5-branes. To illustrate this with an example, the magnetic quiver for the tensor branch SQFT of $D_N^{\mathfrak{su}_{2k}}$ is

$$\mathcal{Q}_{fin} = \begin{array}{c} \overbrace{\begin{array}{ccc} 1 & \cdots & 1 \end{array}}^{N \text{ nodes}} \\ \diagdown \quad \diagup \\ \bullet \\ \diagup \quad \diagdown \\ \begin{array}{ccccccc} 2k & 2k-1 & 2k-2 & \cdots & 2 & 1 \end{array} \end{array} \quad (3.2)$$

The $\mathfrak{usp}(2k)$ node has been drawn as a filled blue circle following the conventions of [60] whilst $\mathfrak{u}(1)$ s in the bouquet have been drawn as an empty red circle anticipating the fact that when the NS5-branes are put on top of the ON^- -plane they give rise to an \mathfrak{so} gauge node that, according to the aforementioned conventions, is drawn as a filled red circle.

In this way, a 3D $\mathcal{N} = 4$ quiver gauge theory can be obtained for each $D_N^{\mathfrak{su}_{2k}}(O)$, where O is an arbitrary generalized partition. This is a magnetic quiver for the Higgs branch of the SQFT living at the generic point of the tensor branch of the associated SCFT. In Sec. III C, we discuss the extension required to understand the Higgs branch of the SCFT at the origin of the tensor branch; however, we can already answer questions about the operators belonging to the Higgs branch of the tensor branch SQFT from this magnetic quiver perspective.

One of the most immediate pieces of information that can be extracted from a magnetic quiver is the global symmetry, to wit, the presence of 1/2-BPS moment map operators in the Higgs branch chiral ring. Of course, this can be directly determined by computing the leading order terms in the (refined) Coulomb branch Hilbert series of the magnetic quiver. Instead, a balance algorithm was introduced in [34] which allows for a straightforward identification of the global symmetry in certain cases. In many of our cases, the balance algorithm only provides a subset of the full global symmetry [61], and more refined computations are necessary. We compute the global symmetry and determine the Coulomb branch Hilbert series for several explicit examples in Sec. IV.

C. Magnetic quivers at infinite coupling

In six dimensions, the Higgs branch can be thought of as the fibers of a fibration over the tensor branch of a given theory [58]. Over the generic point of the tensor branch, the fiber is simply the Coulomb branch of the finite-coupling magnetic quiver discussed in Sec. III B. Moving around on the tensor branch corresponds to adjusting the various distances in the x^6 direction between the

NS5-branes. Special subloci of the tensor branch occur when some number of these distance moduli are taken to zero; typically the fiber, and thus the Higgs branch, is modified along these subloci as some tensionful strings become tensionless. These are referred to as the phases of the theory.

In addition to the finite-coupling phase associated with the generic point of the tensor branch, two interesting phases are the “discretely-gauged” phase and the “infinite-coupling” phase. The former occurs when the distances between all of the N NS5-branes are taken to zero, but the distance between this NS5-brane stack and the ON^- -plane is nonzero. The infinite-coupling phase occurs when all NS5-branes are atop the ON^- -plane; in this latter configuration all of the scales have been removed from the theory and we are at the origin of the tensor branch where the SCFT is located.

The discretely-gauged phase is so-named due to the observation of the phenomenon of discrete gauging as described in [58,62–65] along this subloci of the tensor branch. The magnetic quiver for the Higgs branch in this phase, \mathcal{Q}_{dg} , is related to \mathcal{Q}_{fin} by a discrete gauging of the \mathfrak{S}_N symmetry that permutes the $\mathfrak{u}(1)$ nodes of the bouquet. This replaces the bouquet with a $\mathfrak{u}(N)$ gauge node together with an adjoint hypermultiplet. At the level of the Hilbert series, the discrete-gauging action is rephrased in the following identity:

$$HS(\mathcal{Q}_{dg}) = HS(\mathcal{Q}_{fin})/\mathfrak{S}_N. \quad (3.3)$$

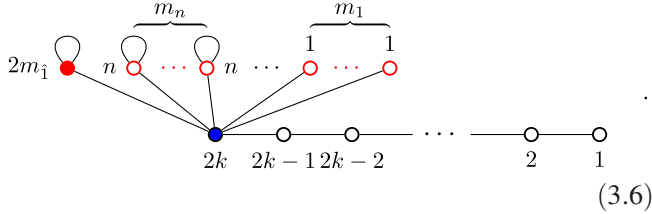
When tuning the x^6 moduli to reach the infinite-coupling phase, a new phenomenon is found that results in a \mathbb{Z}_2 projection of the discretely gauged phase. As a result of the orientifold projection rules mentioned before, the $\mathfrak{u}(N)$ gauge algebra coming from the discrete gauging of the permutation symmetry on the N NS5-branes, and similarly, the coupled adjoint hypermultiplet, are projected onto an $\mathfrak{so}(2N)$ gauge algebra paired with a matter hypermultiplet in the rank two antisymmetric representation. Therefore, the SCFT $D_N^{\mathfrak{su}_{2k}}$ has the following magnetic quiver for the Higgs branch:

$$\mathcal{Q}_{\infty} = \begin{array}{c} \begin{array}{c} \text{loop} \\ \bullet \\ 2N \end{array} \\ \diagdown \quad \diagup \\ \begin{array}{ccccccc} 2k & 2k-1 & 2k-2 & \cdots & 2 & 1 \end{array} \end{array} \quad (3.4)$$

The Coulomb branch Hilbert series of \mathcal{Q}_{∞} , which counts the 1/2-BPS operators belonging to the Higgs branch chiral ring of the 6D SCFT, is related to the Hilbert series of the aforementioned discretely-gauged phase as

$$HS(\mathcal{Q}_\infty) = HS(\mathcal{Q}_{dg})/\mathbb{Z}_2. \quad (3.5)$$

For completeness, we now write the magnetic quiver for the Higgs branch of an arbitrary phase of the SCFT $D_N^{\mathfrak{su}_{2k}}$. The N NS5-branes can be arranged in stacks. Let m_i denote the number of NS5-brane stacks containing i branes, which are not sitting on top of the ON^- . We also assume that there are m_1 NS5-branes on top of the ON^- . In this generic phase, the magnetic quiver for the Higgs branch takes the following form:



$$(3.6)$$

While we have only discussed the $D_N^{\mathfrak{su}_{2k}}$ theories explicitly in this section, the same considerations about phases, discrete gauging, and \mathbb{Z}_2 quotients apply for every theory $D_N^{\mathfrak{su}_{2k}}(O)$ where O is a generalized partition. In particular, we can determine the infinite coupling magnetic quiver in each case, which provides the Higgs branch for each SCFT $D_N^{\mathfrak{su}_{2k}}(O)$.

IV. EXPOLITING THE $A_3 \cong D_3$ ISOMORPHISM

In the previous section, we determined the magnetic quiver for the Higgs branch of the $D_N^{\mathfrak{su}_{2k}}(O)$ SCFTs from the brane engineering of the theory in type IIA string theory. In fact, we have determined the magnetic quiver for the Higgs branch emanating from each sublocus of the tensor branch, not just for the SCFT at the origin. Generically, this is a unitary-orthosymplectic quiver; however, when $N = 3$ we can use the isomorphism between $\mathfrak{so}(6)$ and $\mathfrak{su}(4)$ to write a dual unitary quiver. In this section, we briefly use this isomorphism to provide a cross-check on the unitary-orthosymplectic quivers that we have derived.

At the generic point of the tensor branch, the SCFT $D_3^{\mathfrak{su}_{2k}}$ is described via the curve configuration,

$$\begin{array}{c} \mathfrak{su}_k \\ 2 \\ \mathfrak{su}_k \quad \mathfrak{su}_{2k} \\ 2 \quad 2 \quad [\mathfrak{su}_{2k}]. \end{array} \quad (4.1)$$

Rearranging, we can write this curve configuration as

$$\begin{array}{c} \mathfrak{su}_k \quad \mathfrak{su}_{2k} \quad \mathfrak{su}_k \\ 2 \quad 2 \quad 2, \\ [\mathfrak{su}_{2k}] \end{array} \quad (4.2)$$

which is nothing other than the description at the generic point of the tensor branch of rank four ($\mathfrak{su}(2k), \mathfrak{su}(2k)$)

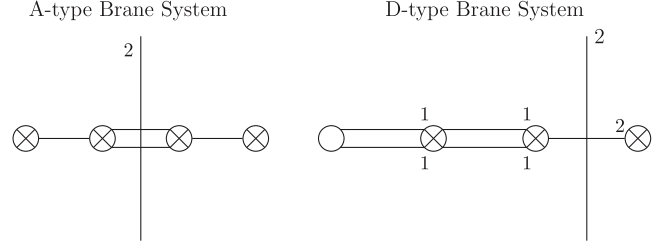


FIG. 7. Two different type IIA brane systems engineering the $\mathfrak{su}_{2k} 2 \ 2 \ 2$ theory at the generic point of the tensor branch.

conformal matter, Higgsed on both the left and the right by the nilpotent orbit associated with the partition $[2^k]$. We refer to this theory as $A_3^{\mathfrak{su}_{2k}}([2^k], [2^k])$. The type IIA brane engineering of this latter theory, and thus the magnetic quiver for the Higgs branch, was studied in [64], where it arises through D6-NS5-D8-branes; however, without the presence of any ON^- -plane.

We consider only the case of $k = 1$; this is sufficient to demonstrate the subtleties of the various phases,¹⁸ and is particularly interesting as the structure of the non-Abelian flavor symmetry is special [11,22,43,45]. That is, we wish to compare the magnetic quivers of

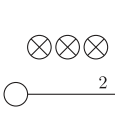
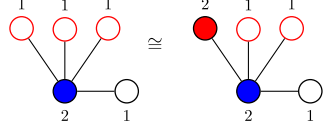
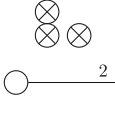
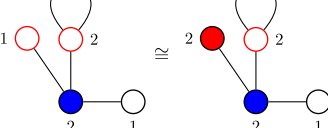
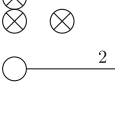
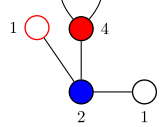
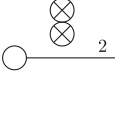
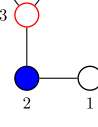
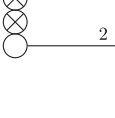
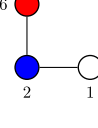
$$\begin{array}{c} \mathfrak{su}_{2k} \\ 2 \ 2 \ 2 \\ [\mathfrak{su}_3] \end{array} \quad \text{and} \quad \begin{array}{c} 2 \\ 2 \ 2 \ [\mathfrak{su}_3], \end{array} \quad (4.3)$$

where we can already see that the flavor symmetry is enhanced from the naive $\mathfrak{su}(2)$ to an $\mathfrak{su}(3)$. The two different type IIA brane systems engineering these theories, at the generic point of the tensor branch, are depicted in Fig. 7. Using the A_3 -type brane description, we have determined the magnetic quivers for each phase, and furthermore, we have determined the Coulomb branch Hilbert series using the standard methods [37]. These quivers and their Coulomb branch Hilbert series appeared already in previous studies [64].

We can then perform the same analysis for the phases of the D_3 -type brane description. *A priori*, there appear to be seven phases, as opposed to five, however, there is a redundancy in the D_3 -type brane description; if only a single NS5-brane is placed on top of the ON^- -plane, then the resulting quiver is the same as if that NS5-brane was placed elsewhere. Removing this redundancy, we find the five phases listed in Table II. Again, we can compute the Coulomb symmetry of the resulting magnetic quivers and their Coulomb branch Hilbert series; these quantities precisely match those from the unitary magnetic quivers listed in Table III.

¹⁸For the generic case the phase structure is identical.

TABLE II. The D-type construction of the phases of the SCFT associated with the tensor branch configuration $2 \ 2 \ 2$, arising from D6-NS5-D8-branes together with the ON^- -plane in type IIA. We list the magnetic quiver for each phase and determine the Coulomb symmetry and the Coulomb branch Hilbert series.

Brane system	Magnetic quiver	Global symmetry	Coulomb branch Hilbert series
		$\mathfrak{su}(8)$	$\frac{(t^2+1)(t^8+17t^6+48t^4+17t^2+1)}{(1-t^2)^{10}}$
		$\mathfrak{su}(7)$	$\frac{(t^2+1)(t^8+10t^6+20t^4+10t^2+1)}{(1-t^2)^{10}}$
		$\mathfrak{su}(4)$	$\frac{t^{20}+10t^{18}+55t^{16}+150t^{14}+288t^{12}+336t^{10}+288t^8+150t^6+55t^4+10t^2+1}{(1-t^2)^{10}(t^2+1)^5}$
		\mathfrak{g}_2	$\frac{(t^2+1)(t^8+3t^6+6t^4+3t^2+1)}{(1-t^2)^{10}}$
		$\mathfrak{su}(3)$	$\frac{t^{20}+3t^{18}+13t^{16}+25t^{14}+46t^{12}+48t^{10}+46t^8+25t^6+13t^4+3t^2+1}{(1-t^2)^5(1-t^4)^5}$

V. HIGGS BRANCH RG FLOW FOR THE $D_N^{\mathfrak{su}_{2k}}(O)$ SCFTS


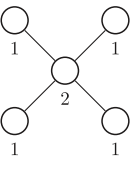

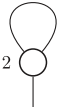
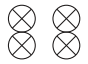
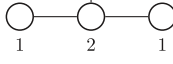
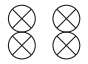
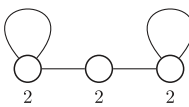
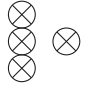
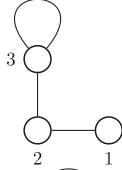


The Coulomb branches of the magnetic quivers that we have just determined are isomorphic to the Higgs branches of the 6D (1, 0) SCFTs that we are interested in. However, we have not yet answered any of the questions posed in Sec. I about the Higgs branch, except in the abstract. We would now like to explore how to extract some of these properties from the magnetic quivers. For example, to understand the operators/generators/relations of the Higgs branch chiral ring, we can use the monopole formula to compute the Coulomb branch Hilbert series of the magnetic quiver. In this section, we utilize the magnetic quiver to enumerate the interacting SCFT fixed points that arise on

different subloci of the Higgs branch and provide some understanding of the operators which trigger the RG flow between a pair of theories on nested subloci.

A. Quiver subtraction for unitary-orthosymplectic quivers

The quiver subtraction algorithm, first formulated in [38] and then extended in [66] to also include instanton moduli spaces, provides a means to read the transverse slice between two 3D $\mathcal{N} = 4$ unitary gauge theories related by a Coulomb branch RG flow. That is, given a unitary quiver theory \mathcal{Q} for which we can turn on some Coulomb branch moduli such that under an RG flow it reaches a quiver theory \mathcal{Q}' , the subtraction $\mathcal{Q} - \mathcal{Q}'$ outputs another

TABLE III. The type IIA brane description, the magnetic quiver, and the Coulomb branch Hilbert series together with global symmetry for the various phases in the A-type description of the theories associated with the tensor branch configuration $2 \ 2 \ 2$ [64]. The last entry is the magnetic quiver for the Higgs branch of the 6D SCFT.

Brane system	Magnetic quiver	Global symmetry	Coulomb branch Hilbert series
		$\mathfrak{so}(8)$	$\frac{(t^2+1)(t^8+17t^6+48t^4+17t^2+1)}{(1-t^2)^{10}}$
		$\mathfrak{so}(7)$	$\frac{(t^2+1)(t^8+10t^6+20t^4+10t^2+1)}{(1-t^2)^{10}}$
		$\mathfrak{su}(4)$	$\frac{t^{20}+10t^{18}+55t^{16}+150t^{14}+288t^{12}+336t^{10}+288t^8+150t^6+55t^4+10t^2+1}{(1-t^2)^{10}(t^2+1)^5}$
		$\mathfrak{su}(4)$	$\frac{t^{20}+10t^{18}+55t^{16}+150t^{14}+288t^{12}+336t^{10}+288t^8+150t^6+55t^4+10t^2+1}{(1-t^2)^{10}(t^2+1)^5}$
		\mathfrak{g}_2	$\frac{(t^2+1)(t^8+3t^6+6t^4+3t^2+1)}{(1-t^2)^{10}}$
		$\mathfrak{su}(3)$	$\frac{t^{20}+3t^{18}+13t^{16}+25t^{14}+46t^{12}+48t^{10}+46t^8+25t^6+13t^4+3t^2+1}{(1-t^2)^5(1-t^4)^5}$

unitary quiver \mathcal{S} , whose Coulomb branch moduli space gives exactly the transverse slice that connects the two theories; in a more physical language, \mathcal{S} gives information about the moduli we had to tune to trigger the flow from \mathcal{Q} to \mathcal{Q}' .

The algorithm stemmed from observations made in the context of brane dynamics in [67]. There, borrowing the definition of the theories \mathcal{Q} and \mathcal{Q}' of the last paragraph, and observing the type IIB D3-D5-NS5-brane system realization of \mathcal{Q} and \mathcal{Q}' , assuming that it exists, it was possible to associate with the Higgsing process and the corresponding transverse slice, a “move” in the brane system. In a subsequent work [68], the same authors explored with the same analysis pure 3D $\mathcal{N} = 4$ orthosymplectic quiver gauge theories, but the observations made in this case culminated only in a partial quiver subtraction algorithm [35] for orthosymplectic quiver theories.

In this section, we pursue the brane dynamics approach to craft a unitary-orthosymplectic quiver subtraction

algorithm that can be applied to the magnetic quivers for the Higgs branch that we wish to study. We consider the following procedure:

- (1) Engineer all the magnetic brane systems and magnetic quivers associated with the Higgsed phases of $D_N^{\mathfrak{su}_{2k}}(O)$ theories, for arbitrary generalized partitions O .
- (2) Look at the magnetic brane system of two theories we believe to be connected by an elementary RG flow according to the ordering in Eq. (2.11), and try to fit this flow to a known transition identified in [67,68] from a brane dynamics perspective.
- (3) When, after such a transition, the brane system obtained is exactly one of the theories we want to flow to, take the quivers of the theories at the two ends of the flow and work out the rules for a quiver subtraction algorithm.

Proceeding in this way, we find that in the brane system description, three kinds of transitions occur, namely the a_n minimal singularity, and the A_N and D_N Kleinian

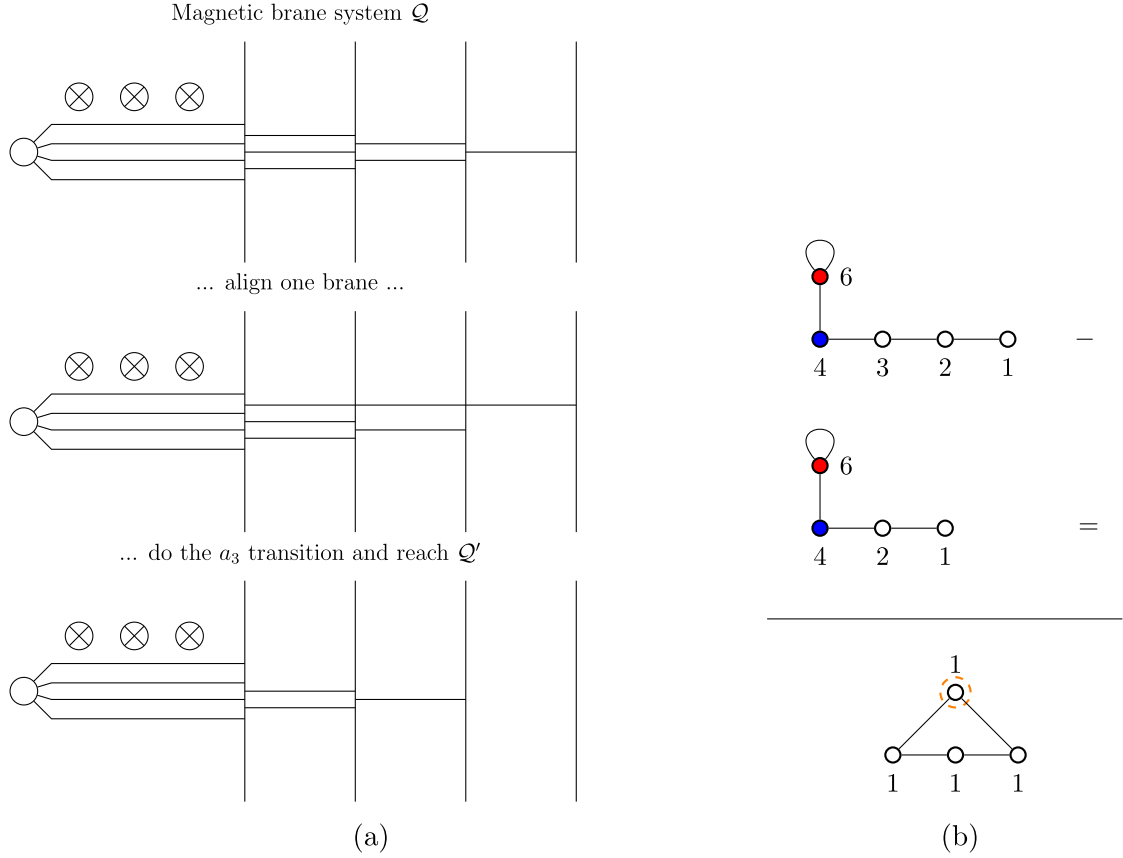


FIG. 8. An example of an a_3 transition via brane dynamics and quiver subtraction transitioning from the $D_3^{\text{su}_4}([1^4])$ theory to the $D_3^{\text{su}_4}([2, 1^2])$ theory. The rebalancing node introduced in the subtraction has been drawn with an orange dashed border. (a) Brane realization. (b) Quiver subtraction.

singularities. In the brane systems, we find that they occur as follows:

- (i) a_n transitions are realized by aligning a single D6-brane between $n + 1$ D8-branes and then pulling the merged D6-brane transversely to infinity, see Fig. 8(a) for an example.
- (ii) A_N transitions occur when only a single D6-brane that sits between D8-branes is pulled away transversely to infinity, and in the intervals adjacent to the boundary D8-branes there are precisely $N + 1$ D6-branes exceeding the number necessary for balance. For an example see Fig. 9(a).
- (iii) D_N transitions: These one-dimensional transitions are realized by pulling away a D6-brane stretching between the ON^- -plane and the D8-brane next to it and are possible only when the adjacent D8 interval hosts D6-branes with balance of at least 2. This minimal move requires the simultaneous pulling of the image D6-brane arising from the ON^- projection as the orientifold plane induces an $SO(2)$ charge on the D6-branes that needs to be neutralized.

The comparison of the magnetic quiver associated with theories connected by the aforementioned brane system transitions leads to the proposal of the following quiver

subtraction rules for unitary-orthosymplectic quiver theories¹⁹:

- (1) Consider all $\mathfrak{so}(2N)$ gauge nodes with matter in the rank-two antisymmetric representation as flavor nodes²⁰;
- (a) The quiver theory \mathcal{Q}' can be subtracted from the theory \mathcal{Q} if there exists an alignment of the two theories such that the gauge nodes in \mathcal{Q}' correspond to gauge nodes in \mathcal{Q} with same type of gauge algebras but ranks not greater than that of \mathcal{Q} .
- (b) The subtraction $\mathcal{Q} - \mathcal{Q}'$ is defined as the quiver gauge theory \mathcal{S} having same links and nodes gauge algebra as \mathcal{Q} , but with gauge group rank given by the difference between that of the node in \mathcal{Q} and the corresponding one in \mathcal{Q}' .

¹⁹We emphasize that these rules are not proposed for arbitrary unitary-orthosymplectic quivers, but for those of the form we consider in this paper.

²⁰We remark that point *) is necessary since there has been no understanding of an analogous concept to “decoration” [66] in the case of nonunitary gauge nodes.

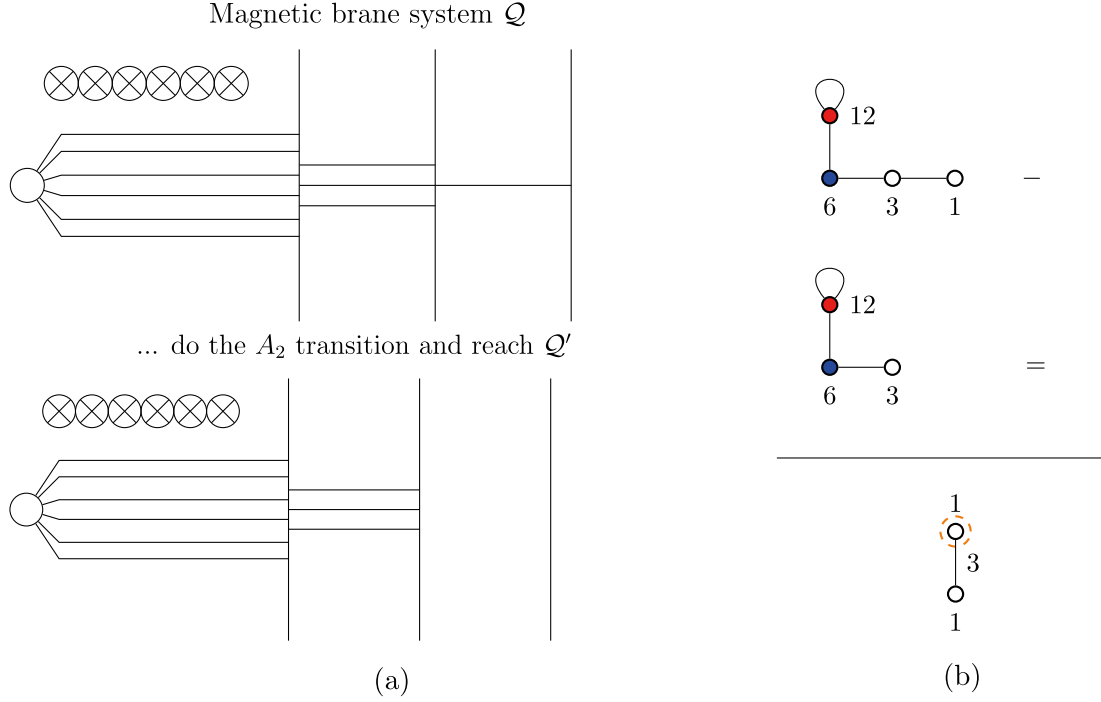


FIG. 9. An example of an A_2 transition via brane dynamics and quiver subtraction taking us from the $D_6^{\text{su}_6}([3, 2, 1])$ theory to the $D_6^{\text{su}_6}([3^2])$ theory. As before, the $U(1)$ rebalancing node introduced into \mathcal{S} has been drawn with a dashed orange border. (a) Brane realization. (b) Quiver subtraction.

(c) The quiver theory \mathcal{S} must be rebalanced according to the following procedure:

- (i) Call N the rank of the flavor node obtained from point *), k the rank of the connected symplectic gauge node, and h the total rank of the unitary nodes connected to the symplectic node. If after the subtraction that very same symplectic gauge node has nonzero rank then

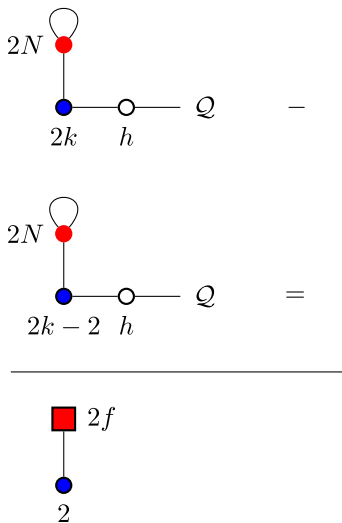


FIG. 10. Quiver subtraction operation on \mathcal{Q} and \mathcal{Q}' that results in a D_f transition. The quantity f is defined in Eq. (5.1).

its flavor symmetry node changes to an $SO(2f)$ node with

$$2f = \begin{cases} 2N + h - 2k & 2N + h = 0 \bmod 2, \\ 2N + h - 2k + 1 & 2N + h = 1 \bmod 2. \end{cases} \quad (5.1)$$

- (ii) If, after the subtraction, the quiver \mathcal{S} splits into a fully orthosymplectic part and a unitary part, the unitary part must be rebalanced via the introduction of the usual $U(1)$ node as in the standard quiver subtraction algorithm [38].

We depicted in Figs. 8(a), 9(a), and 10 some examples of the subtraction algorithm applied to each transition encountered in the Higgsing of the $D_N^{\text{su}_{2k}}(O)$ theories.

A much more direct approach that still manages to reproduce the Higgs branch Hasse diagram of $D_N^{\text{su}_{2k}}(O)$ involves the application of an extended version of the decay and fission algorithm [29,39] to unitary-orthosymplectic quivers.²¹ In fact, while the quiver subtraction algorithm

²¹This extension is valid only for the magnetic quivers that are the subject of this paper. Even a first extension of the decay and fission algorithm to the case of a purely orthosymplectic quiver is deemed to be challenging since “bad” magnetic quivers appear in Higgsed phases of theories associated with “good” magnetic quivers [69]. Such ubiquitous pathologies are absent from the quivers we study here.

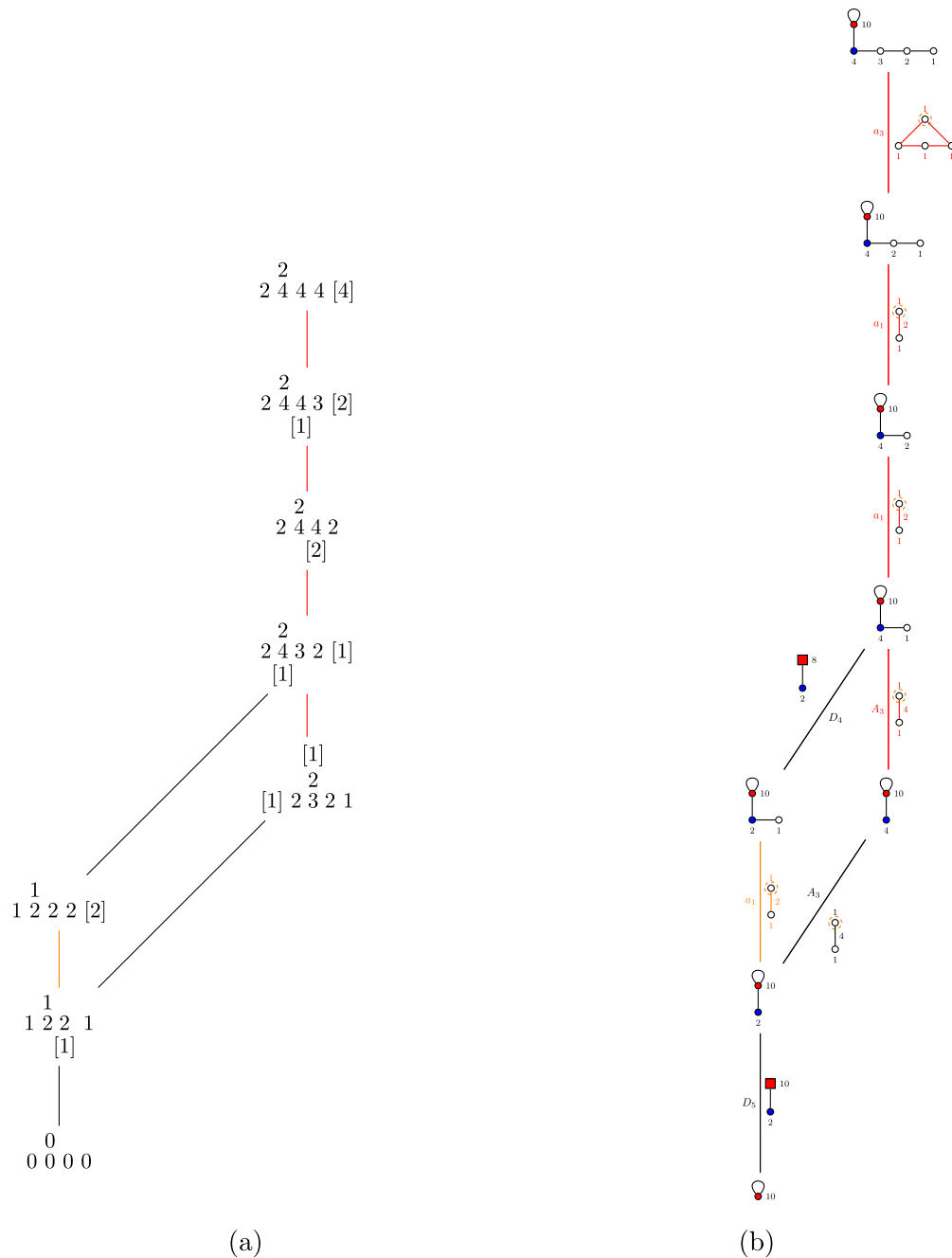


FIG. 11. (a) The Hasse diagram for a $D_5^{\text{su}_4}([1^4])$ theory where each vertex is represented by its tensor branch geometry is depicted. (b) The same Hasse diagram is proposed, but vertices show the corresponding magnetic quiver, and slices are identified via the quiver resulting from quiver subtraction of connected theories, depicted together with the standard nomenclature. (a) Hasse diagram from the tensor branch. (b) Hasse diagram from quiver subtraction.

leverages on the knowledge of a quiver realization of the slice²² one wants to subtract (the \mathcal{Q}' quiver in the aforementioned description of said algorithm), the decay and

²²Here we use the word “slices” to refer to more general Slodowy slices of which transverse slices constitute a particular subset.

fission algorithm is intrinsically free from such a constraint. The approach here is in fact the same as the one adopted in the original paper and consists of writing all the possible good, in the sense of [70], quiver gauge theories with the same shape and type of gauge algebras as the considered theory, but with not greater gauge rank for each node. First, discard the equivalent theories, and then connect them

according to whether, via this very same algorithm, a theory with smaller gauge group ranks can be obtained from a higher dimensional one. This procedure realizes the same Hasse diagram as the quiver subtraction algorithm that we have just delineated.

B. The Higgs branch

Now that we have utilized the brane system both to derive the magnetic quivers for the Higgs branches of the 6D (1, 0) SCFTs Higgsable to the D-type (2, 0) SCFTs, and the quiver subtraction algorithm for such magnetic quivers/brane systems, we are ready to explicate the structure of the Higgs branch. Since it is a straightforward application of the algorithm of Sec. VA to the magnetic quivers for the Higgs branch derived in Sec. III, in this section we simply present some explicit examples.

We begin by considering the $D_5^{\mathfrak{su}_4}([1^4])$ SCFT. We determine each of the tensor branches satisfying Eq. (2.6) and such that the ranks of the gauge algebras

are less than or equal to that of the gauge algebras for the tensor branch of the original theory. That is, we determine all consistent tensor branch configurations satisfying Eq. (2.10), and construct a provisional Hasse diagram using the partial ordering defined in Eq. (2.11). We have depicted this in Fig. 11(a). The next step is to determine the nature of the slices connecting neighboring theories, this feat can be accomplished by extracting the magnetic quiver for all the theories in the provisional Hasse and subtracting, according to the rules explained in Sec. VA, adjacent theories. Each subtraction will produce a 3D quiver whose Coulomb branch moduli space determines the slice nature. Therefore, from this procedure, it is possible to label each edge in the Hasse diagram, as shown in Fig. 11(b).

Having played this exercise with the $D_5^{\mathfrak{su}_4}([14])$ model, we can apply the same philosophy to study more general long $D_N^{\mathfrak{su}_{2k}}([1^{2k}])$ theories. The quiver subtraction algorithm correctly predicts the full nilpotent cone $\mathcal{N}(\mathfrak{su}_{2\ell})$ for $1 \leq 2\ell \leq 2k$ as a subset of the Hasse diagram for each long

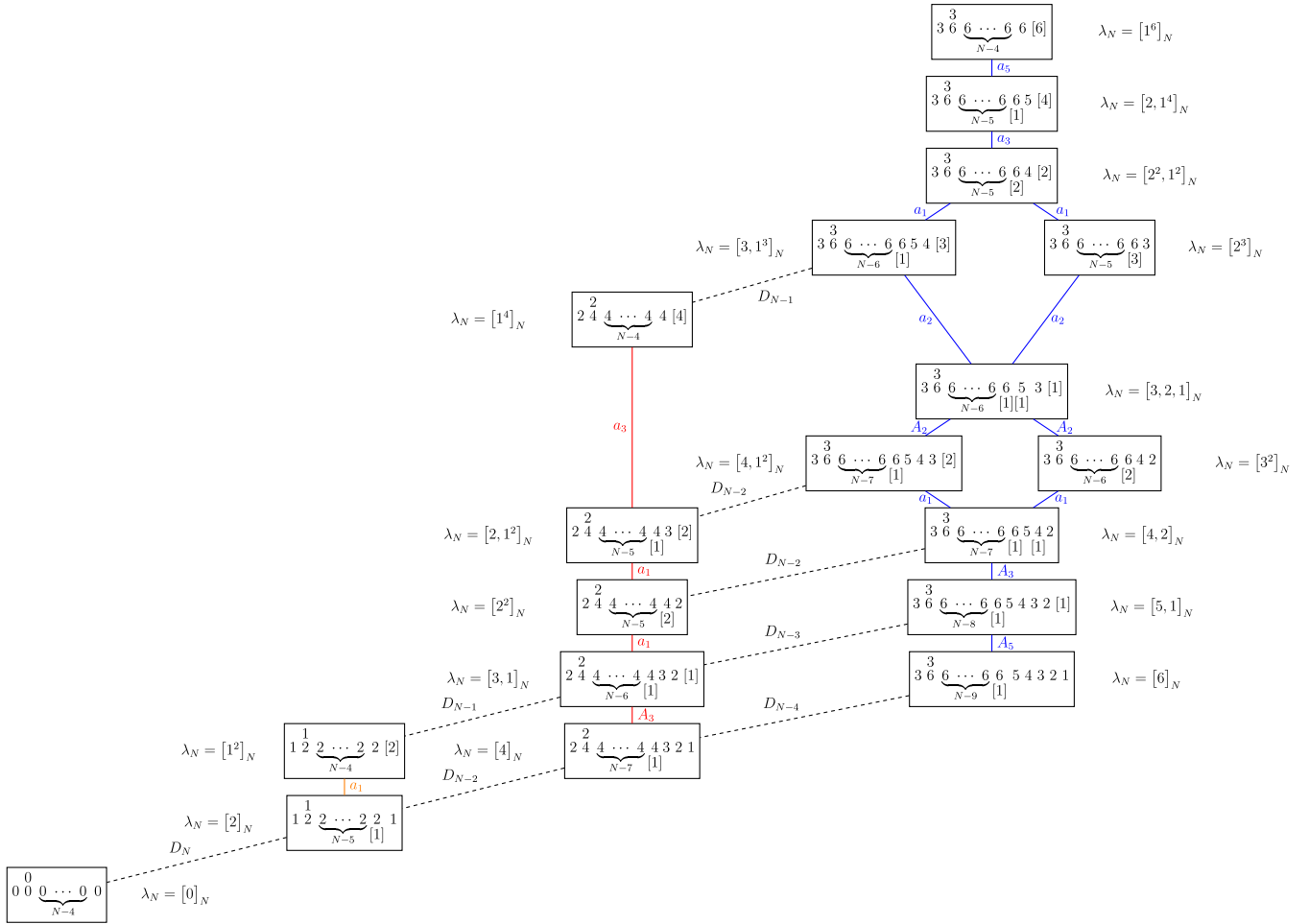


FIG. 12. Hasse diagram for the long $D_{N \geq 9}^{\mathfrak{su}_6}$ theory. At each node, we depict the tensor branch curve configuration. Blue slices refer to the nilpotent cone of $\mathfrak{su}(6)$, whereas red is used for the nilpotent cone of $\mathfrak{su}(4)$, and orange for $\mathfrak{su}(2)$. Dashed lines denote D-type transitions that link cones of different algebras together.

theory. Moreover, nilpotent cones of different algebras are connected by D_n slices, giving a nested inclusion relation. It is interesting to notice that the D_N slice only appears once and at the bottom of the diagram where the supersymmetry enhancement appears. In Fig. 12, we explicitly considered the Higgs branch of the long $D_N^{\mathfrak{su}_6}([1^6])$ theory, while taking care to highlight the different nilpotent cones appearing in the Hasse diagram, namely $\mathcal{N}(\mathfrak{su}_2), \mathcal{N}(\mathfrak{su}_4), \mathcal{N}(\mathfrak{su}_6)$, with different colors. The nested structure of the diagram is rendered explicit from the presence of D-slices interconnecting the various nilpotent subdiagrams, with the D_N slice itself leading to the (2, 0) theory of type D_N .

The case of short theories can be understood as well with the same approach; in fact, the quiver subtraction algorithm, as well as the magnetic quiver for the Higgs branch, is not sensitive to the location of the flavor symmetries in the tensor branch description. Therefore, there is no qualitative distinction between the procedure for determination of the Higgs branch for long and short theories. What is different is the fact that the full nilpotent cone of the ultraviolet flavor algebra is no longer realized as a subset of the Hasse diagram as highlighted in Fig. 1. On the other hand, it is partially realized and still nested to other (partially realized) cones via D-type transverse slices. One further caveat is that there may also be additional theories between one partial nilpotent cone and another. Figures 13 and 14 provide examples of Hasse diagrams for short theories, respectively $D_5^{\mathfrak{su}_6}([1^6])$ and $D_5^{\mathfrak{su}_8}([1^8])$. In these examples, it is clear to see that, in contrast to the long theories of Fig. 12, there are many possibilities for the RG

flow that are not associated with elements of any nilpotent cone.

C. An observation on Higgsing from the tensor branch

We have derived the interacting nonproduct subdiagram of the Higgs branch Hasse diagram of any given 6D (1, 0) SCFT Higgsable to D-type 6D (2, 0) SCFTs, of the form in Eq. (2.5), via quiver subtraction on the associated magnetic quiver. For the (both long and short) theories $D_N^{\mathfrak{su}_{2k}}(O)$, which have a tensor branch description of the form in Eq. (2.5), it is straightforward to observe that whenever the tensor branch geometry takes a specific form, then there exists a Higgs branch RG flow to another SCFT where the transverse slice also takes a particular form. We elucidate this observation in this subsection.

There are precisely three kinds of transverse slices that appear in the Hasse diagram: a_n, A_n , and D_n . The first is the closure of the minimal nilpotent orbit of $\mathfrak{su}(n+1)$, and the latter two are orbifold singularities of AD-type, respectively. By studying the tensor branch geometries before and after such elementary transverse slices, we observe that they occur under the following circumstances:

- (i) An a_n transverse slice exists whenever there is an $\mathfrak{su}(n+1 \geq 2)$ flavor algebra attached to a single curve supporting a nontrivial gauge algebra. After the transition, the rank of that gauge algebra is reduced by one, and the flavor algebras are fixed via anomaly cancellation. To illustrate this, we consider the following example:

$$5 \begin{smallmatrix} 10 \\ 8 \end{smallmatrix} \begin{smallmatrix} 6 \\ 4 \end{smallmatrix} \Rightarrow \begin{cases} \begin{smallmatrix} [1] \\ 5 \\ [1]5 \end{smallmatrix} \begin{smallmatrix} 9 \\ 8 \end{smallmatrix} \begin{smallmatrix} 6 \\ 4 \end{smallmatrix} & \text{Higgsing the } [2] \text{ flavor via an } a_1 \text{ transition,} \\ \begin{smallmatrix} 5 \\ 5 \end{smallmatrix} \begin{smallmatrix} 10 \\ 8 \end{smallmatrix} \begin{smallmatrix} 5 \\ 2 \end{smallmatrix} & \text{Higgsing the } [4] \text{ flavor via an } a_3 \text{ transition.} \end{cases} \quad (5.2)$$

That is, the Higgsable to D_5 tensor branch on the left has two elementary Higgsings where the transverse slice is of a_n type, to the two tensor branch configurations on the right. We emphasize that we know that these two transitions exist via the construction of the magnetic quiver and the application of the quiver subtraction algorithm; however, *a posteriori*, we note that are observed to correspond to the presence of the $[2]$ and the $[4]$, respectively.

- (ii) An A_n transverse slice occurs whenever there are two curves supporting nontrivial gauge algebras each with a single dangling fundamental flavor (that is, each has a $[1]$), and an inclusive linear chain of n curves, without attached flavor algebras, between them. After the Higgsing, the ranks of the gauge algebras on each of the n curves are reduced by one.

Again, it is best to illustrate via an example. There exists the following elementary transition between the SCFTs associated with the tensor branches:

$$\begin{smallmatrix} [1] \\ 4 \\ 2 \end{smallmatrix} \begin{smallmatrix} 4 \\ 7 \\ 1 \end{smallmatrix} \begin{smallmatrix} 6 \\ 3 \\ [2] \end{smallmatrix} \xrightarrow{A_3} \begin{smallmatrix} [1]2 \end{smallmatrix} \begin{smallmatrix} 3 \\ 6 \\ 3 \end{smallmatrix} \begin{smallmatrix} 3 \\ [3] \end{smallmatrix}. \quad (5.3)$$

We can see there is a linear chain of three curves of the form

$$[1]474[1], \quad (5.4)$$

indicating the existence of a Higgsing to a new SCFT where the transverse slice in the foliation of the

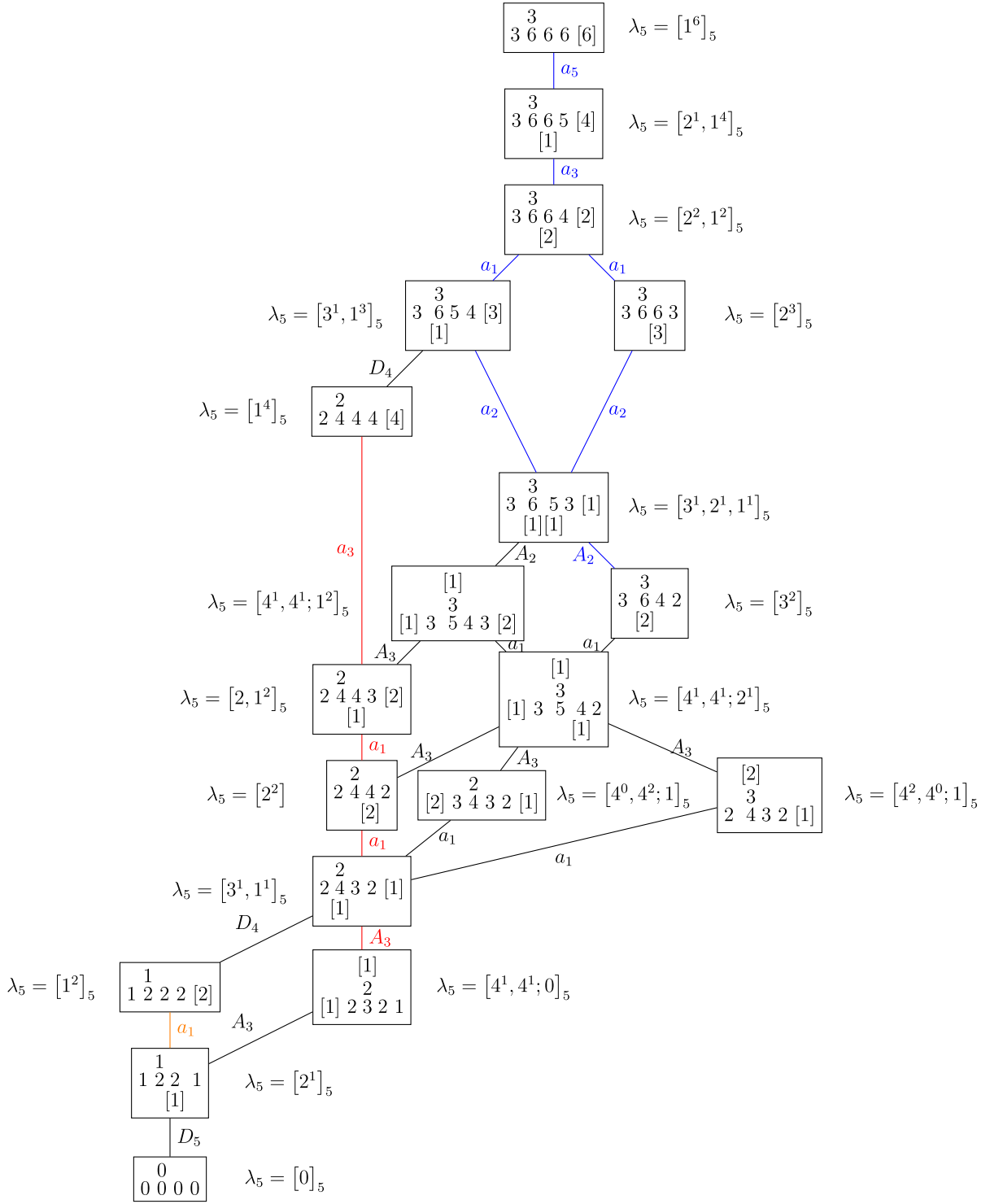


FIG. 13. Hasse diagram for the $D_5^{\mathfrak{su}_6}$ theory. At each vertex, the tensor branch curve configuration is drawn. Blue transitions are used to identify slices in the nilpotent cone of $\mathfrak{su}(6)$, whereas red is used for the nilpotent cone of $\mathfrak{su}(4)$. We note that there are also black edges which do not correspond to any nilpotent cone.

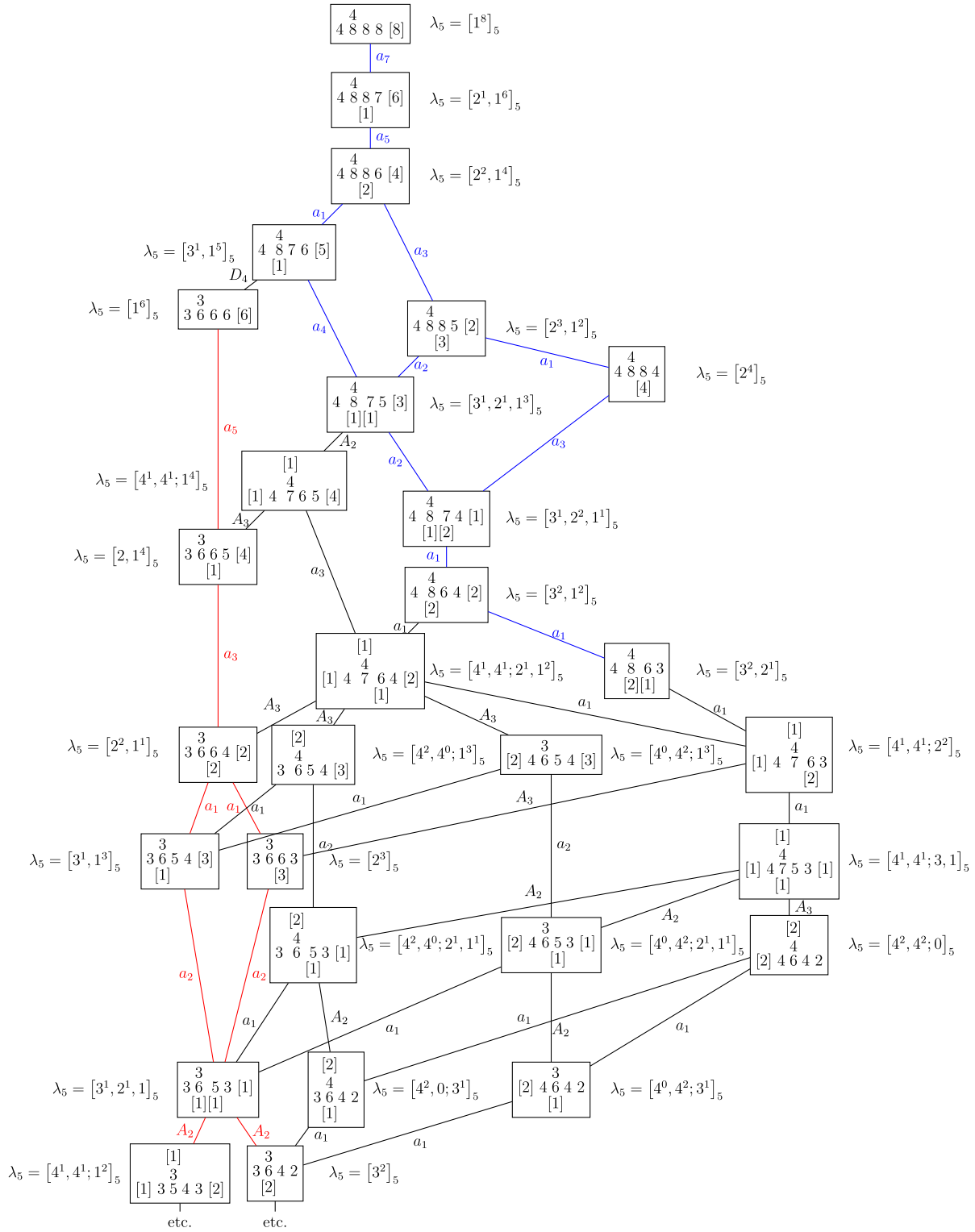


FIG. 14. The (partial) Higgs branch Hasse diagram for the $D_5^{\mathfrak{su}_8}$ SCFT. We have drawn the tensor branch curve configuration in each vertex. Blue transitions are used to identify slices in the nilpotent cone of $\mathfrak{su}(8)$, whereas red is used for the nilpotent cone of $\mathfrak{su}(6)$.

symplectic singularity is A_3 . Turning to, for example, Fig. 14, we can see this structure realized in each instance of such a tensor branch configuration.

- (iii) Finally, we turn to the D_n transverse slice. Such a transition occurs whenever we have a tensor branch configuration of the form

$$k_1 k_3 k_4 \cdots k_{n-1} k_n \cdots, \quad (5.5)$$

[1]

where $k_1, k_2, k_n \geq 1$ and $k_i \geq 2$ for $i = 3, \dots, n-1$. It is important to note that there are no dangling hypermultiplets attached to any of the depicted curves. After Higgsing, each of the k_1, k_2, k_n is decreased by one, the k_i for $i = 3, \dots, n-1$ are each decreased by two, and the infrared flavor symmetry is determined from anomaly cancellation. An example is the following elementary Higgsing:

$$\begin{array}{c} 3 \\ 6 \end{array} 5 4 [3] \xrightarrow{D_4} \begin{array}{c} 2 \\ 4 \end{array} 4 4 [4]. \quad (5.6)$$

[1]

There is one special case of the D_n transverse slice, which occurs at the bottom of the Hasse diagram, i.e., the final Higgsing before the $(2, 0)$ supersymmetry enhancement occurs. This Higgsing is always between tensor branches of the form,

$$\begin{array}{c} 1 \\ 122 \cdots 21 \end{array} \xrightarrow{D_N} \begin{array}{c} 0 \\ 000 \cdots 00 \end{array}, \quad (5.7)$$

[3/2]

where there are N compact curves in the configuration. In this case, there is a $[3/2]$ instead of a $[1]$, but otherwise, the standard rule for the D_n transverse slice applies.

From this experimental reverse engineering of the transverse slices in terms of the tensor branch configurations, we can produce a catalog of “slices” that need to be subtracted from the tensor branch to generate the Higgs branch Hasse diagrams for $D_N^{\mathfrak{su}_{2k}}(O)$. To wit, we denote these tensor branch slices as

$$a_n := 1 - [n + 1], \quad (5.8)$$

$$A_n := [1] - \underbrace{1 - \cdots - 1}_{n \text{ curves}} - [1], \quad (5.9)$$

$$D_n := 1 - \begin{array}{c} 1 \\ 2 \end{array} - \underbrace{2 - \cdots - 2}_{n-5 \text{ curves}} - \begin{array}{c} 2 \\ 1 \end{array} - 1. \quad (5.10)$$

In particular, if the tensor branch configuration contains one of these subgraphs, then there exists an elementary Higgs branch RG flow, with transverse slice as given, to a

new SCFT where the ranks of the gauge algebras on the tensor branch are obtained via subtracting the gauge ranks of the subgraph. We refer to this as performing “slice subtraction” directly on the 6D tensor branch.

Working out the Higgsing pattern for $D_N^{\mathfrak{su}_{2k}}(O)$ theories and drawing the associated Hasse diagram is a straightforward computation with the slice subtraction algorithm, and it can be checked from the previously drawn Hasse diagrams in Fig. 12 for long theories and in Figs. 13 and 14 for short theories.

We emphasize once again that this is an experimental observation, based on the transverse slices as worked out from the quiver subtraction algorithm as applied to the magnetic quiver for the Higgs branch. The slice subtraction pattern holds for the $D_N^{\mathfrak{su}_{2k}}(O)$ SCFTs, but it does not *a priori* hold beyond that regime. In the case of the family of the 6D $(1, 0)$ SCFTs known as conformal matter, there is a similar set of slice subtraction rules, which can be understood microscopically in terms of giving vacuum expectation values to specific Higgs branch chiral ring operators directly in 6D. For conformal matter, this analysis appears in [49], and the generalization to the microscopics of the slice subtraction algorithm for Higgsable to D-type $(2, 0)$ SCFTs can be determined.

VI. GEOMETRIC APPROACH TO PRODUCT HIGGSING

In the previous section, one of the approaches to understanding the Higgs branch of $D_N^{\mathfrak{su}_{2k}}$ was via a magnetic quiver for the Higgs branch. That is, we applied the quiver subtraction algorithm to the magnetic quiver for the Higgs branch worked out in Sec. III. Such a procedure allows us to extract both the symplectic leaves and the transverse slices between them; however, due to the incompleteness of the quiver subtraction algorithm for the unitary-orthosymplectic quivers that we are considering [see, e.g., Eq. (3.4)], we do not see the structure of the full Higgs branch in this way, only the leaves/slices corresponding to interacting nonproduct 6D $(1, 0)$ SCFTs. In particular, the subtlety arises from the $\mathfrak{so}(2N)$ gauge node with the antisymmetric hypermultiplet.

We can partially overcome this limitation if instead of the structure of the Higgs branch, i.e., knowing both the leaves and the transverse slices between them, we only focus on the possible Higgsing results, i.e., only the leaves. The geometry itself automatically encodes the Higgsing pattern of an SCFT, since the former is realized as complex structure deformation of the elliptically fibered Calabi-Yau threefold Y on which F-theory is compactified. Thus we can study such complex structure deformations to extract the Hasse diagram of a 6D SCFT. One drawback of this approach is that the information about the transverse slice corresponding to any particular Higgsing is obscured.

The second drawback is that, given a noncompact elliptically-fibered Calabi-Yau threefold engineering a 6D (1, 0) SCFT, it is generally challenging to study the space of complex structure deformations. In particular, it is not straightforward to explore the complex structure moduli space of the geometry engineering the tensor branch SQFT, which has the advantage of a smooth base and only minimal singularities in the fiber, to learn about the complex structure deformations of the SCFT geometry. Therefore, in this section, we review the complex structure deformation approach as applied to the geometries engineering the 6D (2, 0) SCFTs. From the magnetic quiver of those theories that are Higgsable to 6D (2, 0) SCFTs of type Γ , we have seen that the “end” of the Hasse diagram corresponds to the 6D (2, 0) theory of type Γ itself. In fact, these (2, 0) theories themselves possess a nontrivial Higgs branch, which must be further studied; this continuation of the Higgs branch Hasse diagram is what we explore here. Recall that the (2, 0) theories are realized geometrically as a trivial fibration over a base space of the form \mathbb{C}^2/Γ , with $\Gamma \subset SU(2)$ a finite subgroup.

The deformation space of a \mathbb{C}^2/Γ orbifold singularity was worked out in [71], following [72–75], amongst others. We first consider a simple example; the $A_{N-1} = \mathbb{C}^2/\mathbb{Z}_N$ orbifold can be written as the zero-locus of the polynomial

$$uv = z^N, \quad (6.1)$$

in \mathbb{C}^3 , where the singular point is at the origin. There exists a complex structure deformation which modifies this hypersurface equation as follows:

$$uv = z^N \longrightarrow uv = (z - t_1)^{N_1}(z - t_2)^{N_2}, \quad (6.2)$$

where $N_1 + N_2 = N$. Now, there is locally a $\mathbb{C}^2/\mathbb{Z}_{N_1}$ singularity at $u = v = z - t_1 = 0$ and a $\mathbb{C}^2/\mathbb{Z}_{N_2}$ singularity at $u = v = z - t_2 = 0$. The space of all such deformations, together with the foliation structure of the symplectic singularity, is simply $\text{Sym}^N(\mathbb{C}^2)$, as discussed previously in [66]. The general result can be summarized as follows. By abuse of notation, let Γ denote the Dynkin diagram of the Lie algebra associated with the finite group Γ via the McKay correspondence. Let Γ_0 denote a subgraph of Γ . The graph

$$\Gamma' = \Gamma - \Gamma_0 = \bigsqcup_{i=1}^n \Gamma'_i, \quad (6.3)$$

consists of a disjoint union of Dynkin diagrams Γ'_i . There exists a deformation of \mathbb{C}^2/Γ to a space with n isolated singular points locally of the form

$$\mathbb{C}^2/\Gamma'_i, \quad (6.4)$$

TABLE IV. Complex structure deformations of a \mathbb{C}^2/Γ singularity. Such deformations can be applied recursively. Here, we implicitly allowed the trivial A_0 and D_0 cases.

Γ	Possible deformations
A_n	$A_{n-k} \times A_{k-1}$
D_n	$D_{n-k} \times A_{k-1}$
E_6	$D_5, A_5, A_4 \times A_1, A_2 \times A_2 \times A_1$
E_7	$E_6, D_6, A_6, D_5 \times A_1, A_5 \times A_1, A_4 \times A_2, A_3 \times A_2 \times A_1$
E_8	$E_7, D_7, A_7, E_6 \times A_1, A_6 \times A_1, D_5 \times A_2, A_4 \times A_3, A_4 \times A_2 \times A_1$

respectively. Again, we have abused notation and used Γ'_i to denote both the Dynkin diagrams and the associated finite subgroups of $SU(2)$.

It is clear that a partial ordering exists on such deformations given via inclusion of subgraphs. Let Γ' denote the (possibly disconnected) Dynkin diagram after an arbitrary number of deformations, then the elementary transitions under this partial ordering occur when the subgraph removed from Γ' consists only of a single vertex, that is, removing an A_1 Dynkin diagram. Thus, the Hasse diagram of deformations of \mathbb{C}^2/Γ under this partial ordering can be straightforwardly determined once the single vertex deletions of each simple Dynkin diagram are known. For convenience, we list these in Table IV.²³ This provides the symplectic leaves of the Hasse diagram for the Higgs branch of the 6D (2, 0) SCFTs of type Γ , however, it does not, in general, provide the data of the transverse slice, even though it is easy to see that each of these slices is one-dimensional.

In the first case in Table IV, where an A-type orbifold splits into two, we do have an understanding of the transverse slice [66]. The slice is A_1 if the orbifold splits into two copies of the same Dynkin diagram, otherwise it is m ,²⁴

$$\begin{aligned} A_{2k+1} &\xrightarrow{A_1} A_k \times A_k, \\ A_k &\xrightarrow{m} A_{k-1-p} \times A_p, \quad p \geq 0. \end{aligned} \quad (6.5)$$

While it is unknown for the generic case, the geometry allows us to draw Hasse diagrams, without the slice data, for cases where brane constructions are not viable or only partially understood. As an example, we have depicted the Hasse diagram of the complex structure deformations of the \mathbb{C}^2/D_5 singularity in Fig. 15; we have labeled each vertex by the resolution of the deformed singularity. This is then the Hasse diagram for the Higgs branch of the 6D (2, 0)

²³We thank Amihay Hanany for pointing out that this procedure determines the Levi subgroups of the algebra \mathfrak{g} associated with Γ .

²⁴For the definition of the one-dimensional m slice, see [76].

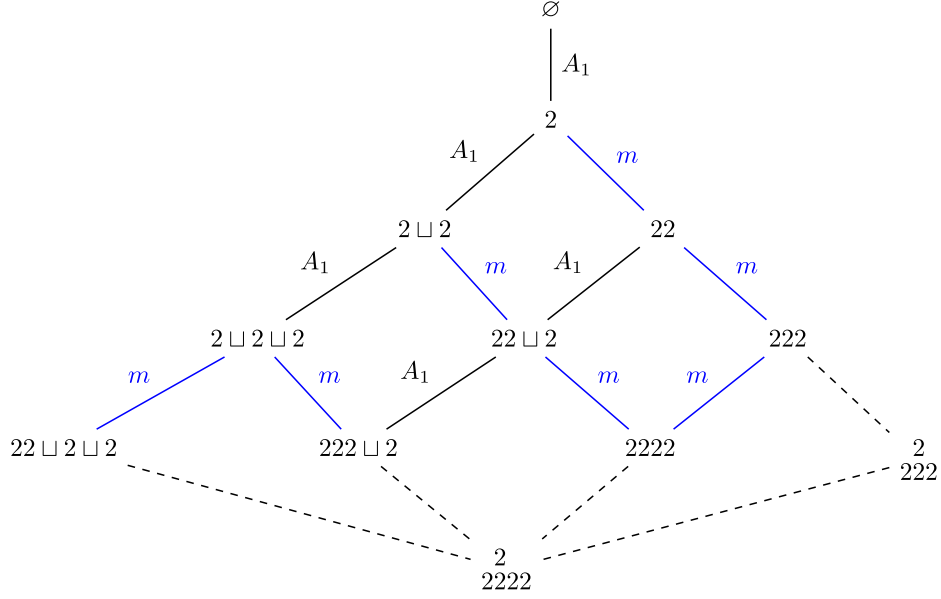


FIG. 15. Hasse diagram of the 6D $\mathcal{N} = (2, 0)$ SCFT of type D_5 . Known slices are labeled and colored according to their nature (black for A_1 slices and blue for m ones), whereas unknown slices are depicted with dashed lines.

SCFT of type D_5 . Even more, since we have a brane construction from each of the theories appearing in the D_5 -type Hasse diagram of Fig. 15, and in general for every theory in the D_n -type Hasse diagram, we can associate a

magnetic quiver to each of the theories as done in Fig. 16 and take it as a future starting point for a more systematic understanding of subtraction in the context of orthosymplectic quivers.

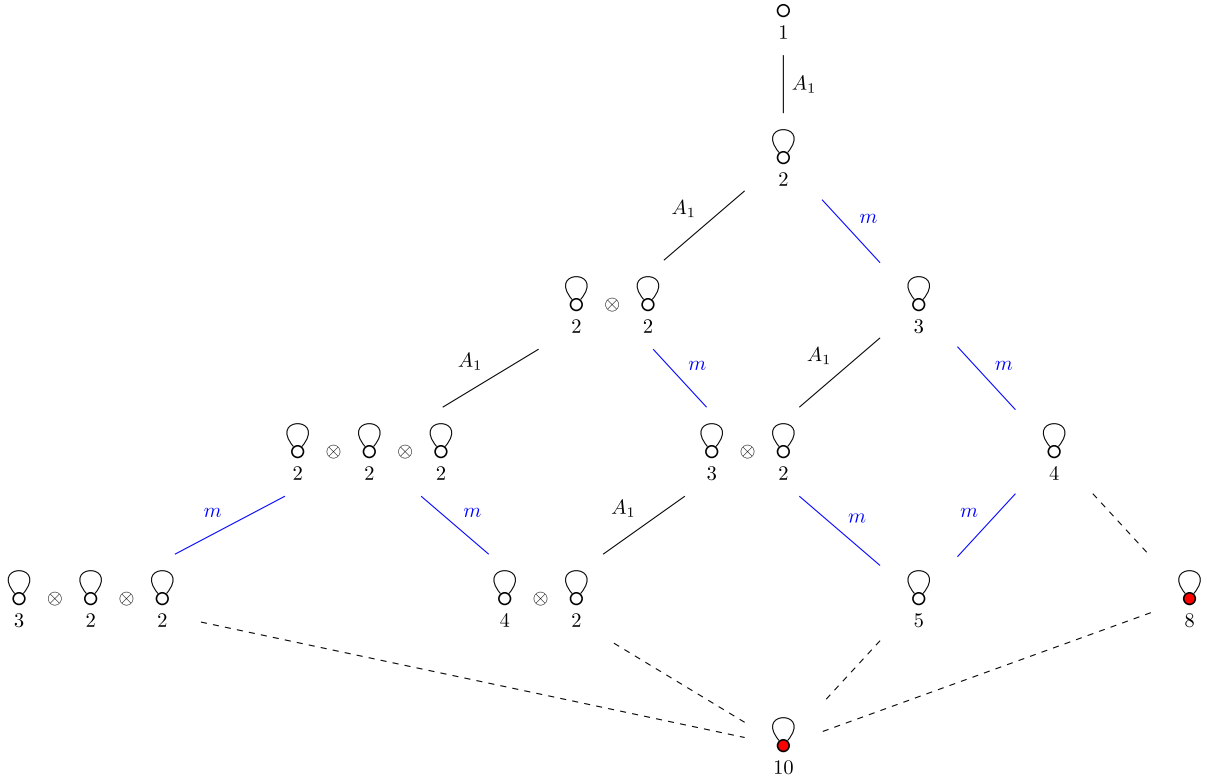


FIG. 16. Hasse diagram of the 6D $\mathcal{N} = (2, 0)$ SCFT of type D_5 with the magnetic quiver for the Higgs branch of the theory at each vertex depicted. Known slices are labeled and colored according to their nature (black for A_1 slices and blue for m), whereas unknown slices are depicted via dashed lines.

VII. HIGGS BRANCH OF HIGGSABLE TO E-TYPE (2, 0) SCFTS

In addition to the Higgsable to D-type (2, 0) SCFTs, $D_N^{\mathfrak{su}(2k)}(O)$, in Sec. II we also introduced the SCFTs $E_N(k_1, \dots, k_N)$ which have supersymmetry-enhancing Higgs branch RG flows to the E-type (2, 0) SCFTs. While we could determine the (interacting, nonproduct subdiagram of the) Higgs branch Hasse diagram from the geometric perspective, following Eq. (2.31), there is no known brane description of these theories and thus no magnetic quiver for the Higgs branches.²⁵ As a result, we lack a method to learn about the structure of the Higgs branch as a foliation of a symplectic singularity; this is, we are missing the information on the transverse slices. Specifically, given an elementary Higgsing,

$$E_N(k_1, \dots, k_N) \xrightarrow{S} E_N(k'_1, \dots, k'_N), \quad (7.1)$$

what can we learn about the transverse slice S ?

In Sec. VC, we proposed an empirical “slice subtraction algorithm” that allowed for the determination of the transverse slice directly via studying the structure of the tensor branch field theory before Higgsing. This algorithm is conjectural and based on the matching with the transverse slices as determined from the magnetic quiver for the $D_N^{\mathfrak{su}(2k)}(O)$ SCFTs. However, we may suppose that the algorithm applies more broadly, in particular to the $E_N(k_1, \dots, k_N)$ SCFTs, and test whether it provides a transverse slice consistent with the known properties of the 6D (1, 0) theories before and after the flow.

The a_n slice subtraction involves reducing the rank of a single gauge algebra by one. It is straightforward to check the change in the Higgs branch dimension using Eq. (2.30). Let i denote the index of the compact curve to which the $\mathfrak{su}(n+1)$ flavor algebra is attached, and we find that the difference in the Higgs branch dimension is

$$\delta \dim(\mathcal{H}) = \sum_{j=1}^N A^{ij} k_j - \frac{1}{2} A^{ii} = m_i - 1 = n. \quad (7.2)$$

This is the dimension of the closure of the minimal nilpotent orbit of $\mathfrak{su}(n+1)$, as expected for an a_n transverse slice. Similar arguments can be made to show that the change in the Higgs branch dimension whenever there is an A_n or D_n transition according to Eq. (5.8) is one. This provides a consistency check that the transverse slices that we have associated via slice subtraction are consistent with the expectation from the Higgs branch dimension.

²⁵In the spirit of Sec. IV, if we were to obtain a potential magnetic quiver for the E_N series with arbitrary N , we should match following the isomorphisms $E_4 \cong A_4$ and $E_5 \cong D_5$.

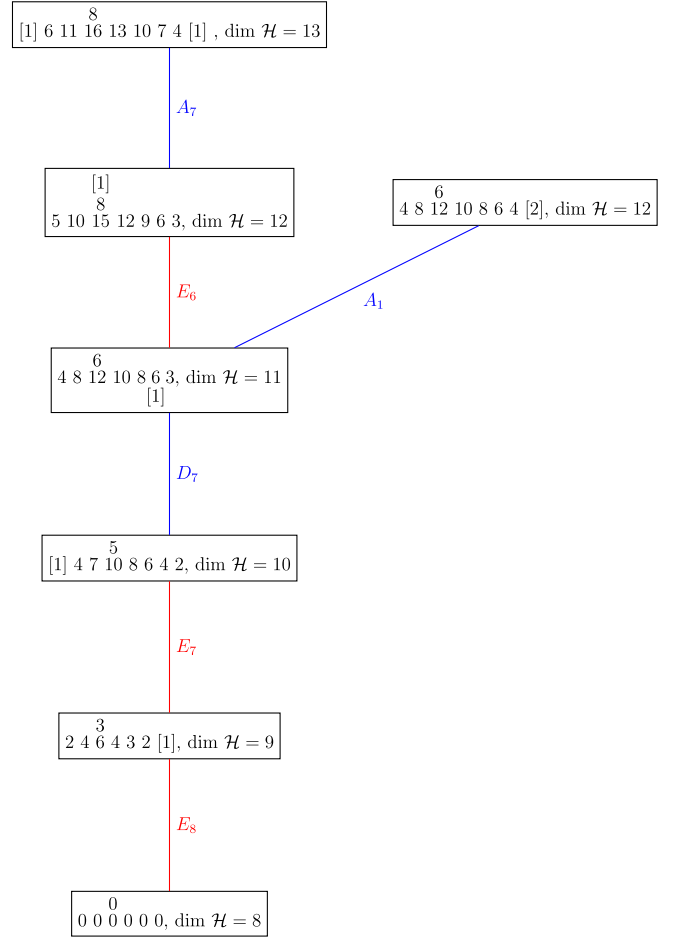


FIG. 17. The bottom of the (intersecting, non-product part of the) Hasse diagram for the $E_8(k_1, \dots, k_8)$ SCFTs; we depict only configurations with $k_5 \leq 16$. At each vertex we write the tensor branch description of the SCFT as well as the dimension of the Higgs branch. Vertices are connected according to Eq. (2.31), and the transverse slice labeling each link is conjectured from the slice subtraction algorithm in Eqs. (5.8) and (7.3).

However, we can see that there are a small number of transitions in the Higgs branch Hasse diagram of the $E_N(k_1, \dots, k_N)$ SCFTs where there is no transverse slice associated via the slice subtraction rules. In each of these cases, the transverse slices must be one-dimensional due to the known change in the Higgs branch dimension. These are best illustrated by the lower part of the $E_8(k_1, \dots, k_8)$ Hasse diagram, which we depict in Fig. 17. Blue transitions denote elementary Higgsings where the transverse slice follows from the slice subtraction rules in Eq. (5.8), whereas the red transitions do not. However, these red transitions have a very evocative form; they appear to involve the subtraction of an E_N type Dynkin diagram, weighted by the Dynkin labels, from the gauge ranks of the tensor branch configuration. This suggests that we should propose the following slice subtraction rules, in addition to those in Eq. (5.8):

$$\begin{aligned}
E_6 &:= 1 - 2 - \overset{[1]}{\underset{2}{3}} - 2 - 1, & E_7 &:= [1] - 2 - 3 - \overset{2}{\underset{4}{3}} - 2 - 1, \\
E_8 &:= 2 - 4 - \overset{3}{\underset{6}{5}} - 4 - 3 - 2 - [1].
\end{aligned} \tag{7.3}$$

Interestingly, the slice subtraction rules in Eqs. (5.8) and (7.3) are sufficient to provide a transverse slice, with the correct change in the Higgs branch dimension, to each link in the Hasse diagram of interacting nonproduct theories on the Higgs branch of $E_N(k_1, \dots, k_N)$. For example, see Fig. 18 where we have taken the Hasse diagram from the F-theory geometric engineering (for $N = 6$) that was drawn in Fig. 2 and added the transverse slices obtained using the slice subtraction algorithm. Of course, the change in the Higgs branch dimension is a relatively crude invariant, and further study is necessary to verify that this algorithm is producing the correct transverse slices for this class of Higgsable to E-type $(2, 0)$ SCFTs.

Further evidence for these assignments of transverse slices arises from the 3D reduction of the tensor branch SQFT, which we briefly summarize here. For an arbitrary $E_6(k_1, \dots, k_6)$ SCFT, it is believed that the T^3 reduction of the tensor branch theory gives rise to the following unitary 3D $\mathcal{N} = 4$ quiver:

$$\begin{array}{c}
\begin{array}{c} [m_6] \\ k_6 \\ k_1 \ k_2 \ k_3 \ k_4 \ k_5 \\ [m_1] [m_2] [m_3] [m_4] [m_5] \end{array} \xrightarrow{T^3} \begin{array}{c} m_6 \\ \square \\ \circ \quad k_6 \\ \circ \quad k_3 \\ \square \quad m_1 \quad \square \quad m_2 \quad \square \quad m_3 \quad \square \quad m_4 \quad \square \quad m_5 \end{array},
\end{array} \tag{7.4}$$

and similarly for the $N = 7$ and $N = 8$ cases. Since these 3D reductions have only unitary gauge/flavor nodes and bifundamental matter, we can apply the technique of inversion [77] to understand their Higgs branches,²⁶ which are isomorphic to the Higgs branches of the 6D tensor branch SQFTs. Inversion notes that the Coulomb branch Hasse diagram and the Higgs branch Hasse diagram are identical as graphs, and the only difference is the labeling of the edges via transverse slices. If a transition in the Coulomb branch is labeled by the closure of a minimal nilpotent orbit of a simple and simply-laced Lie algebra \mathfrak{g} , $\overline{\min.\mathfrak{g}}$, then the corresponding transition in the Higgs

²⁶More precisely, if the Coulomb branch Hasse diagram only has transverse slices which are closures of minimal nilpotent orbits or Kleinian singularities, then we can use inversion to derive the Higgs branch Hasse diagram.

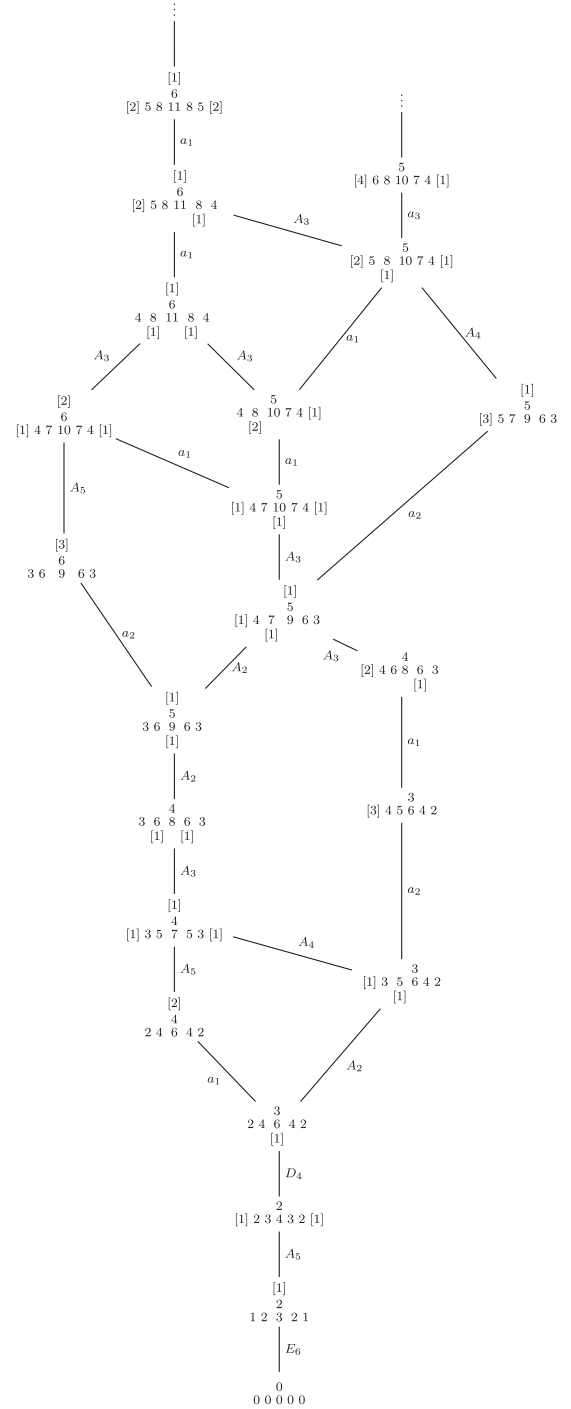


FIG. 18. Portion of the bottom part of the Higgs branch Hasse diagram obtained via slice subtraction on a Higgsable to $E_6(2, 0)$ theory: $E_6(k_1, \dots, k_6)$. This figure is the same as Fig. 2, but with the addition of the transverse slice labeling.

branch is labeled by the Kleinian singularity $\mathbb{C}^2/\Gamma_{\mathfrak{g}}$, where $\Gamma_{\mathfrak{g}}$ is the finite subgroup of $SU(2)$ related to \mathfrak{g} via the McKay correspondence, and vice versa. To wit,

$$\overline{\min.\mathfrak{g}} \leftrightarrow \mathbb{C}^2/\Gamma_{\mathfrak{g}}. \tag{7.5}$$

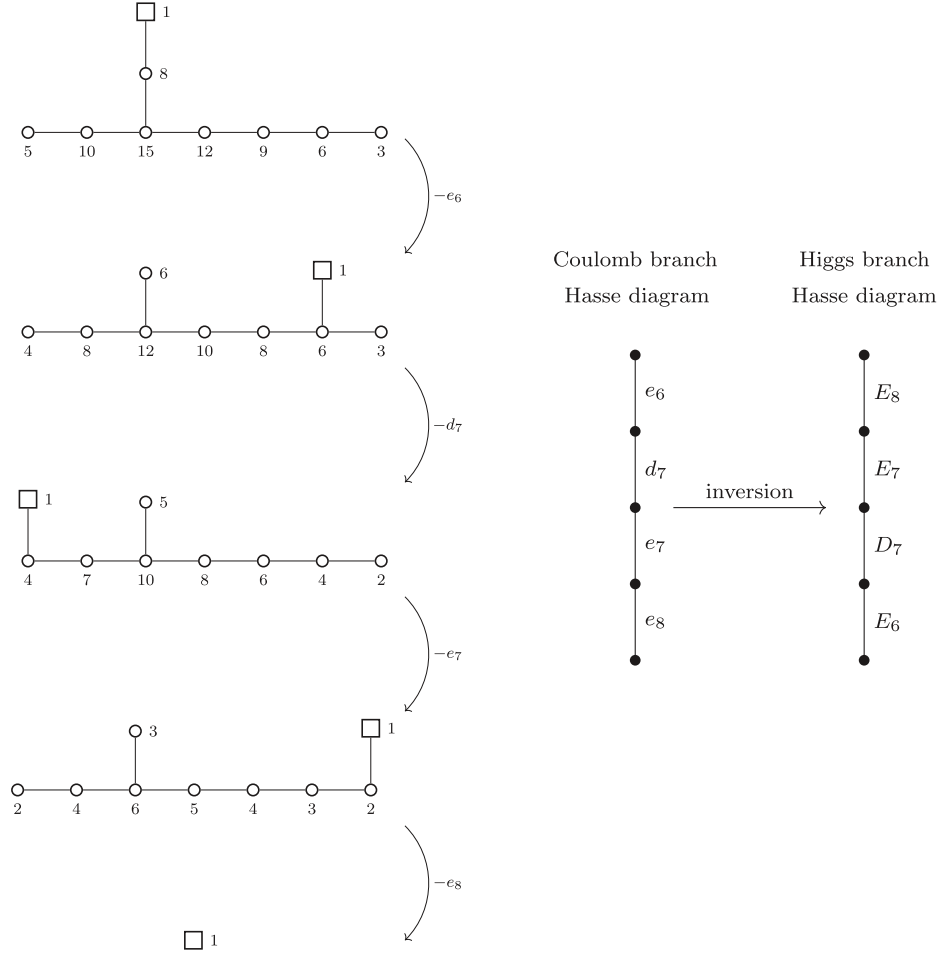


FIG. 19. Quiver subtraction technique applied to the 3D reduction of the tensor branch SQFT of the $E_8(5, 10, 15, 12, 9, 6, 3, 8)$ SCFT together with its Coulomb branch Hasse diagram and its Higgs branch Hasse diagram derived via inversion. The Hasse diagrams are ordered according to the foliation induced by the underlying symplectic singularity, which is converse to the ordering used in other figures of this paper that decrease in Higgs branch dimension.

Therefore, we can use quiver subtraction to determine the Coulomb branch Hasse diagram of the 3D reduction and use inversion to determine the transverse slices in the Higgs branch Hasse diagram. When performing this process, we note that the slices obtained in this way are the same as the slices obtained when following the slice subtraction algorithm. As an example, we carry this out in Fig. 19 for a Higgsable to E_8 -type theory, where the resulting Higgs branch Hasse diagram can be compared to that from slice subtraction in Fig. 17. While this is a statement about the Higgs branch of the tensor branch theories, as opposed to the SCFT Higgs branches, we generally (though not always) expect that operators of the Higgs branch chiral ring on the generic point of the tensor branch survive the contraction to the SCFT point, and thus can still trigger Higgsing.

We would also like to understand such a Higgsing microscopically in six dimensions. For example: when considering the E_8 transverse slice that appears in Fig. 17, it is natural to ask: what is the operator in the Higgs branch

chiral ring of the UV 6D (1, 0) SCFT to which a vacuum expectation value is given to trigger this renormalization group flow? First, one can analyze the 1/2-BPS Higgs branch operators belonging to the tensor branch SQFT, and attempt to understand how the E_8 transition is triggered between the tensor branch SQFTs in the UV and the IR. Then, it is necessary to make an argument that the relevant operators survive in the SCFT limit where all of the compact curves are shrunk to zero volume. Some of these questions are answered in the conformal matter theories (or Higgsable to A-type (2, 0) SCFTs) in [49]. We leave the general case for future work.

VIII. 6D (2, 0) LSTs WITH SUSY-ENHANCING RG FLOWS

Thus far, we have considered 6D (1, 0) SCFTs which have supersymmetry-enhancing renormalization group flows. There exists a closely related class of six-dimensional theories known as LSTs. These are nongravitational

TABLE V. We list 6D (1, 0) LSTs that have SUSY-enhancing Higgs branch renormalization group flows to the (2, 0) LSTs. For their properties, we list the dimension of the Coulomb branch of the S^1 compactification, and the generalized symmetry structure constant κ_R .

LST	Curve configuration	$\dim(\mathcal{C})$	κ_R
$\hat{A}_{N-1}^{\mathfrak{su}_K}$	$\underbrace{// \underbrace{\begin{smallmatrix} \mathfrak{su}_K & \mathfrak{su}_K & & \mathfrak{su}_K & \mathfrak{su}_K \\ 2 & 2 & \cdots & 2 & 2 \end{smallmatrix}}_{N(-2)\text{-curves}} //}$	$NK - 1$	NK
$\hat{A}_{N-1}^{\mathfrak{so}_{2K}}$	$\underbrace{// \underbrace{\begin{smallmatrix} \mathfrak{so}_{2K} & \mathfrak{sp}_{K-4} & & \mathfrak{so}_{2K} & \mathfrak{sp}_{K-4} \\ 4 & 1 & \cdots & 4 & 1 \end{smallmatrix}}_{N(-4)\text{-curves}} //}$	$2N(K - 1) - 1$	$4NK - 8N$
$\hat{A}_{N-1}^{e_6}$	$\underbrace{// \underbrace{\begin{smallmatrix} e_6 & \mathfrak{su}_3 & & e_6 & \mathfrak{su}_3 \\ 6 & 1 & \cdots & 6 & 1 \end{smallmatrix}}_{N(-6)\text{-curves}} //}$	$12N - 1$	$24N$
$\hat{A}_{N-1}^{e_7}$	$\underbrace{// \underbrace{\begin{smallmatrix} e_7 & \mathfrak{su}_2 & \mathfrak{so}_7 & \mathfrak{su}_2 & & e_7 & \mathfrak{su}_2 & \mathfrak{so}_7 & \mathfrak{su}_2 \\ 8 & 1 & 2 & 3 & 2 & 1 & \cdots & 8 & 1 & 2 & 3 & 2 & 1 \end{smallmatrix}}_{N(-8)\text{-curves}} //}$	$18N - 1$	$48N$
$\hat{A}_{N-1}^{e_8}$	$\underbrace{// \underbrace{\begin{smallmatrix} e_8 & \mathfrak{su}_2 & \mathfrak{g}_2 & \mathfrak{f}_4 & \mathfrak{g}_2 & \mathfrak{su}_2 & & e_8 & \mathfrak{su}_2 & \mathfrak{g}_2 & \mathfrak{f}_4 & \mathfrak{g}_2 & \mathfrak{su}_2 \\ (12) & 12 & 2 & 3 & 15 & 13 & 2 & 21 & \cdots & (12) & 12 & 2 & 3 & 15 & 13 & 2 & 21 \end{smallmatrix}}_{N(-12)\text{-curves}} //}$	$30N - 1$	$120N$
$\hat{D}_N^{\mathfrak{su}_{2K}}$	$\underbrace{\begin{smallmatrix} \mathfrak{su}_{2K} & & \mathfrak{su}_{2K} \\ 2 & & 2 \\ \mathfrak{su}_K & \mathfrak{su}_K & \mathfrak{su}_{2K} & \mathfrak{su}_{2K} & \mathfrak{su}_K & \mathfrak{su}_K \\ 2 & 2 & 2 & \cdots & 2 & 2 \end{smallmatrix}}_{N-5(-2)\text{-curves}}$	$2K(N - 1) - 1$	$4NK - 8K$
$\hat{D}_N^{\mathfrak{su}_3}$	$\underbrace{\begin{smallmatrix} 2 & & 2 \\ \mathfrak{su}_2 & & \mathfrak{su}_3 & \mathfrak{su}_3 & \mathfrak{su}_2 \\ 2 & 2 & 2 & \cdots & 2 & 2 \end{smallmatrix}}_{N-5(-2)\text{-curves}}$	$3N - 8$	$6N - 18$
$\hat{D}_N^{\mathfrak{so}_8}$	$\underbrace{\begin{smallmatrix} \mathfrak{su}_2 & & \mathfrak{su}_2 \\ 2 & & 2 \\ \mathfrak{su}_2 & \mathfrak{so}_7 & \mathfrak{so}_8 & \mathfrak{so}_8 & \mathfrak{so}_7 & \mathfrak{su}_2 \\ 2 & 3 & 1 & 4 & 1 & \cdots & 4 & 1 & 3 & 2 \end{smallmatrix}}_{N-5(-4)\text{-curves}}$	$6N - 14$	$16N - 48$
$\hat{D}_N^{e_6}$	$\underbrace{\begin{smallmatrix} \mathfrak{su}_3 & & \mathfrak{su}_3 \\ 3 & & 3 \\ 1 & & 1 \\ \mathfrak{su}_3 & e_6 & \mathfrak{su}_3 & e_6 & \mathfrak{su}_3 & e_6 & \mathfrak{su}_3 \\ 3 & 1 & 6 & 1 & 3 & 16 & 1 & 3 & 1 & \cdots & 6 & 1 & 3 & 1 & 6 & 1 & 3 \end{smallmatrix}}_{N-5(-6)\text{-curves}}$	$12N - 26$	$48N - 144$

theories, but they differ from their SCFTs cousins as they are nonlocal and have an intrinsic length scale M_{string} . While the UV completion of such theories is not a standard quantum field theory, below the scale set by M_{string} , we can treat the theory as a QFT with a cutoff [78,79]. This nonlocal nature allows LSTs to experience T-duality; in [20] it was recognized that a robust feature for the exploration of the T-duality landscape of LSTs is the magnetic quiver of the Higgs branch.

As we have mentioned in Sec. II, 6D (1, 0) LSTs have a similar geometric construction in F-theory to the 6D (1, 0) SCFTs [41]. In this construction, the 6D (2, 0) LSTs arise when the curve configuration consists of an affine ADE Dynkin diagram formed out of (-2) -curves, with no reducible singular fibers supported over the compact curves. Thus, in this section, we consider 6D (1, 0) LSTs, and the magnetic quivers for their Higgs branches, which have Higgs branch renormalization group flows that evince SUSY-enhancement. This class of 6D (1, 0) LSTs has been considered, for example, in [41,80–87].

First, we revisit the 6D (1, 0) LSTs that are Higgsable to the 6D (2, 0) LSTs of A-type. These theories consist of a ring of conformal matter theories fused together. The LSTs that result from fusing N copies of $(\mathfrak{g}, \mathfrak{g})$ conformal matter, where \mathfrak{g} is an ADE Lie algebra, in this way are denoted $\hat{A}_{N-1}^{\mathfrak{g}}$. We have written their tensor branch curve configurations in Table V,²⁷ together with a variety of their well-studied properties. In fact, for Higgsable to (2, 0) LSTs of types A_1 and A_2 there are additional configurations; these occur when the endpoint configuration, obtained by repetitively blowing-down all (-1) -curves, consists of either two smooth rational curves of self-intersection (-2) intersecting at the single point of multiplicity two, or of three smooth rational curves of self-intersection (-2) all intersecting at a single point. These endpoints are referred to as *III* and *IV*, as these intersection patterns

²⁷A note on the notation of [41], when we write $// \cdots //$, we are indicating that the leftmost and rightmost curves in \cdots intersect, with intersection number one.

match those of the Kodaira-Neron fibers of the same labelling. Since we are principally concerned with DE-type SUSY enhancement in this paper, we do not enumerate these exceptional Higgsable to A-type $(2, 0)$ LSTs.

Let us now consider 6D (1, 0) LSTs Higgsable to D-type (2, 0) LSTs. The generic class takes the form,²⁸

$$\begin{array}{ccccccc} & \frac{\mathfrak{su}_{k_2}}{2} & & & \frac{\mathfrak{su}_{k_{N+1}}}{2} & & \\ \frac{\mathfrak{su}_{k_1}}{2} & & \frac{\mathfrak{su}_{k_3}}{2} & \frac{\mathfrak{su}_{k_4}}{2} & \cdots & \frac{\mathfrak{su}_{k_{N-2}}}{2} & \frac{\mathfrak{su}_{k_{N-1}}}{2} & \frac{\mathfrak{su}_{k_N}}{2} \\ & & \underbrace{\hspace{10em}}_{N-5} & & & & & \end{array}. \quad (8.1)$$

Anomaly cancellation fixes that the k_i must satisfy the condition that

$$A^{ij}k_j = m_i \geq 0, \quad (8.2)$$

where A^{ij} is the affine Cartan matrix of D_N . In fact, almost all solutions are parametrized by a single positive integer K , and take the form

$$\frac{\mathfrak{su}_K}{2} \quad \frac{\mathfrak{su}_K}{2} \quad \frac{\mathfrak{su}_K}{2} \quad \frac{\mathfrak{su}_{2K}}{2} \quad \underbrace{\frac{\mathfrak{su}_{2K}}{2} \cdots \frac{\mathfrak{su}_{2K}}{2}}_{N-5} \quad \frac{\mathfrak{su}_{2K}}{2} \quad \frac{\mathfrak{su}_K}{2} . \quad (8.3)$$

Therefore, we refer to this class of LSTs as

$$\hat{D}_N^{\mathfrak{su}_{2K}}. \quad (8.4)$$

Here, we have removed those solutions of Eq. (8.2) which are incompatible with the F-theory geometry, as discussed around Eq. (2.7).

We can also consider the LSTs that arise as the affinization of the tensor branch configuration in Eq. (2.20)

$$\begin{array}{cccccccccccccccccccc} & & \mathfrak{su}_3 & & & & & & & & & & & & & & & \mathfrak{su}_3 & & \\ & & 3 & & & & & & & & & & & & & & & 3 & & \\ & & 1 & & & & & & & & & & & & & & & 1 & & \\ & & & & & \overbrace{\hspace{1.5cm}}^{N=5} & & & & & & & & & & & & & & & \\ \mathfrak{su}_3 & e_6 & \mathfrak{su}_3 & e_6 & \mathfrak{su}_3 & & e_6 & \mathfrak{su}_3 & & e_6 & \mathfrak{su}_3 & & e_6 & \mathfrak{su}_3 & & e_6 & \mathfrak{su}_3 & & \\ 3 & 1 & 6 & 1 & 3 & 16 & 1 & 3 & 1 & \cdots & 6 & 1 & 3 & 1 & 6 & 1 & 3 & . \end{array} \quad (8.5)$$

Finally, we note that there are two additional 6D (1, 0) LSTs Higgsable to 6D (2, 0) D-type LSTs, analogous to those appearing in Eq. (2.21). These have tensor branch configurations of the following forms:

²⁸Recall that a 6D (1, 0) LST is associated with a tensor branch curve configuration together with a choice of contraction map. Such contraction maps are in general not unique [88], and thus we should consider each curve configuration as being associated with a family of LSTs parametrized by possible contraction maps.

$$\begin{array}{c} 2 \\ \text{\tiny \mathfrak{su}_2} \\ 2 \end{array} \begin{array}{c} 2 \\ \text{\tiny \mathfrak{su}_3} \\ 2 \end{array} \underbrace{\begin{array}{c} 2 \\ \text{\tiny \mathfrak{su}_3} \\ 2 \end{array} \cdots \begin{array}{c} 2 \\ \text{\tiny \mathfrak{su}_2} \\ 2 \end{array}}_{N-5} \begin{array}{c} 2 \\ \text{\tiny \mathfrak{su}_2} \\ 2 \end{array} \quad \text{and} \quad \begin{array}{c} \text{\tiny \mathfrak{su}_2} \\ 2 \\ \text{\tiny \mathfrak{su}_2} \end{array} \begin{array}{c} \text{\tiny \mathfrak{su}_7} \\ 3 \end{array} \begin{array}{c} \text{\tiny \mathfrak{su}_8} \\ 1 \end{array} \underbrace{\begin{array}{c} \text{\tiny \mathfrak{su}_8} \\ 4 \end{array} \cdots \begin{array}{c} \text{\tiny \mathfrak{su}_8} \\ 4 \end{array}}_{N-5} \begin{array}{c} \text{\tiny \mathfrak{su}_7} \\ 3 \end{array} \begin{array}{c} \text{\tiny \mathfrak{su}_2} \\ 2 \end{array} . \quad (8.6)$$$

In Eqs. (8.3) and (8.5), and the left of Eq. (8.6),²⁹ we can take $N = 4$, in which case the two curves which intersect three other curves are identified. Note: for particularly small values of N , there are additional 6D (1, 0) LSTs that are Higgsable to the (2, 0) LSTs of D-type, however, we do not consider them further in this work.

A similar analysis can be performed for the 6D (1, 0) LSTs that are Higgsable to the 6D (2, 0) LSTs of E-type. For E_6 the only possibilities are

[illegible]

For E_7 there is still one exceptional theory, in addition to the standard family; altogether,

[illegible]

whereas for E_8 we have simply,

$$\frac{\mathfrak{su}_{3K}}{2} \frac{\mathfrak{su}_K}{2} \frac{\mathfrak{su}_{2K}}{2} \frac{\mathfrak{su}_{3K}}{2} \frac{\mathfrak{su}_{4K}}{2} \frac{\mathfrak{su}_{5K}}{2} \frac{\mathfrak{su}_{6K}}{2} \frac{\mathfrak{su}_{4K}}{2} \frac{\mathfrak{su}_{2K}}{2} . \quad (8.10)$$

Each of the 6D (1, 0) LSTs which have SUSY-enhancing Higgs branch RG flows to the 6D (2, 0) LSTs that we have just found are written in Tables V and VI.

We now turn to a discussion of the physical properties of little string theories. LSTs possess a $\mathfrak{u}(1)_{\text{LST}}^{(1)}$ one-form symmetry. The symmetry structure of LSTs typically involves combined transformations involving the

²⁹For the configuration on the right in Eq. (8.6), when we take the $N = 4$ limit we have the configuration,

$$\frac{g_{u_2}}{2} \frac{g_2}{2} \frac{g_{u_2}}{2} . \quad (8.7)$$

TABLE VI. The continuation of Table V; see the caption there for the details.

LST	Curve configuration	$\dim(\mathcal{C})$	κ_R
$\hat{E}_6^{\mathfrak{su}_{3K}}$	\mathfrak{su}_K 2 \mathfrak{su}_{2K} 2 $\mathfrak{su}_K \mathfrak{su}_{2K} \mathfrak{su}_{3K} \mathfrak{su}_{2K} \mathfrak{su}_K$ $2 \ 2 \ 2 \ 2 \ 2$	$12K - 1$	$24K$
$\hat{E}_6^{\mathfrak{q}_2}$	2 \mathfrak{su}_2 2 $\mathfrak{su}_2 \mathfrak{q}_2 \mathfrak{su}_2$ $2 \ 2 \ 2 \ 2 \ 2$	11	27
$\hat{E}_6^{e_7}$	\mathfrak{su}_2 2 \mathfrak{so}_7 3 \mathfrak{su}_2 2 1 $\mathfrak{su}_2 \mathfrak{so}_7 \mathfrak{su}_2$ $2 \ 3 \ 2 \ 1 \ 8 \ 1 \ 2 \ 3 \ 2$	34	144
$\hat{E}_7^{\mathfrak{su}_{4K}}$	\mathfrak{su}_{2K} 2 $\mathfrak{su}_K \mathfrak{su}_{2K} \mathfrak{su}_{3K} \mathfrak{su}_{4K} \mathfrak{su}_{3K} \mathfrak{su}_{2K} \mathfrak{su}_K$ $2 \ 2 \ 2 \ 2 \ 2 \ 2 \ 2$	$18K - 1$	$48K$
$\hat{E}_7^{\mathfrak{f}_4}$	\mathfrak{su}_3 3 1 $\mathfrak{su}_2 \mathfrak{q}_2 \mathfrak{f}_4 \mathfrak{q}_2 \mathfrak{su}_2$ $2 \ 2 \ 3 \ 1 \ 5 \ 13 \ 2 \ 2$	22	96
$\hat{E}_8^{\mathfrak{su}_{6K}}$	\mathfrak{su}_{3K} 2 $\mathfrak{su}_K \mathfrak{su}_{2K} \mathfrak{su}_{3K} \mathfrak{su}_{4K} \mathfrak{su}_{5K} \mathfrak{su}_{6K} \mathfrak{su}_{4K} \mathfrak{su}_{2K}$ $2 \ 2 \ 2 \ 2 \ 2 \ 2 \ 2 \ 2$	$30K - 1$	$120K$

background field of the one-form symmetry, together with the background fields of the zero-form symmetries; $\mathfrak{su}(2)_R$, \mathfrak{p} , and \mathfrak{f} [89,90]. Here, $\mathfrak{su}(2)_R$ is the R-symmetry, \mathfrak{p} denotes the Poincaré symmetry, and \mathfrak{f} encodes any additional flavor symmetry. This symmetry structure, sometimes referred to as Green-Schwarz symmetry,³⁰ can be written as

$$(\mathfrak{su}(2)_R \oplus \mathfrak{p} \oplus \mathfrak{f})^{(0)} \times \kappa_R, \kappa_P, \kappa_F \mathfrak{u}(1)_{\text{LST}}^{(1)}. \quad (8.11)$$

The quantities κ_R , κ_P , and κ_F capture how the R-symmetry, Poincaré symmetry, and flavor symmetries, respectively, mix with the one-form symmetry; they are referred to as the generalized symmetry structure constants. For each of the LSTs that have SUSY-enhancing Higgs branch RG flows, we have $\kappa_P = 0$ and there generically is no non-Abelian flavor symmetry³¹; therefore, we only consider κ_R from this point onwards. One of

³⁰See [91], for a careful analysis of such continuous Green-Schwarz symmetries, highlighting several major subtleties.

³¹Even in the cases of (2, 0) LSTs realized as a cluster of undecorated (−2)-curves intersecting as an affine Dynkin diagram where an $SU(2)$ flavor symmetry can be identified, we choose not to consider κ_F for simplicity.

the key results of [90,92] is that the structure constants can be determined from the F-theory geometry; in particular,

$$\kappa_R = \sum_i \ell_i h_{\mathfrak{g}_i}^\vee. \quad (8.12)$$

Here, the sum runs over the compact curves at the generic point of the tensor branch, ℓ_i is the normalized zero eigenvector associated with the zero eigenvalue of the intersection matrix,

$$A^{ij} \ell_j = 0 \quad \text{such that} \quad \ell_j > 0 \quad \text{and} \quad \gcd(\ell_1, \ell_2, \dots) = 1, \quad (8.13)$$

and $h_{\mathfrak{g}_i}^\vee$ is the dual Coxeter number of the algebra \mathfrak{g}_i supported over the i th curve.³²

Furthermore, we can consider moduli spaces of supersymmetric vacua associated with the LSTs. We can consider the dimension of the Coulomb branch of the five-dimensional theory that is obtained via compactification of the LST on an S^1 . This quantity can be obtained from the configuration at the generic point of the tensor branch as follows:

$$\dim(\mathcal{C}) = \sum_i (1 + \text{rank}(\mathfrak{g}_i)) - 1. \quad (8.14)$$

The sum runs over the compact curves C_i supporting algebras \mathfrak{g}_i .

For each of the Higgsable to (2, 0) LSTs that we study in this paper, we compute these two physical quantities, κ_R and $\dim(\mathcal{C})$, and we list them in Tables V and VI. We remind the reader that these quantities depend only on the tensor branch curve configuration, and not the choice of contraction map, and thus we can write them down without specifying the latter.

One of the exciting features of LSTs that follows from their nonlocal nature is T-duality. Two LSTs are said to be T-dual if they give rise to the same theory after circle compactification. More specifically, if \mathcal{T}_1 and \mathcal{T}_2 are 6D LSTs, then we can consider the S^1 compactifications, with radii R_1 and R_2 , where, along the circles, we can turn on Wilson lines valued in the (continuous) flavor symmetry of the LSTs. We denote these compactified theories as

$$\mathcal{T}_1 \langle S_{R_1}^1, \text{WL}_1 \rangle \quad \text{and} \quad \mathcal{T}_2 \langle S_{R_2}^1, \text{WL}_2 \rangle, \quad (8.15)$$

where WL_i abstractly specifies which Wilson lines are turned on. If these two 5D theories are identical, at some point on the Coulomb branch and for some choices of WL_1 and WL_2 , then \mathcal{T}_1 and \mathcal{T}_2 are said to be T-dual.

To identify a T-dual pair, we should see that both \mathcal{T}_1 and \mathcal{T}_2 are engineered in string theory from the same compactification space, up to inequivalent fibration structures

³²If the singular fiber is irreducible over the curve C_i , then we define $h_{\mathfrak{g}_i}^\vee = 1$.

on that space; this approach was pioneered in [88]. Alternatively, one can identify putative T-dual pairs by determining invariants of the theories \mathcal{T}_1 and \mathcal{T}_2 which are known to either be unchanged or change predictably under the S^1 -compactification with Wilson lines. Some examples of such T-duality invariant properties are [90]

$$\kappa_P, \quad \kappa_R, \quad \kappa_F, \quad \dim(\mathcal{C}), \quad \text{rank}(\mathfrak{f}), \quad (8.16)$$

where the latter is the rank of the 6D flavor algebra. This provides a necessary, but not sufficient, condition for T-duality. In general, the 6D Higgs branch does not match across T-duality, as the choice of Wilson lines modifies the 5D Higgs branch from the 6D Higgs branch. However, in cases where there is no flavor symmetry in 6D, there are no Wilson lines to turn on, and the 5D Higgs branch is identical to the 6D Higgs branch, and thus any T-dual pair $(\mathcal{T}_1, \mathcal{T}_2)$ must satisfy

$$\mathcal{H}_{\mathcal{T}_1} = \mathcal{H}_{\mathcal{T}_2}, \quad (8.17)$$

where $\mathcal{H}_{\mathcal{T}}$ denotes the Higgs branch of theory \mathcal{T} . For some of the Higgsable to DE-type (2, 0) LSTs that we consider in this paper, there is no 6D flavor symmetry, and thus the Higgs branches of any T-dual pair must match.

In Tables V and VI, we have written the putative T-dual for each 6D (1, 0) LSTs evincing DE-type SUSY enhancement by identifying another LSTs where the numerical invariants in Eq. (8.16) match. Importantly, each of these quantities is independent of the choice of contraction map, and thus they can be determined directly from the curve configuration; the Higgs branch itself is sensitive to the choice of contraction map, and we discuss this particular subtlety anon.

Since we have enumerated a collection of LSTs that realize Higgs branch RG flows with SUSY enhancement in Tables V and VI, together with their T-duality invariant properties, we can identify pairs of LSTs for which $\dim(\mathcal{C})$ and κ_R [as well as κ_P , κ_F , and $\text{rank}(\mathfrak{f})$] match. We find that the putative T-duals for each of the five classes of LSTs whose base geometry is a ring of (-2) -curves are as follows:

$$\begin{aligned} \hat{A}_{N-1}^{\mathfrak{su}_K} &\leftrightarrow \hat{A}_{K-1}^{\mathfrak{su}_N}, \\ \hat{A}_{N-1}^{\mathfrak{so}_{2K}} &\leftrightarrow \hat{D}_K^{\mathfrak{su}_{2N}}, \\ \hat{A}_{N-1}^{e_6} &\leftrightarrow \hat{E}_6^{\mathfrak{su}_{3N}}, \\ \hat{A}_{N-1}^{e_7} &\leftrightarrow \hat{E}_7^{\mathfrak{su}_{4N}}, \\ \hat{A}_{N-1}^{e_8} &\leftrightarrow \hat{E}_8^{\mathfrak{su}_{6N}}. \end{aligned} \quad (8.18)$$

We note that this is expected from fiber-base duality, as was already pointed out in [41]; see also [83] for a careful analysis of the second row. Next, we can consider a possible T-dual for the $\hat{D}_N^{e_6}$ LST. It is easy to see that there is no other theory in Tables V or VI for which the numerical

invariants match. Instead, consider the LSTs associated with the following tensor branch curve configuration:

$$\begin{array}{c} \mathfrak{so}_{2N} \\ 4 \\ \mathfrak{sp}_{2N-8} \\ 1 \\ \mathfrak{so}_{2N} \quad \mathfrak{sp}_{2N-8} \quad \mathfrak{so}_{6N-16} \quad \mathfrak{sp}_{2N-8} \quad \mathfrak{so}_{2N} \\ 4 \quad 1 \quad 4 \quad 1 \quad 4 \end{array}. \quad (8.19)$$

The endpoint configuration for this theory is type IV; that is, it is three (-2) -curves that intersect simultaneously at one point. We label the associated LSTs as $IV^{\mathfrak{so}_{6N-16}}$. We can determine the T-duality invariant numerical quantities,

$$\dim(\mathcal{C}) = 12N - 26, \quad \kappa_R = 48N - 144. \quad (8.20)$$

Therefore, as all the numerical invariants we can compute agree, we have the putative T-duality,

$$\hat{D}_N^{e_6} \leftrightarrow IV^{\mathfrak{so}_{6N-16}}. \quad (8.21)$$

While a similar discussion for the putative LSTs T-dual to the $\hat{D}_N^{\mathfrak{su}_3}$, $\hat{D}_N^{\mathfrak{so}_8}$, $\hat{E}_6^{e_2}$, $\hat{E}_6^{e_7}$, and $\hat{E}_7^{f_4}$ theories can be carried out, it is beyond the scope of this paper and we leave it for future work.³³ Here, following the theme of this paper, we discuss the Higgs branches of some of these LSTs.

There are two approaches that we can take to determine the Higgs branch of the LSTs under discussion. We would like to capture a Higgs branch by providing a magnetic quiver, that is, a 3D $\mathcal{N} = 4$ Lagrangian quiver such that the Coulomb branch is isomorphic to the Higgs branch of the theory we are interested in. The first approach is to engineer the LSTs via a brane system in type IIA (or type I) string theory, and then pass to the magnetic phase; this is the approach we have taken for SCFTs throughout this paper.

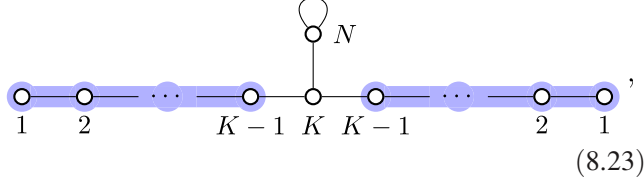
Alternatively, we can take advantage of the fact that LSTs satisfy the tensor decoupling condition [41], that is, if one takes the volume of any compact curve in the curve configuration of an LST to infinity, then one obtains either an SCFT or a product of SCFTs. In reverse, we can think of an LST as arising from the fusion of a non-Abelian flavor algebra of a product of SCFTs. If we know magnetic quivers for the Higgs branches of the fused SCFTs, then we can determine the magnetic quiver for the LST via Coulomb gauging of the Coulomb symmetry of the SCFT magnetic quivers.

We first consider the LSTs that we denote via $\hat{A}_{N-1}^{\mathfrak{su}_K}$; the tensor branch curve configuration of such LSTs takes the form of a ring of (-2) -curves, each supporting an $\mathfrak{su}(K)$ algebra. This LST can be obtained from the rank N ($\mathfrak{su}(K), \mathfrak{su}(K)$) conformal matter theory, and fusing the two $\mathfrak{su}(K)$ flavor factors. We depict this as

³³A detailed analysis of T-duality for nonheterotic LSTs recently appeared in [93].

$$[\mathfrak{su}(K)] \underbrace{2 \cdots 2}_{N-1} [\mathfrak{su}(K)] \xrightarrow{\text{fusion}} // \underbrace{2 \cdots 2}_N //. \quad (8.22)$$

The magnetic quiver for the Higgs branch of rank N ($\mathfrak{su}(K), \mathfrak{su}(K)$) conformal matter is [64]

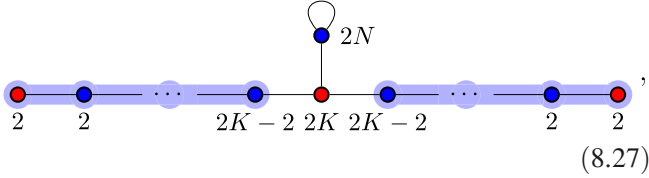


$$(8.23)$$

where the $\mathfrak{su}(K) \oplus \mathfrak{su}(K)$ Coulomb symmetry arises from the balanced nodes highlighted in blue. The behavior of the 3D quiver under Coulomb gauging follows from [94], and thus we find that the Higgs branch of the LST $\hat{A}_{N-1}^{\mathfrak{su}_K}$ is

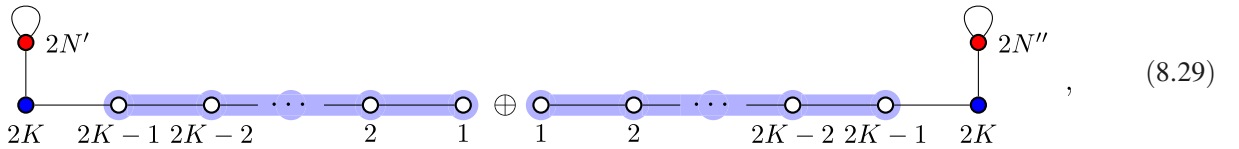
$$[\mathfrak{so}(2K)] \underbrace{\mathfrak{sp}_{K-4} \mathfrak{so}_{2K} \cdots \mathfrak{sp}_{K-4} \mathfrak{so}_{2K} \mathfrak{sp}_{K-4}}_{N-1(-4)\text{-curves}} [\mathfrak{so}(2K)] \xrightarrow{\text{fusion}} // \underbrace{\mathfrak{sp}_{K-4} \mathfrak{so}_{2K} \cdots \mathfrak{sp}_{K-4} \mathfrak{so}_{2K}}_{N(-4)\text{-curves}} //. \quad (8.26)$$

The magnetic quiver for the conformal matter theory is known [64]; it is



$$(8.27)$$

where, again, we have highlighted the balanced nodes giving rise to the $\mathfrak{so}(2K) \oplus \mathfrak{so}(2K)$ Coulomb symmetry.³⁵ The Coulomb gauging is described in [94], and thus we find that the magnetic quiver for the LST $\hat{A}_{N-1}^{\mathfrak{so}_{2K}}$ is



$$(8.29)$$

simply the Coulomb branch of the following quiver:



$$(8.24)$$

As we can see, this quiver is identical under $K \leftrightarrow N$, which is consistent with the T-duality³⁴

$$\hat{A}_{N-1}^{\mathfrak{su}_K} \leftrightarrow \hat{A}_{K-1}^{\mathfrak{su}_N}. \quad (8.25)$$

Next, we consider the LSTs $\hat{A}_{N-1}^{\mathfrak{so}_{2K}}$; these theories can be obtained via the diagonal fusion of the $\mathfrak{so}(2K) \oplus \mathfrak{so}(2K)$ flavor algebra of rank N ($\mathfrak{so}(2K), \mathfrak{so}(2K)$) conformal matter. Pictorially, we have



$$(8.28)$$

We are now ready to turn to the LSTs $\hat{D}_N^{\mathfrak{su}_{2K}}$. Such LSTs can be obtained via the diagonal fusion of the $\mathfrak{su}(2K)$ flavor symmetry of the SCFTs $D_{N'}^{\mathfrak{su}_{2K}}$ and $D_{N''}^{\mathfrak{su}_{2K}}$ where $N' + N'' = N$. The magnetic quivers of the Higgsable to D-type (2, 0) SCFTs have been determined in this paper; therefore, for the LSTs $\hat{D}_N^{\mathfrak{su}_{2K}}$, we have

³⁴Notice that this theory actually enjoys the triality [81]; $\hat{A}_{N-1}^{\mathfrak{su}_K} \leftrightarrow \hat{A}_{K-1}^{\mathfrak{su}_N} \leftrightarrow \hat{A}_{\ell-1}^{\mathfrak{su}_{N/K}}$ with $\ell = \gcd(N, K)$, not seen from the magnetic quiver.

³⁵The loop on the $\mathfrak{usp}(2N)$ gauge node denotes an antisymmetric hypermultiplet.

where the \oplus indicates Coulomb gauging along the Coulomb symmetries that arise from the blue-highlighted balanced nodes. When Coulomb gauging $\mathfrak{su}(2K)$ symmetries that are connected to $\mathfrak{usp}(2K)$ gauge nodes, the post-gauging $\mathfrak{usp}(2K)$ node picks up an antisymmetric hypermultiplet due to the decomposition of the adjoint representation of $\mathfrak{su}(2K)$, as discussed in [94–96]. Therefore, the result of the Coulomb gauging is

$$(8.30)$$

We can see that there are different Higgs branches for each of the combinations of $(N', N'') \geq (3, 3)$ such that $N' + N'' = N$ and $N' \leq N''$. This reflects the fact that to prescribe an LST we must give both a tensor branch curve configuration and a contraction map; the contraction map is not unique, and the choice can be captured by the splitting of N into N' and N'' . We require that both N' and N'' are ≥ 3 as we have engineered this LST via fusion of $D_{N'}^{\mathfrak{su}_{2K}}$ and $D_{N''}^{\mathfrak{su}_{2K}}$ SCFTs, and we have only defined such theories when the number of (-2) -curves in the tensor branch configuration is at least three. The Higgs branch given by Eq. (8.30) does not match, under interchange of N and K , the Higgs branch

of the putative T-dual as given in Eq. (8.28) for any such choice of N' and N'' . However, the fusions that we have written here are not necessarily all of the distinct contraction maps for the tensor branch configuration in Eq. (8.3); with a sensible analytic continuation, we could believe that formally $N' = 0$ and $N'' = N$ captures a valid contraction map, and does in fact result in the same Higgs branch across the T-duality. A more careful matching and verification of these Higgs branches under T-duality would be an interesting subject for future research.

As a final point in this section, we highlight a family of LSTs which arise from the fusion of a $D_N^{\mathfrak{su}_{2K}}$ SCFT together with a rank N' ($\mathfrak{e}_8, \mathfrak{su}(2K)$) orbi-instanton SCFT. The latter is the SCFT that arises on a stack of N' M5-branes probing a $\mathbb{C}^2/\mathbb{Z}_{2K}$ orbifold singularity, and contained inside of an M9-brane [23]. We can depict this fusion as follows:

$$\begin{aligned}
 & \underbrace{\begin{array}{c} \mathfrak{su}_K \\ 2 \\ \mathfrak{su}_K \mathfrak{su}_{2K} \mathfrak{su}_{2K} \dots \mathfrak{su}_{2K} \\ 2 \quad 2 \quad 2 \quad \dots \quad 2 \end{array}}_{N(-2)\text{-curves}} [\mathfrak{su}(2K)] \oplus [\mathfrak{su}(2K)] \underbrace{\begin{array}{c} \mathfrak{su}_{2K} \mathfrak{su}_{2K} \mathfrak{su}_{2K-1} \mathfrak{su}_2 \\ 2 \dots 2 \quad 2 \dots 2 \end{array}}_{N'-1(-2)\text{-curves}} \\
 & \longrightarrow \underbrace{\begin{array}{c} \mathfrak{su}_{2K} \\ 2 \\ \mathfrak{su}_K \mathfrak{su}_K \mathfrak{su}_{2K} \mathfrak{su}_{2K} \dots \mathfrak{su}_{2K} \mathfrak{su}_{2NK} \mathfrak{su}_{2K-1} \dots \mathfrak{su}_2 \\ 2 \quad 2 \quad 2 \quad \dots \quad 2 \quad \dots \quad 2 \end{array}}_{N+N'(-2)\text{-curves}} \dots 21,
 \end{aligned} \quad (8.31)$$

where the \oplus denotes the fusion of two $\mathfrak{su}(2K)$ flavor symmetries. We note that these LSTs have $\kappa_P = 2$, and thus they cannot be T-dual to the Higgsable to $(2, 0)$ LSTs we have discussed above; in fact, one can recognise the quiver structure as a frozen phase of F-theory³⁶ [97] corresponding to a $\text{Spin}(32)/\mathbb{Z}_2$ model without vector structure, from which T-dual models can be found in the realm of heterotic LSTs, recently been explored in, for

example, [20,98–103] by matching the generalized symmetry structure constants. The magnetic quiver for the orbi-instanton theory and its Higgsed products is well-known [34,104] (see [20] for a recent summary). Therefore, the procedure of Coulomb gauging again reveals the magnetic quiver for the Higgs branch of this family of LSTs; we find that it is the Coulomb branch of the following quiver:

$$(8.32)$$

³⁶We thank Paul-Konstantin Oehlmann for this observation.

where the \oplus now indicates the Coulomb gauging of the two highlighted $\mathfrak{su}(2K)$ Coulomb symmetries.

From the magnetic quivers for the Higgs branches of the LSTs, we can determine the foliation of the symplectic singularity capturing the fixed points under Higgs branch RG flow via the technique of quiver subtraction, as we have done for Higgsable to D-type SCFTs throughout this paper. We leave a careful analysis of the structure of the Higgs branches of LSTs, and the implications with regards to T-duality, for future work.

IX. DISCUSSION

In this paper, we have studied the renormalization group flows along the Higgs branch of 6D (1, 0) SCFTs which present supersymmetry enhancement along some locus inside of the Higgs branch. In particular, we were interested in the lesser-studied 6D (1, 0) SCFTs that have an enhancement to the DE-type (2, 0) SCFTs. From the geometric engineering perspective, almost all such theories are constructed in terms of elliptically fibered Calabi–Yau threefolds where the base contains a collection of (-2) -curves intersecting according to the associated DE-type Dynkin diagram. The singular fibers over these curves were of special unitary type, and interacting nonproduct SCFTs on the Higgs branch were obtained by (consistently) reducing the ranks of these special unitary algebras. Thus, this geometric picture allows the derivation (of the interacting nonproduct subdiagram) of the Higgs branch Hasse diagram, but without the information of the transverse slices in the foliation of the symplectic singularity.

Focusing on the Higgsable to D-type (2, 0) theories, a type IIA realization is explicitly given via a system of D6-D8-NS5-branes in the presence of an ON^- -plane. This brane construction of the theory is crucial since it allows, with due extensions, the application of the magnetic quiver technique to study the Higgs branch of the six-dimensional theory. In fact, from a joint approach intertwining tensor branch geometries and magnetic quivers, it has been rendered possible to describe not only the various leaves in the Higgs branch of $D_N^{\mathfrak{su}_{2k}}(O)$ theories but also the transverse slices between them. The lessons learnt from the D-type case can then be conjectured to extend to Higgsable to E-type (2, 0) models, for which a controlled type IIA brane system is not available. Therefore, the proposed new slice subtraction method allows the construction of the Hasse diagram by simply looking at the tensor branch curve configuration and subtracting the Dynkin labels of the appropriate Dynkin diagram from the ranks of the gauge algebras.

While most of this paper was concerned with the 6D (1, 0) SCFTs that have a Higgs branch renormalization group flow to the 6D (2, 0) SCFTs; the same techniques can be used to study the Higgs branch of little string theories. We considered the natural “affinized extension” of the SCFTs considered in this paper, that is, the 6D (1, 0)

LSTs that are Higgsable to the 6D (2, 0) LSTs. We derive the magnetic quivers for the Higgs branches and determine the structure constants of the generalized symmetries, which led to some interesting observations about T-dualities of LSTs.

Quiver subtraction for (unitary-)orthosymplectic quivers: As we highlighted throughout Sec. V, when constructing the Hasse diagram from the unitary-orthosymplectic magnetic quiver there are several subtleties. One important caveat was that the unitary-orthosymplectic quiver subtraction algorithm that we motivated from the brane dynamics perspective is incomplete; subtractions involving the special orthogonal gauge node with antisymmetric matter were not defined. Thus, the Hasse diagram as derived via the subtraction algorithm is only a subdiagram of the Higgs branch Hasse diagram of the 6D SCFT. This subtlety is deeply connected to the orthosymplectic analog of the notion of decoration [58], which has yet to be understood. Relatedly, the 6D (2, 0) SCFT that lives at the “end” of the Higgs branch RG flow still has a nontrivial Higgs branch, indicating that there exist further Higgsings which we have not captured; in Sec. VI, we understood some of these Higgsings from a geometric perspective.

An extreme example of this subtlety with decoration in the unitary-orthosymplectic case can be seen in the $D_3^{\mathfrak{su}_2}([1^2])$ SCFT. In addition to the unitary-orthosymplectic magnetic quiver for the Higgs branch that has been the principle object of study in this paper, there exist two unitary 3D $\mathcal{N} = 4$ quivers which have the same Coulomb branch Hilbert series as the unitary-orthosymplectic quiver [62]. These three quivers are depicted on the right in Fig. 20. Whereas in the unitary case, the extraction of the Hasse diagram (shown on the left in Fig. 20) from the quiver is fully under control and reproduces that expected from the 6D geometry, for the unitary-orthosymplectic quiver the lack of a notion of decoration hinders an analogous procedure, and only a subdiagram of the full Hasse diagram can be produced.³⁷ This plurality of descriptions, from the geometry and alternative unitary quivers, should provide an important hint at the nature of decoration for orthosymplectic quivers.

Noninvertible symmetries across the Higgs branch: The 6D (2, 0) SCFTs of type D_{2n} have noninvertible global symmetries [105], realized via the duality defect construction [106,107]. This occurs because the intermediate defect group, $\mathbb{Z}_2 \oplus \mathbb{Z}_2$, admits distinct polarizations, related via gauging of two-form symmetries, and there exists a Green-Schwarz automorphism/duality [108] which acts on the charge lattice of stringlike defects. When combined, these lead to noninvertible duality defects; see [105,109] for

³⁷In fact, in this $D_3^{\mathfrak{su}_2}([1^2])$ example, the subdiagram observable from the unitary-orthosymplectic quiver consists only of a single vertex; in more general examples it is a more involved subdiagram.

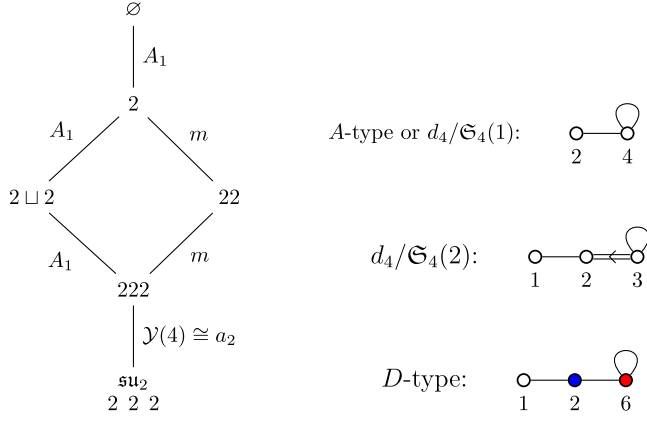


FIG. 20. Hasse diagram for the $D_3^{su_2}([1^2])$ theory, along with the different magnetic quiver realizations of the Higgs branch.

details and references. For long 6D (1, 0) SCFTs $D_N^{su_{2k}}(O)$, the \mathbb{Z}_2 Green-Schwarz automorphism still exists, and thus the noninvertible symmetries are also realized in such theories; that is, at any interacting nonproduct fixed point on the Higgs branch of these Higgsable to D-type (2, 0) SCFTs, the noninvertible symmetry is preserved. In contrast, for short quivers, certain choices of generalized partition can break the \mathbb{Z}_2 Green-Schwarz automorphism, thereby destroying the duality defect construction of the noninvertible symmetries. Thus, for short quivers, the noninvertible symmetries appear to be alternatively broken and emergent along various loci in the Higgs branch. It would be interesting to make a detailed study of the microscopic behavior of such noninvertible symmetries along Higgs branch renormalization group flows.

Higgs branches and 4d reductions: While we have studied the Higgs branches of 6D (1, 0) SCFTs in this paper, it is well-known that compactifying on a d -dimensional torus T^d leads to a lower-dimensional field theory which has the same Higgs branch as the original 6D SCFT. Such lower-dimensional theories may have dual constructions, and this may lead to different perspectives on the Higgs branch. For example, a 6D (1, 0) SCFT compactified on a T^2 may have a dual description via the class \mathcal{S} construction [110,111]. That is, starting from a 6D (2, 0) SCFT and compactifying on a punctured Riemann surface. Class \mathcal{S} theories have known magnetic quivers, see e.g., [94], and thus any class \mathcal{S} duals can lead to distinct magnetic quivers for the 6D Higgs branch, and patching together these different descriptions may lead to an understanding of aspects of the Higgs branch that are obscured in one formulation. This plurality of origins was vital for studying the Higgs branch of 6D conformal matter in [45,49].

Furthermore, when compactifying on a torus, one is free to turn on a nontrivial Stiefel-Whitney twist, which leads to classes of novel 4D $\mathcal{N} = 2$ SCFTs related to S -folds [112–117]; these theories often have an interesting Higgs branch structure that can be related to the magnetic quiver for the 6D (1, 0) Higgs branch via folding-type operations [118,119]. Determining the structure of the Higgs branch of such SCFTs originating in the 6D (1, 0) SCFTs Higgsable to D-type would be a natural extension of the current work. In another direction, the 6D (1, 0) SCFTs Higgsable to the A-type (2, 0) SCFT were important for proving subtle dualities amongst class \mathcal{S} theories in [120]; it is natural to ask if there are analogous dualities that can also be studied from the perspective of the Higgs branch in the D-type sector.

Complex structure deformations of CY_3 : From the geometric engineering perspective, the Higgs branch of 6D (1, 0) SCFTs is encoded in the complex structure deformations of the associated Calabi-Yau threefold. A systematic study of such deformation spaces has not been carried out (however, see [121,122]), even at the level of determining when two Calabi-Yau threefolds associated with 6D (1, 0) SCFTs are connected, let alone the extraction of the transverse slice between them. Given that the approach via the magnetic quiver for the Higgs branch, for theories which admit a brane engineering description, can be utilized to determine the structure of the Higgs branch, it should be possible to draw a clearer connection between the quiver subtraction algorithm for 3D $\mathcal{N} = 4$ quivers and complex structure deformations of singular elliptically-fibered Calabi-Yau threefolds. For specific geometries engineering little string theories, steps have been taken in this direction in [102], where all the deformations have been tracked and associated with different transverse slices in the Hasse diagram for LSTs where the tensor branch geometry involves a single curve of self-intersection 0. We hope to return to such questions in the future.

ACKNOWLEDGMENTS

We thank Florent Baume, Jacques Distler, Julius Grimminger, Monica Jinwoo Kang, and Deshuo Liu for interesting discussions. The authors acknowledge support from DESY (Hamburg, Germany), a member of the Helmholtz Association HGF. This work was partially supported by the Deutsche Forschungsgemeinschaft under Germany’s Excellence Strategy—EXC 2121 “Quantum Universe”—390833306 and the Collaborative Research Center—SFB 1624 “Higher Structures, Moduli Spaces, and Integrability”—506632645.

- [1] W. Nahm, Supersymmetries and their representations, *Nucl. Phys.* **B135**, 149 (1978).
- [2] N. Seiberg, Nontrivial fixed points of the renormalization group in six-dimensions, *Phys. Lett. B* **390**, 169 (1997).
- [3] A. Strominger, Open p-branes, *Phys. Lett. B* **383**, 44 (1996).
- [4] E. Witten, Some comments on string dynamics, in *STRINGS 95: Future Perspectives in String Theory* (1995), Vol. 7, pp. 501–523, [arXiv:hep-th/9507121](#).
- [5] M. Buican, J. Hayling, and C. Papageorgakis, Aspects of superconformal multiplets in $D > 4$, *J. High Energy Phys.* **11** (2016) 091.
- [6] C. Cordova, T. T. Dumitrescu, and K. Intriligator, Anomalies, renormalization group flows, and the a-theorem in six-dimensional $(1, 0)$ theories, *J. High Energy Phys.* **10** (2016) 080.
- [7] C. Cordova, T. T. Dumitrescu, and K. Intriligator, Deformations of superconformal theories, *J. High Energy Phys.* **11** (2016) 135.
- [8] C. Cordova, T. T. Dumitrescu, and K. Intriligator, Multiplets of superconformal symmetry in diverse dimensions, [arXiv:1612.00809](#).
- [9] J. Louis and S. Lüst, Supersymmetric AdS_7 backgrounds in half-maximal supergravity and marginal operators of $(1, 0)$ SCFTs, *J. High Energy Phys.* **10** (2015) 120.
- [10] P. C. Argyres, J. J. Heckman, K. Intriligator, and M. Martone, Snowmass white paper on SCFTs, [arXiv:2202.07683](#).
- [11] J. J. Heckman, D. R. Morrison, T. Rudelius, and C. Vafa, Atomic classification of 6D SCFTs, *Fortschr. Phys.* **63**, 468 (2015).
- [12] J. J. Heckman, D. R. Morrison, and C. Vafa, On the classification of 6D SCFTs and generalized ADE orbifolds, *J. High Energy Phys.* **05** (2014) 028.
- [13] J. J. Heckman and T. Rudelius, Top down approach to 6D SCFTs, *J. Phys. A* **52**, 093001 (2019).
- [14] J. J. Heckman, T. Rudelius, and A. Tomasiello, Fission, fusion, and 6D RG flows, *J. High Energy Phys.* **02** (2019) 167.
- [15] E. Witten, Small instantons in string theory, *Nucl. Phys.* **B460**, 541 (1996).
- [16] J. McKay, Graphs, singularities, and finite groups, in *The Santa Cruz Conference on Finite Groups (University of California, Santa Cruz, California, 1979), Proceedings of Symposia in Pure Mathematics* (American Mathematical Society, Providence, RI, 1980), Vol. 37, pp. 183–186.
- [17] D. R. Morrison and C. Vafa, Compactifications of F theory on Calabi–Yau threefolds. 1, *Nucl. Phys.* **B473**, 74 (1996).
- [18] C. Vafa, Evidence for F theory, *Nucl. Phys.* **B469**, 403 (1996).
- [19] D. R. Morrison and C. Vafa, Compactifications of F theory on Calabi–Yau threefolds. 2, *Nucl. Phys.* **B476**, 437 (1996).
- [20] C. Lawrie and L. Mansi, The Higgs branch of heterotic LSTs: Hasse diagrams and generalized symmetries, [arXiv:2312.05306](#).
- [21] K. Ohmori, H. Shimizu, Y. Tachikawa, and K. Yonekura, 6d $\mathcal{N} = (1, 0)$ theories on T^2 and class S theories: Part I, *J. High Energy Phys.* **07** (2015) 014.
- [22] K. Ohmori, H. Shimizu, Y. Tachikawa, and K. Yonekura, 6d $\mathcal{N} = (1, 0)$ theories on S^1/T^2 and class S theories: Part II, *J. High Energy Phys.* **12** (2015) 131.
- [23] M. Del Zotto, J. J. Heckman, A. Tomasiello, and C. Vafa, 6d conformal matter, *J. High Energy Phys.* **02** (2015) 054.
- [24] J. Chen, B. Haghighat, S. Liu, and M. Sperling, 4d $N = 1$ from 6d D-type $N = (1, 0)$, *J. High Energy Phys.* **01** (2020) 152.
- [25] H. Hayashi, S.-S. Kim, K. Lee, M. Taki, and F. Yagi, More on 5d descriptions of 6d SCFTs, *J. High Energy Phys.* **10** (2016) 126.
- [26] A. Beauville, Symplectic singularities, *Inventiones Math.* **139**, 541 (2000).
- [27] N. J. Hitchin, A. Karlhede, U. Lindstrom, and M. Rocek, Hyperkahler metrics and supersymmetry, *Commun. Math. Phys.* **108**, 535 (1987).
- [28] A. Bourget, S. Cabrera, J. F. Grimminger, A. Hanany, M. Sperling, A. Zajac, and Z. Zhong, The Higgs mechanism—Hasse diagrams for symplectic singularities, *J. High Energy Phys.* **01** (2020) 157.
- [29] A. Bourget, M. Sperling, and Z. Zhong, Decay and fission of magnetic quivers, [arXiv:2312.05304](#).
- [30] J. J. Heckman, D. R. Morrison, T. Rudelius, and C. Vafa, Geometry of 6D RG flows, *J. High Energy Phys.* **09** (2015) 052.
- [31] G. Ferlito, A. Hanany, N. Mekareeya, and G. Zafrir, 3d Coulomb branch and 5d Higgs branch at infinite coupling, *J. High Energy Phys.* **07** (2018) 061.
- [32] A. Hanany and E. Witten, Type IIB superstrings, BPS monopoles, and three-dimensional gauge dynamics, *Nucl. Phys.* **B492**, 152 (1997).
- [33] A. Hanany and A. Zaffaroni, Branes and six-dimensional supersymmetric theories, *Nucl. Phys.* **B529**, 180 (1998).
- [34] S. Cabrera, A. Hanany, and M. Sperling, Magnetic quivers, Higgs branches, and 6d $N = (1, 0)$ theories, *J. High Energy Phys.* **06** (2019) 071.
- [35] S. Cabrera, A. Hanany, and M. Sperling, Magnetic quivers, Higgs branches, and 6d $\mathcal{N} = (1, 0)$ theories—orthogonal and symplectic gauge groups, *J. High Energy Phys.* **02** (2020) 184.
- [36] A. Hanany and N. Mekareeya, The small E_8 instanton and the Kraft Procesi transition, *J. High Energy Phys.* **07** (2018) 098.
- [37] S. Cremonesi, A. Hanany, and A. Zaffaroni, Monopole operators and Hilbert series of Coulomb branches of 3d $\mathcal{N} = 4$ gauge theories, *J. High Energy Phys.* **01** (2014) 005.
- [38] S. Cabrera and A. Hanany, Quiver subtractions, *J. High Energy Phys.* **09** (2018) 008.
- [39] A. Bourget, M. Sperling, and Z. Zhong, Higgs branch RG-flows via decay and fission, [arXiv:2401.08757](#).
- [40] A. Kapustin, D(n) quivers from branes, *J. High Energy Phys.* **12** (1998) 015.
- [41] L. Bhardwaj, M. Del Zotto, J. J. Heckman, D. R. Morrison, T. Rudelius, and C. Vafa, F-theory and the classification of little strings, *Phys. Rev. D* **93**, 086002 (2016); **100**, 029901 (E) (2019).
- [42] J. Distler, M. J. Kang, and C. Lawrie, Distinguishing 6D $(1, 0)$ SCFTs: An extension to the geometric construction, *Phys. Rev. D* **106**, 066011 (2022).

- [43] D. R. Morrison and T. Rudelius, F-theory and unpaired tensors in 6D SCFTs and LSTs, *Fortschr. Phys.* **64**, 645 (2016).
- [44] F. Baume and C. Lawrie, The bestiary of 6d (1, 0, 0) SCFTs: Nilpotent orbits and anomalies, [arXiv:2312.13347](#).
- [45] F. Baume, M. J. Kang, and C. Lawrie, Two 6D origins of 4D SCFTs: Class S and 6D (1, 0) on a torus, *Phys. Rev. D* **106**, 086003 (2022).
- [46] K. Intriligator, 6d, $\mathcal{N} = (1, 0)$ Coulomb branch anomaly matching, *J. High Energy Phys.* **10** (2014) 162.
- [47] K. Ohmori, H. Shimizu, and Y. Tachikawa, Anomaly polynomial of E-string theories, *J. High Energy Phys.* **08** (2014) 002.
- [48] K. Ohmori, H. Shimizu, Y. Tachikawa, and K. Yonekura, Anomaly polynomial of general 6d SCFTs, *Prog. Theor. Exp. Phys.* **2014**, 103B07 (2014).
- [49] J. Distler, M. J. Kang, and C. Lawrie (to be published).
- [50] F. Baume, J. J. Heckman, and C. Lawrie, 6D SCFTs, 4D SCFTs, Conformal matter, and spin chains, *Nucl. Phys. B* **967**, 115401 (2021).
- [51] F. Baume, J. J. Heckman, and C. Lawrie, Super-spin chains for 6D SCFTs, *Nucl. Phys. B* **992**, 116250 (2023).
- [52] S. S. Razamat, E. Sabag, and G. Zafrir, From 6d flows to 4d flows, *J. High Energy Phys.* **12** (2019) 108.
- [53] O. Bergman, M. Fazzi, D. Rodríguez-Gómez, and A. Tomasiello, Charges and holography in 6d (1, 0) theories, *J. High Energy Phys.* **05** (2020) 138.
- [54] J. J. Heckman, T. Rudelius, and A. Tomasiello, 6D RG flows and nilpotent hierarchies, *J. High Energy Phys.* **07** (2016) 082.
- [55] N. Mekareeya, T. Rudelius, and A. Tomasiello, T-branes, anomalies and moduli spaces in 6D SCFTs, *J. High Energy Phys.* **10** (2017) 158.
- [56] A. Hanany and A. Zaffaroni, Issues on orientifolds: On the brane construction of gauge theories with $SO(2n)$ global symmetry, *J. High Energy Phys.* **07** (1999) 009.
- [57] A. Hanany and A. Zaffaroni, Chiral symmetry from type IIA branes, *Nucl. Phys. B* **509**, 145 (1998).
- [58] A. Bourget and J. F. Grimminger, Fibrations and Hasse diagrams for 6d SCFTs, *J. High Energy Phys.* **12** (2022) 159.
- [59] G. Ferlito and A. Hanany, A tale of two cones: The Higgs branch of $Sp(n)$ theories with $2n$ flavours, [arXiv:1609.06724](#).
- [60] M. Sperling and Z. Zhong, Balanced B and D-type orthosymplectic quivers—magnetic quivers for product theories, *J. High Energy Phys.* **04** (2022) 145.
- [61] K. Gledhill and A. Hanany, Coulomb branch global symmetry and quiver addition, *J. High Energy Phys.* **12** (2021) 127.
- [62] A. Hanany, G. Kumaran, C. Li, D. Liu, and M. Sperling, Actions on the quiver—Discrete quotients on the Coulomb branch, [arXiv:2311.02773](#).
- [63] A. Hanany and M. Sperling, Discrete quotients of 3-dimensional $\mathcal{N} = 4$ Coulomb branches via the cycle index, *J. High Energy Phys.* **08** (2018) 157.
- [64] A. Hanany and G. Zafrir, Discrete gauging in six dimensions, *J. High Energy Phys.* **07** (2018) 168.
- [65] A. Hanany and A. Zajac, Discrete gauging in Coulomb branches of three dimensional $\mathcal{N} = 4$ supersymmetric gauge theories, *J. High Energy Phys.* **08** (2018) 158.
- [66] A. Bourget, J. F. Grimminger, A. Hanany, and Z. Zhong, The Hasse diagram of the moduli space of instantons, *J. High Energy Phys.* **08** (2022) 283.
- [67] S. Cabrera and A. Hanany, Branes and the Kraft-Procesi transition, *J. High Energy Phys.* **11** (2016) 175.
- [68] S. Cabrera and A. Hanany, Branes and the Kraft-Procesi transition: Classical case, *J. High Energy Phys.* **04** (2018) 127.
- [69] A. Hanany and M. Sperling, Magnetic quivers and negatively charged branes, *J. High Energy Phys.* **11** (2022) 010.
- [70] D. Gaiotto and E. Witten, S-duality of boundary conditions in $N = 4$ super Yang-Mills theory, *Adv. Theor. Math. Phys.* **13**, 721 (2009).
- [71] S. Katz and D. R. Morrison, Gorenstein threefold singularities with small resolutions via invariant theory for Weyl groups (1992).
- [72] H. C. Pinkham, Factorization of birational maps in dimension 3, in *Singularities, Part 2 (Arcata, California, 1981)*, Proceedings of Symposia in Pure Mathematics Vol. 40 (American Mathematical Society, Providence, RI, 1983), pp. 343–371.
- [73] M. Reid, Minimal models of canonical 3-folds, in *Algebraic Varieties and Analytic Varieties (Tokyo, 1981)*, Advanced Studies in Pure Mathematics Vol. 1 (North-Holland, Amsterdam, 1983), pp. 131–180.
- [74] J. M. Wahl, Equisingular deformations of normal surface singularities. I, *Ann. Math.* **104**, 325 (1976).
- [75] J. M. Wahl, Elliptic deformations of minimally elliptic singularities, *Math. Ann.* **253**, 241 (1980).
- [76] B. Fu, D. Juteau, P. Levy, and E. Sommers, Generic singularities of nilpotent orbit closures, *Adv. Math.* **305**, 1 (2017).
- [77] J. F. Grimminger and A. Hanany, Hasse diagrams for 3d $\mathcal{N} = 4$ quiver gauge theories—Inversion and the full moduli space, *J. High Energy Phys.* **09** (2020) 159.
- [78] N. Seiberg, New theories in six-dimensions and matrix description of M theory on T^5 and T^5Z_2 , *Phys. Lett. B* **408**, 98 (1997).
- [79] O. Aharony, A brief review of “little string theories”, *Classical Quantum Gravity* **17**, 929 (2000).
- [80] B. Bastian, S. Hohenegger, A. Iqbal, and S.-J. Rey, Dual little strings and their partition functions, *Phys. Rev. D* **97**, 106004 (2018).
- [81] B. Bastian, S. Hohenegger, A. Iqbal, and S.-J. Rey, Triality in little string theories, *Phys. Rev. D* **97**, 046004 (2018).
- [82] B. Filoche, S. Hohenegger, and T. Kimura, Non-perturbative symmetries of little strings and affine quiver algebras, *J. High Energy Phys.* **02** (2024) 233.
- [83] B. Haghighat, J. Kim, W. Yan, and S.-T. Yau, D-type fiber-base duality, *J. High Energy Phys.* **09** (2018) 060.
- [84] S. Hohenegger, A. Iqbal, and S.-J. Rey, Self-duality and self-similarity of little string orbifolds, *Phys. Rev. D* **94**, 046006 (2016).

- [85] S. Hohenegger, A. Iqbal, and S.-J. Rey, Dual little strings from F-theory and flop transitions, *J. High Energy Phys.* **07** (2017) 112.
- [86] J. Kim and K. Lee, Little strings on D_n orbifolds, *J. High Energy Phys.* **10** (2017) 045.
- [87] X.-Y. Wei, Y. Sugimoto, F. Yagi, and S.-S. Kim, DE-type little strings from glued brane webs, *J. High Energy Phys.* **05** (2023) 214.
- [88] P. S. Aspinwall and D. R. Morrison, Point—like instantons on K3 orbifolds, *Nucl. Phys.* **B503**, 533 (1997).
- [89] C. Cordova, T. T. Dumitrescu, and K. Intriligator, 2-group global symmetries and anomalies in six-dimensional quantum field theories, *J. High Energy Phys.* **04** (2021) 252.
- [90] M. Del Zotto and K. Ohmori, 2-group symmetries of 6D little string theories and T-duality, *Ann. Henri Poincaré* **22**, 2451 (2021).
- [91] M. J. Kang and S. Kang, Central extensions of higher groups: Green–Schwarz mechanism and 2-connections, [arXiv:2311.14666](#).
- [92] M. Del Zotto, M. Liu, and P.-K. Oehlmann, 6D heterotic little string theories and F-theory geometry: An introduction, [arXiv:2303.13502](#).
- [93] F. Baume, P.-K. Oehlmann, and F. Ruehle, Bounds and dualities of type II little string theories, [arXiv:2405.03877](#).
- [94] F. Benini, Y. Tachikawa, and D. Xie, Mirrors of 3d Sicilian theories, *J. High Energy Phys.* **09** (2010) 063.
- [95] E. Beratto, S. Giacomelli, N. Mekareeya, and M. Sacchi, 3d mirrors of the circle reduction of twisted A_{2N} theories of class S, *J. High Energy Phys.* **09** (2020) 161.
- [96] M. J. Kang, C. Lawrie, K.-H. Lee, M. Sacchi, and J. Song, Higgs branch, Coulomb branch, and Hall-Littlewood index, *Phys. Rev. D* **106**, 106021 (2022).
- [97] P.-K. Oehlmann, F. Ruehle, and B. Sung, The frozen phase of heterotic F-theory duality, *J. High Energy Phys.* **07** (2024) 295.
- [98] L. Bhardwaj, Discovering T-dualities of little string theories, *J. High Energy Phys.* **02** (2024) 046.
- [99] M. Del Zotto, M. Fazzi, and S. Giri, The Higgs branch of heterotic ALE instantons, [arXiv:2307.11087](#).
- [100] M. Del Zotto, M. Liu, and P.-K. Oehlmann, Back to heterotic strings on ALE spaces: Part II—Geometry of T-dual little strings, [arXiv:2212.05311](#).
- [101] M. Del Zotto, M. Liu, and P.-K. Oehlmann, Back to heterotic strings on ALE spaces. Part I. Instantons, 2-groups and T-duality, *J. High Energy Phys.* **01** (2023) 176.
- [102] L. Mansi and M. Sperling, Unravelling T-duality: Magnetic quivers in rank-zero little string theories, [arXiv:2312.12510](#).
- [103] H. Ahmed, P.-K. Oehlmann, and F. Ruehle, T-duality and flavor symmetries in little string theories, [arXiv:2311.02168](#).
- [104] M. Fazzi, S. Giri, and P. Levy, Proving the 6d a-theorem with the double affine Grassmannian, [arXiv:2312.17178](#).
- [105] C. Lawrie, X. Yu, and H. Y. Zhang, Intermediate defect groups, polarization pairs, and noninvertible duality defects, *Phys. Rev. D* **109**, 026005 (2024).
- [106] Y. Choi, C. Cordova, P.-S. Hsin, H. T. Lam, and S.-H. Shao, Noninvertible duality defects in $3 + 1$ dimensions, *Phys. Rev. D* **105**, 125016 (2022).
- [107] J. Kaidi, K. Ohmori, and Y. Zheng, Kramers-Wannier-like duality defects in $(3 + 1)$ D gauge theories, *Phys. Rev. Lett.* **128**, 111601 (2022).
- [108] F. Apruzzi, J. J. Heckman, and T. Rudelius, Green-Schwarz automorphisms and 6D SCFTs, *J. High Energy Phys.* **02** (2018) 157.
- [109] S. Gukov, P.-S. Hsin, and D. Pei, Generalized global symmetries of $T[M]$ theories. Part I, *J. High Energy Phys.* **04** (2021) 232.
- [110] D. Gaiotto, $N = 2$ dualities, *J. High Energy Phys.* **08** (2012) 034.
- [111] D. Gaiotto, G. W. Moore, and A. Neitzke, Wall-crossing, Hitchin systems, and the WKB approximation, *Adv. Math.* **234**, 239 (2013).
- [112] S. Giacomelli, M. Martone, Y. Tachikawa, and G. Zafrir, More on $\mathcal{N} = 2$ S-folds, *J. High Energy Phys.* **01** (2021) 054.
- [113] S. Giacomelli, R. Savelli, and G. Zoccarato, $\mathcal{N} = 2$ orbi-S-folds, [arXiv:2405.00101](#).
- [114] J. J. Heckman, C. Lawrie, L. Lin, H. Y. Zhang, and G. Zoccarato, 6D SCFTs, center-flavor symmetries, and Stiefel-Whitney compactifications, *Phys. Rev. D* **106**, 066003 (2022).
- [115] J. J. Heckman, C. Lawrie, T. B. Rochais, H. Y. Zhang, and G. Zoccarato, S-folds, string junctions, and $\mathcal{N} = 2$ SCFTs, *Phys. Rev. D* **103**, 086013 (2021).
- [116] F. Apruzzi, S. Giacomelli, and S. Schäfer-Nameki, 4d $\mathcal{N} = 2$ S-folds, *Phys. Rev. D* **101**, 106008 (2020).
- [117] S. Giacomelli, C. Meneghelli, and W. Peelaers, New $\mathcal{N} = 2$ superconformal field theories from S-folds, *J. High Energy Phys.* **01** (2021) 022.
- [118] A. Bourget, S. Giacomelli, J. F. Grimminger, A. Hanany, M. Sperling, and Z. Zhong, S-fold magnetic quivers, *J. High Energy Phys.* **02** (2021) 054.
- [119] A. Bourget, J. F. Grimminger, M. Martone, and G. Zafrir, Magnetic quivers for rank 2 theories, *J. High Energy Phys.* **03** (2022) 208.
- [120] J. Distler, G. Elliot, M. J. Kang, and C. Lawrie, Isomorphisms of 4D $N = 2$ SCFTs from 6D, *Phys. Rev. D* **107**, 106005 (2023).
- [121] L. B. Anderson, J. J. Heckman, and S. Katz, T-branes and geometry, *J. High Energy Phys.* **05** (2014) 080.
- [122] L. B. Anderson, J. J. Heckman, S. Katz, and L. P. Schaposnik, T-branes at the limits of geometry, *J. High Energy Phys.* **10** (2017) 058.